

Propeller Aircraft Design Optimization for Climate Impact Reduction

R. A. Thijssen

Technische Universiteit Delft



 TU Delft

Cover image: Ifik Ismoedjati <https://unsplash.com/photos/qY8au30b7wI>

Propeller Aircraft Design Optimization for Climate Impact Reduction

by

R. A. Thijssen

to obtain the degree of Master of Science
at the Delft University of Technology,
to be defended publicly on Friday February 11, 2022 at 9:30 AM.

Student number:	4439112	
Project duration:	February 18, 2021 – February 11, 2022	
Thesis committee:	Prof. dr. ir. L. L. M. Veldhuis	TU Delft, Chair
	Dr. ir R. Vos,	TU Delft, supervisor
	Dr. I. C. Dedoussi	TU Delft, Examiner
	Ir. P. Proesmans,	TU Delft, supervisor

An electronic version of this thesis is available at <http://repository.tudelft.nl/>.

Preface

This study marks the end of my MSc student life at the faculty of Aerospace Engineering in Delft. First and foremost there are a few people I would like to thank Ir. Pieter-Jan Proesmans for the guidance and help over past year. Many meetings and questions later, this document signifies the end of the thesis project. Next, I would also like to thank Dr. ir. Roelof Vos for additional guidance and have a critical look on the study where applicable.

As my student career comes to an end, I would not be here without the many friends over the past 6.5 years. This all included random beer nights, interesting discussions, and even the most random walks over the past year. This made me enjoy my student time here to the fullest. A special mention to both of my roommates for way to heated game nights, a critical view, and listened to all my struggles over the past year.

Lastly I would like to thank my parents and my two brothers, who supported my big adventure to Delft over the past years. They continued to support me without hesitation. Even though it was asked many times when I would finally graduate, the day has finally come receive that question no more.

*R. A. Thijssen
Delft, January 2022*

Abstract

The impact of the aviation industry on the atmospheric conditions are significant. The global warming effect that the emitted CO_2 , NO_x , H_2O , and soot in combination with the formation aircraft induced cloudiness (AIC) have is starting to increase due to the growth of the industry. Over the past years, technological advancements were made, but are outperformed by the growth of the industry. For that reason a different approach is required. This study focuses on climate impact reduction by utilizing propeller aircraft on similar routes for turbofan aircraft. Additionally, a direct comparison is made with turbofan data to help determine the potential benefits gained from the utilization of propeller aircraft.

The propeller aircraft is optimized for minimum fuel mass (FM), a minimum direct operating costs (DOC), and minimum average temperature response (ATR). The optimized aircraft are subjected to both a medium-range route and regional route. The former allows a direct comparison with a turbofan aircraft and determine if employing propeller aircraft results in a lower ATR. The regional route is where propeller aircraft are often utilized and allows to see the impact of range on the design variables. Using airframe, engine, and mission design variables the optimal aircraft are designed according to traditional design methods, which are verified with existing aircraft data.

For design case, the aircraft is subject to two different scenarios. The first is where the fleet size is held constant for all objectives, while the second is where the productivity is held constant. It is observed that optimizing for the different objectives either results in a loss of productivity of 50% or an increase in fleet size of 35% when shifting from the DOC objective to either the FM or ATR objective. In the constant productivity scenario the shift from the DOC to the ATR objective reduces the climate impact by 16%, increases the costs by 21% and reduces the fuel mass by 16%. For the design variables, the shift in objective sees a decrease in Mach number, turbine inlet temperature (TIT), and cruise altitude. The compressor pressure ratio and wing-loading remain equal.

Interestingly, the FM and ATR objective are aligned objectives. The low cruise altitude (≈ 5.0 km) causes both unfavorable conditions for the formation of persistent contrails and a limited impact by NO_x . This causes the climate impact to be fully attributed by CO_2 and short-lived emissions, which are directly dependent on the amount of fuel consumption of the aircraft. Minimizing the total fuel consumption during the mission, then directly minimizes the climate impact of the aircraft as well.

The trends seen in scenarios and objectives are generally also applicable to the regional design case. The exception is the wing-loading, which is unconstrained, due to the lower aircraft mass.

When compared to the turbofan data, utilization of propeller aircraft sees a 32% decrease in climate impact between both ATR objectives. This employment also sees an increase in 33% in fleet size, because of the difference in block time between the two distinct aircraft. The benefit gained from employing propeller aircraft is lessened to 22% if a similar fleet size to that of the turbofan aircraft is wanted. The costs and fuel mass reduction, with the lower block time, are 13% and 26% respectively. The cost benefit is viewed critically and likely overestimated, considering the fuel price assumed.

The increase and decrease in costs, fuel mass, ATR and fleet size an optimistic propeller efficiency of 88% is assumed. If a ATR advantage is wanted a propeller efficiency of 75% is required. This increases to 80% if a similar fleet size is wanted. This also affects the costs and fuel mass of the aircraft.

It is concluded that the benefit for employing propeller aircraft for a reduction in climate impact is certainly possible, if a certain efficiency is achieved. This requirement greatly effects the possible utilization of the propeller aircraft, but with the current efficiencies achieved the climate impact is reduced by utilizing propeller aircraft on medium-range routes.

Contents

Abstract	v
Nomenclature	xi
List of Figures	xvii
List of Tables	xxi
1 Introduction	1
1.1 Research Objective	2
1.2 Research Questions	2
1.3 Thesis Structure	3
2 Literature	5
2.1 Propeller Aircraft Conceptual Design & Benefits	5
2.1.1 Propeller Propulsion Characteristics	5
2.1.2 Conceptual Propeller Aircraft Design in Literature	6
2.1.3 Potential Propeller Aircraft Utilization Benefits	7
2.2 Aircraft Climate Impact and Metrics	8
2.2.1 Aircraft Emissions	8
2.2.2 Aircraft Climate Impact Modelling	9
2.3 Aircraft Climate Impact Optimization	11
3 Optimization & Design Methodology	15
3.1 optimization Problem	15
3.1.1 Constraints	16
3.1.2 Aircraft & Engine Configuration	17
3.1.3 Overview	17
3.2 XDSM Diagram and Approach	17
3.2.1 Aircraft Sizing Module	18
3.2.2 Propulsion Module	18
4 Aircraft Design Methodology	21
4.1 Aircraft Sizing Module	21
4.1.1 Class I Weight Estimation	21
4.1.2 Loading Diagram	22
4.1.3 Geometry Layout Generation	23
4.1.4 Aerodynamic Update	24
4.1.5 Class II Weight Estimation	25
4.1.6 Mission Analysis	25
4.2 Propulsion Module	26
4.2.1 Internal Engine Architecture	26
4.2.2 Propulsion Design Analysis	27
4.2.3 Engine, Propeller & Nacelle Size Estimation	30
4.2.4 Propulsion Mass Estimation	31
4.3 Direct Operating Cost Estimation	32
4.3.1 Flight Costs	32
5 Aircraft Climate Impact & Mission Modeling	35
5.1 Aircraft Climate Impact & Emission Modeling	35
5.1.1 Aircraft Emission Modeling	35

5.1.2 Aircraft Climate Impact	36
5.2 Numerical Aircraft Mission Modeling	40
5.2.1 Takeoff Segment	41
5.2.2 Climb & Descent Segment	41
5.2.3 Cruise Segment	42
5.2.4 Landing Segment	42
6 Verification & Validation	43
6.1 Propulsion Module Verification	43
6.1.1 Parametric analyses verification	43
6.1.2 Performance Analyses	44
6.2 Aircraft Synthesizer Verification	45
7 Aircraft Design Cases & Emission Scenario	49
7.1 Aircraft Design Cases	49
7.1.1 Regional Design Case	49
7.1.2 medium-range Design Case	49
7.2 Future Fleet Scenarios	50
8 Aircraft Design Case Results	53
8.1 medium-range Design Case	53
8.1.1 Constant Fleet Size Scenario	53
8.1.2 Constant Productivity Scenario	56
8.1.3 Turbofan Comparison	59
8.1.4 Block Time Constraint	61
8.2 Regional Design Case	64
8.2.1 Constant Fleet Scenario	64
8.2.2 Constant Productivity Scenario	65
8.3 Regional and medium-range Design Case Trends	67
8.3.1 Constant Fleet Size versus Constant productivity scenario	67
8.3.2 Objective Values	68
8.3.3 Design Variables	68
8.3.4 Summary	68
9 Sensitivity Analysis	69
9.1 Aircraft Performance Overestimation	69
9.2 Propeller Efficiency Sensitivity Analysis	69
9.3 Block Time Sensitivity Analysis	72
10 Conclusion	75
11 Future Recommendations	77
A Input Data Engine Verification	79
A.1 Parametric Paper Verification Inputs & Results	79
A.2 GasTurb Verification Input Parameters	80
B Regional Design Case Values	81
C Power-Loading Diagrams	83
C.1 Medium-Range Design Case	83
C.2 Medium-Range Design Case with Block Time Constraint	84
C.3 Regional Design Case	85
D Performance Discussion	87
D.1 Aircraft Design Cases	87
D.2 Sensitivity Analysis	89
E Contrail Formation	91

Nomenclature

Latin Symbols

A	Aspect ratio	[–]
ATR_{100}	Average Temperature Response over a time horizon of 100 years	[K]
b	Span	[m]
C	Work interaction coefficient	[–]
C_L	Lift coefficient	[–]
$C_{L,buffer}$	Buffet onset lift coefficient	[–]
C_D	Drag coefficient	[–]
$C_{D,0}$	Zero-lift drag coefficient	[–]
$C_{D,E}$	Excrescence drag coefficient	[–]
c	Chord length	[m]
c	Climb rate	[m/s]
c_f	Skin friction coefficient	[–]
c_p	Specific fuel consumption	[kg/(s · kg)]
D	Drag	[N]
$D_{prop-fus}$	Propeller fuselage clearance	[m]
$D_{prop-ground}$	Propeller ground clearance	[m]
D_{prop}	Propeller diameter	[N]
E	Endurance	[s]
E	Amount emitted	[kg]
EI	Emission index	[kg/kg]
e	Oswald efficiency factor	[–]
F	Thrust	[N]
f	Efficacy	[–]
f_m	Fuel-to-air ratio	[]
g_0	Gravitational acceleration of the earth	[m/s ²]
H	Time horizon	[Yearx]
H_0	Specific ambient humidity	[g/kg]
h_0	Free stream specific enthalpy	[–]
h_e	Energy height	[J]

h	Height	[m]
h	Altitude	[m]
L	Lift	[N]
LHV	Lower Heating Value	[J/kg]
l	Length	[m]
M	Mach number	[–]
m_{fuel}	Fuel mass	[kg]
m_{payload}	Payload mass	[kg]
m	Mass	[kg]
\dot{m}	Mass flow	[kg/s]
n_{ult}	Ultimate load factor	[–]
P	Power	[W]
P_{TO}	Takeoff power	[W]
P_r	Range parameter	[–]
P_{AC}	Aircraft price	[\$]
p	Pressure	[Pa]
RF	Radiative Forcing	[W/m ²]
RF^*	Normalized radiative forcing	[–]
R_H	Harmonic range	[W –]
R	Range	[m]
S	Wing area	[m ²]
T	Temperature	[K]
TIT	Turbine Inlet Temperature	[K]
t	Time	[s]
t/c	Thickness to chord ratio	[–]
t_{block}	Block time	[hours]
U_{annual}	Yearly utilization	[hours]
V_0	Free stream velocity	[m/s]
V_j	(Equivalent) jet velocity	[m/s]
V_{block}	Block velocity	[m/s]
W	Weight	[N]
W/P	Power-loading	[N/W]
W/S	Wing-loading	[N/m ²]
w	Width	[m]

x Distance [m]

Greek Symbols

$\eta_{\text{propulsive}}$ Propulsive efficiency [-]

η_{prop} Propeller efficiency [-]

η_{total} Total engine efficiency [-]

γ Climb gradient [°]

γ Specific gas constant [J/K]

λ Shape factor [-]

Π Pressure ratio [-]

$\Pi_{\text{compressor}}$ Compressor pressure ratio [-]

ρ Density [kg/m³]

τ_{tH} HPT enthalpy ratio [-]

τ_{tL} LPT enthalpy ratio [-]

τ_t Total turbine enthalpy ratio [-]

χ Atmospheric concentration [ppmv]

Sub- Superscripts

0 Free stream or start

AC Aircraft

app Approach

cg Center of gravity

core Core of the engine

cruise Cruise condition

ec Engine control

fg Fuselage group

fs Fuel system

fus-wing, connec Fuselage wing connection

GEOM Geometry

le Leading edge

max maximum value

osc Oil system control

pers Persistent

prop Propeller

ps Propulsion system

ref Reference

s	Static value for e.g. pressure or temperature
t	Total value for e.g. pressure or temperature
TO	Takeoff condition
total	Combination of other value making it total
wet	Wetted
wg	Wing group

List of Abbreviations

AC	Aerodynamic Center
AGTP	Absolute Global Temperature Potential
AGWP	Absolute Global Warming Potential
AIC	Aircraft Induced Cloudiness
ATR	Average Temperature Response
BPR	Bypass Ratio
Contrails	Condensation trails
CROR	Contra Rotating Open Rotor
DOC	Direct Operating Costs
FM	Fuel Mass
GHG	Greenhouse gas
GTP	Global Temperature Potential
GWP	Global Warming Potential
HPT	High Pressure Turbine
LPT	Low Pressure Turbine
LTO	Landing and takeoff
MAC	Mean Aerodynamic Chord
MDF	Multidisciplinary Feasible
MTOM	Maximum Takeoff Mass
NB	Narrow-Body
OEI	One Engine Inoperative
OEM	Operative Empty Mass
PR	Turboprop
RJ	Regional Jet
TF	Turbofan
TLAR	Top-Level Aircraft Requirements
TP	Turboprop

UAV Unmanned Aerial Vehicle

UHC Unburned Hydrocarbons

XDSM Extended Design Structure Matrix

Relevant Chemical Formulas

CH₄ Methane

CO₂ Carbon dioxide

H₂O Water vapor

NO_x Nitrogen oxides

O₃ Ozone

SO₄ Sulfate

List of Figures

2.1	The propulsive efficiency of various aircraft propulsion, adapted from Torenbeek [22]	6
2.2	Comparison of direct operating costs for a narrow body (NB), a regional jet (RJ) and a turboprop (PR) aircraft, obtained from Ryerson and Hansen [32].	7
2.3	Change in aircraft allocated with increasing carbon pricing for the ATR 72, obtained from Reid et al. [35]	8
2.4	The difference in radiative forcing for aircraft emissions in 2005, obtained from Schwartz [9]	9
2.5	Pareto front showing different aircraft design for different objectives, relating to costs, noise LTO NO _x and fuel carried, obtained from Antoine [43]	11
2.6	Constant fleet scenario (left) and constant productivity (right) scenario visualized, obtained from Proesmans and Vos [15]	13
3.1	Buffet onset lift coefficient with changing mach number for normal and maneuver operation	17
3.2	Full XDSM Diagram for the optimization, adapted from Proesmans and Vos [15]	18
3.3	Workflow of the aircraft sizing module (step 2, 4, and 5 in Figure 3.2)	19
3.4	Workflow of the propulsion sizing module (step 3 in Figure 3.2)	19
4.1	Statistical relation between the OEM and MTOM for turboprop aircraft with wing mounted engines	22
4.2	Power-loading diagram example including the performance requirements, reference data, and the design point	23
4.3	Top-view geometry example for the aircraft configuration used	23
4.4	Normal and reserve aircraft mission, adapted from Proesmans and Vos [15]	26
4.5	Turboprop engine architecture, adapted from Mattingly et al. [45]	27
5.1	Workflow for determining sea-level temperature change, adapted from Dallara Schwartz [44]	37
5.2	The forcing factor for the NO _x climate effects and AIC, obtained from Dallara Schwartz et al. [44]	39
5.3	Geometrical analysis of contrail, based on the Schmidt-Appleman criterion [76]	40
5.4	Numerical missions analysis workflow for the cruise segment, including the engine analysis time-step (dt_{engine})	41
6.1	Payload-Range diagram comparison for the ATR 72	47
6.2	Payload-range diagram comparison for the Dash 8	47
7.1	Overview of the air craft design cases, objectives and future fleet scenarios	51
8.1	Fleet size and number of flights performed for the medium-range design case, assuming constant fleet size	54
8.2	Sea-level temperature change comparison for the medium-range design case, assuming constant fleet size	55
8.3	Optimal aircraft geometry comparison for the medium-range design case, assuming constant fleet size	56
8.4	optimal aircraft geometry comparison for the medium-range design case, assuming constant productivity	56
8.5	Fleet size and number of flights performed for the medium-range design case, assuming constant productivity	57
8.6	Sea-level temperature change for the medium-range design case, assuming constant productivity	59
8.7	Sea-level temperature change for the turboprop and turbofan objectives for the medium-range design case, assuming constant productivity	60
8.8	Fleet size comparison between the turboprop and turbofan aircraft, assuming constant productivity	61

8.9	Optimal aircraft geometry comparison between the turboprop and turbofan ATR_{100}^* objective, assuming constant productivity	61
8.10	Optimal aircraft geometry for the turboprop, with the block time constraint applied, and turbofan objective ATR_{100}^* , assuming constant productivity	61
8.11	Fleet size comparison between the turboprop with the block time constraint applied and the turbofan objectives, assuming constant productivity	62
8.12	Sea-level temperature change comparison between the turboprop, with the block time constraint applied and turbofan objectives	64
8.13	Fleet size and number of flights performed for the regional design case, assuming constant fleet size	65
8.14	Fleet size and number of flights performed for the regional design case, assuming constant productivity	66
8.15	Optimal aircraft geometry comparison for the regional design case, assuming constant productivity	67
8.16	Sea-level temperature change for the regional design case, assuming constant productivity	67
9.1	Sea-level temperature change for ATR_{100}^* objective for various propeller efficiencies, including ATR_{100}^* turbofan objective	72
9.2	Optimal geometry comparison for the ATR_{100}^* objective with a propeller efficiency of 65%, 75%, and 85%	72
9.3	Optimal geometry comparison for the ATR_{100}^* turbofan objective and the ATR_{100}^* turboprop objective with a propeller efficiency of 75%	72
9.4	Sea-level temperature change for ATR_{100}^* objective, with block time constraint applied, for various propeller efficiencies, including ATR_{100}^* turbofan objective	74
A.1	Parametric analysis verification for specific engine parameters for the paper by Dinç [77]	80
B.1	Optimal aircraft geometry comparison for the regional design case, assuming constant fleet size	82
C.1	Power-Loading diagram of the FM objective for the medium-range design case, assuming constant productivity	83
C.2	Power-Loading diagram of the DOC objective for the medium-range design case, assuming constant productivity	83
C.3	Power-Loading diagram of the ATR_{100}^* optimised objective for the medium-range design case, assuming productivity	84
C.4	Power-Loading diagram of the FM objective for the medium-range design case with block time constraint applied, assuming constant productivity	84
C.5	Power-Loading diagram of the ATR_{100}^* objective for the medium-range design case with block time constraint applied, assuming constant productivity	84
C.6	Power-Loading diagram of the FM objective for the regional design case, assuming constant productivity	85
C.7	Power-Loading diagram of the DOC objective for the regional design case, assuming constant productivity	85
C.8	Power-Loading diagram of the ATR_{100}^* objective for the regional design case, assuming constant productivity	85
D.1	Payload-range diagram for the regional design case, assuming constant productivity	88
D.2	Payload-range diagram for the medium-range design case, assuming constant productivity	88
D.3	Payload-range diagram for medium-range design case, with the block time constraint applied, assuming constant productivity	89
D.4	Payload-range diagram for the turbofan objectives, assuming constant productivity	89
D.5	Payload-range diagram for the ATR_{100}^* objective for various assumed propeller efficiencies	90
D.6	Payload-range diagram for the ATR_{100}^* objective with the block time constraint applied for various assumed propeller efficiencies	90
E.1	Critical contrail formation plot during cruise for the DOC turboprop objective for the medium-range design case	91

E.2	Critical contrail formation plot during cruise for the DOC turbofan objective	91
E.3	Critical contrail formation plot during cruise for the FM turboprop objective for the medium-range design case	92
E.4	Critical contrail formation plot during cruise for the DOC turbofan objective	92
E.5	Critical contrail formation plot during cruise for the ATR_{100}^* turboprop objective for the medium-range design case	92
E.6	Critical contrail formation plot during cruise for the ATR_{100}^* turbofan objective	92

List of Tables

2.1	Table showing design variables and aircraft characteristics for different objective functions, obtained from Schwartz [9]	12
3.1	optimization Design Variables, including the initial values and the bounds	16
4.1	Mission segments numbering	26
4.2	Engine station numberings [45]	27
5.1	Overview of the EI for the various emitted gasses [15]	36
5.2	Efficacy of the different climate impact species [44]	37
5.3	Coefficients for the impulse response function for CO ₂ concentration, used in Equation 5.8 [39]	37
6.1	Input parameters for three on-design point missions, obtained from Dinc [77]	43
6.2	Paper and propulsion module parametric analysis comparison [77]	44
6.3	Input parameters for the Gasturb parametric and the two performance analysis verification	44
6.4	GasTurb and propulsion module parametric analysis comparison	45
6.5	GasTurb and propulsion module performance analysis comparison	45
6.6	Aircraft synthesizer verification input parameters	46
6.7	Aircraft synthesizer validation with the ATR-72 and the DHC Dash 8-400	46
7.1	Aircraft design requirements and both mission- and future fleet scenario variables	50
8.1	Objective function values for the medium-range design case, assuming constant fleet size	53
8.2	Optimal design variables values for the medium-range design case, assuming constant fleet size	55
8.3	Aircraft parameters and characteristics for the medium-range design case, assuming constant fleet size	55
8.4	Objective function values for the medium-range design case, assuming constant productivity	56
8.5	Optimal design variables values for the medium-range design case, assuming constant productivity	58
8.6	Aircraft parameters and characteristics for the medium-range design case, assuming constant productivity	58
8.7	Objective function values comparison between the turboprop and turbofan objectives, including block time and EI _{NO_x}	60
8.8	Objective function values comparison between the turboprop, with the block time constraint applied, and turbofan objectives, including block time and EI _{NO_x}	62
8.9	Optimal design variables for the medium-range design case with the block time constraint applied	63
8.10	Aircraft parameter comparison between the turboprop, with the block time constraint applied, and turbofan objectives	63
8.11	Objective function values for the regional design case, assuming constant fleet size	64
8.12	Objective function values for the regional design case, assuming constant productivity	65
8.13	Optimal design variables values for the regional design case, assuming constant productivity	66
8.14	Aircraft parameters and characteristics for the regional design case, assuming constant productivity	66
9.1	Objective function value comparison for the ATR ₁₀₀ [*] for various propeller efficiencies	70
9.2	Objective function values for the turbofan objectives	70
9.3	Optimal design variables comparison for the ATR ₁₀₀ [*] for various propeller efficiencies	70
9.4	Aircraft parameter and characteristics comparison for the ATR ₁₀₀ [*] , with the block time constraint applied, for various propeller efficiencies	71

9.5	Optimal turbofan aircraft parameters and characteristics	71
9.6	Objective function value comparison for the ATR_{100}^* , with the block time constraint applied, for various propeller efficiency	73
9.7	Optimal design variables value comparison for the ATR_{100}^* , with the block time constraint applied, for various propeller efficiencies	73
9.8	Aircraft parameter and characteristics comparison for the ATR_{100}^* , with the block time constraint applied, for various propeller efficiencies	73
A.1	Input parameters for the different engine parameters	79
A.2	Constant input parameters for the parametric analysis verification with the paper by Dinç [77]	79
A.3	Parametric and Performance analysis GasTurb input parameters	80
B.1	Optimal design variables values for the regional design case, assuming constant fleet size	81
B.2	Aircraft parameters and characteristics for the medium-range design case, assuming constant productivity	81
D.1	Maximum fuel mass and range parameter for the objective within each design case	87
D.2	Maximum fuel mass and range parameter for the turbofan objectives	88
D.3	Maximum fuel mass and the range parameter for $ATR_{thesensitivity}^*$ for various propeller efficiencies	89
D.4	Maximum fuel mass and the range parameter for $ATR_{thesensitivity}^*$ with the block time constraint applied, for various propeller efficiencies	89

1

Introduction

The impact of the aviation industry, due to aircraft emissions, is well established [1, 2]. The current aviation industry is responsible for a total of 5% of all anthropogenic CO₂ emitted in the world [3]. Comparing that to the 24% anthropogenic CO₂ emitted by the transport industry in total, it might seem insignificant. The aviation industry was expected to grow around 3% each year before the corona pandemic hit the world [4]. This growth is estimated to be even larger when travel restrictions will be lifted in the future [5]. Combining this with the knowledge that pollution near airports can cause severe health problems, a reduction in emissions by aircraft is of great importance [6]. For the health problems regulations have been imposed to reduce the landing and takeoff (LTO) NO_x emissions, while CO₂ emissions are currently restricted for the whole flight [7]. This indicates that the emissions water vapor (H₂O) and soot aerosols are not restricted, while their climate impact is clear [8, 9]. Lastly, aircraft induced cloudiness (AIC), if persistent, potentially have a large impact that is often neglected [10, 11]. Overall the emissions can be reduced with the technological advancements made in the future, however the growth of the industry is outpacing the advancements [12]. This gives the need for a different approach to reduce the climate impact.

Studies on the reduction of the have already been performed. Antoine and Kroo [13], performed an optimization for minimum LTO NO_x emitted, minimum noise and minimum mission fuel mass. This is simple way to compare the climate impact early in the design phase, however it is lacking other emission types. The same is true for Henderson et al. [14]. A large amount of design variables are used, showing more aircraft design trends for the reduction of the CO₂ emitted. This does come with the downside that it is hard to distinguish the effects of each design variable. These studies have been majorly improved upon by Dallara Schwartz [9] and Proesmans and Vos [15]. Both studies use core design variables to guide the design of the aircraft for minimum climate impact. The climate impact is measured with the average temperature response (ATR), which takes both long-lived and short-lived emissions into account if the time horizon is chosen correctly. Additionally, AIC is also taken into account. Which is a great improvement on the amount emitted [16].

From the latter two studies, which focused on turbofan aircraft, it is clear that the climate optimal turbofan aircraft has a lower cruise Mach number (≈ 0.6) and cruise altitude (≈ 7 km). The combination of the altitude and Mach number reduces the effect of NO_x on the climate and prevent the formation of AIC, specifically persistent contrails. These cruise conditions the climate optimal turbofan aircraft attains to reduce the climate impact is the region where propeller aircraft are known to have a larger propulsive efficiency. Propeller aircraft have been studied heavily as part of the AGILE 3.0 project¹. Different innovative configurations are tested on performance and climate impact. For example the study of Stingo et al. [17] compares a wing mounted propeller aircraft with an tail mounted propeller aircraft. Della Vecchia et al. [18] measure the climate impact of a propeller aircraft using the global warming potential (GWP), however GWP is not the best metric without sufficient comparison [19]. Next to the turboprop, the contra-rotating open rotor (CROR) has regained interest since its main introduction in advanced turboprop project by Hager et al. [20]. The regained interest is mainly studies by Guynn et al. [21]. The CROR has high potential, but lacks applicability that the turboprops for that reason the turboprop is often preferred in studies.

Combining the knowledge of lower cruise Mach number and altitude of the climate optimal turbofan aircraft with higher propulsive efficiency of propeller aircraft, makes it of interest to study the climate impact

¹See: <https://www.agile-project.eu/>

of propeller aircraft. In other words, can the climate impact for the same route be reduced even more if propeller aircraft are employed. For This for more sustainable aviation industry in the future. To get a better view of the study a research objective and research questions have been constructed.

1.1. Research Objective

Based on the study that showed a gap in literature for climate impact optimized propeller aircraft, the main research objective has been constructed to fill the research gap:

"The research objective is to minimize the global warming impact of a medium-range propeller powered aircraft by optimizing airframe, engine, and mission design variables for the same objective."

The research objective shows both the goal of the study and the means that will help fulfill the objective. The airframe, engine and mission design variables will help shape the aircraft design and guide it to the climate impact optimal aircraft design. From the main objective, sub-objectives are constructed to help fulfill the main objective. One is to adapt and extend the current aircraft design methodology to design propeller aircraft as well. A different engine sizing module being the main expansion. Additionally, the aircraft will be optimized for a fuel mass and direct operating costs (DOC) objective. This will give additional insight in the differences and makes a better comparison. The propeller aircraft will also be compared to turbofan aircraft which is optimized for the same objectives. This will extra insight int he values obtained and puts the results into perspective.

1.2. Research Questions

Following from the research objective and the literature study performed, two main research questions have been constructed. These need to be answered for the study and help reach the research objective. The first main research question is as follows:

What are the changes in airframe, engine and mission design variables for a medium-range, propeller powered aircraft when the optimization objective is changed from direct operating costs or fuel mass to climate impact for a given mission?

The main research question is supported by a number of sub-questions that will help answer the main research question:

- What design variables are needed to model a medium-range propeller powered aircraft in the conceptual design phase to study the climate impact of the aircraft?
- What changes are to be made in the aircraft conceptual design modules to incorporate propeller aircraft?
- What would the climate impact be relating to direct operating costs and minimum fuel mass for a medium-range propeller powered aircraft?
- What are the changes seen in the design variables when designed for a regional route?

The above mentioned main research question has the focus on a the propeller aircraft on its own and how the design variables are shaped for the three objective functions. Additionally, the sensitivity of the mission range is taken into account the last sub-question. These can be compared to see the impact of the range on the design variables and objectives.

The second research question does tie in with the first research question and helps determine the advantages and disadvantages from utilizing propeller aircraft on a similar route to that of the turbofan aircraft. This is accomplished by direct comparison between the design variables and the objective values. The second main research question is shown below:

What is the difference in direct operating costs, mission fuel and climate impact between an optimized propeller powered aircraft and a turbofan powered aircraft optimized for the same objectives and mission?

For this question also a number of sub-question have been made. The sub-questions are as follows:

- What are the changes in overlapping design variables for a propeller powered aircraft in comparison to the optimized turbofan powered aircraft?
- What is the difference in climate impact, costs and mission fuel between the turbofan powered and propeller powered aircraft?

Both research questions help answer the question if propeller aircraft are a suitable option for the climate reduction of the aviation industry. In other words should, for the climate impact reduction, propeller aircraft be used in contrast to the current turbofan aircraft with an insight in the change in costs as well.

1.3. Thesis Structure

This document is structured into different Chapters that will each discuss a different topic. Chapter 2 discusses the literature study performed and gives background information on various topics regarding this study. Followed by the explanation and setup for the optimization problem in Chapter 3. Chapter 4 explains the aircraft design methodology & cost estimation, which is followed by the climate impact analysis. Chapter 6 verifies and validates the design methodology explained in Chapter 4. Chapter 7 discusses the aircraft requirements and the emission scenario for this study, while Chapter 8 discusses the results for the discussed emission scenarios. Chapter 9 focuses on the performed sensitivity analysis. Lastly, the conclusion and future recommendations are discussed in Chapter 10 and Chapter 11.

2

Literature

It is important for the study to have general knowledge about the design of propeller aircraft and the climate impact caused by aircraft emissions. Additionally, the potential utilization is of interest. In order to understand this all a literature study is performed on these topics.

Within this Chapter, Section 2.1 discusses the characteristics, benefits, and drawbacks of propellers. Additionally, propeller aircraft in literature are discussed. Section 2.2 elaborates the cause of the climate impact by aircraft emissions and how this can be measured. Lastly, Section 2.3 discusses the most prominent aircraft climate impact studies and their results and trends.

2.1. Propeller Aircraft Conceptual Design & Benefits

While the conceptual design of propeller aircraft is present in literature for medium-range routes, it is lacking in quantity. This is a logical consequence of drive to reduce costs and for that turbofan are often chosen. Over the last years there has been a shift into more propeller aircraft with new propulsion types and aircraft configurations. This Sections is divided into three Subsections. Subsection 2.1.1 discusses the characteristics of propellers and propeller propulsion, while Subsection 2.1.2 discusses conceptual propeller aircraft design in literature. Lastly, Subsection 2.1.3 discusses about the potential benefits of utilizing propeller aircraft.

2.1.1. Propeller Propulsion Characteristics

Even with the different types of propeller propulsion, they all share the main advantage of propellers. At lower Mach numbers, when compared to turbofan aircraft, the propulsive efficiency is, compared to a turbofan engine, higher [22]. The cause is best explained with the equation for the propulsive efficiency, which is shown in Equation 2.1.

$$\eta_{\text{propulsive}} = \frac{2}{1 + \frac{V_j}{V_0}} \quad (2.1)$$

In this equation the propulsive efficiency is maximized when the equivalent exit jet velocity (V_j), is slightly higher than the free stream velocity (V_0). This is a characteristic of a propeller engine, where a large amount, or total, thrust is provided by the propeller. Propeller thrust is generated by putting power to the propeller, which makes it spin and accelerates the flow behind the propeller. The large air-mass is accelerated a little amount, resulting in a higher propulsive efficiency. This is contrary to a turbofan or turbojet aircraft, where a small amount of air is accelerated by a large amount. This is offset with more recent turbofan engines, where the bypass ratio keeps increasing. The slight increase with a larger mass flow is better for the propulsive efficiency, as mentioned. The downside however is that for propellers the propeller efficiency drops rapid at Mach numbers as seen in Figure 2.1, where the propulsive efficiencies for different propulsors are compared [22, 23].

At lower Mach numbers the propeller propulsion is a solid option, however it also has its downsides. As the propeller rotates the tips can reach sonic speeds and create shock-waves. These shock-waves cause the wave drag to increase and make the propeller less efficient [23]. Additionally, these shock-waves generate considerable amount of noise for the passengers and around airports. Even when the actual noise is lower, the experienced noise is often seen as higher, due to the moving parts [24, 25]. The more stringent noise

regulations imposed and reduction in performance often limits the use of propeller aircraft greatly, especially for medium or long-haul routes. The long mission duration favors the turbofan in this aspect greatly. This is especially seen in Figure 2.1, where the high bypass ratio (BPR) turbofan has a higher propulsive efficiency at the higher Mach numbers. The high propulsive efficiency can be extended by utilizing CROR engines on the aircraft [20].

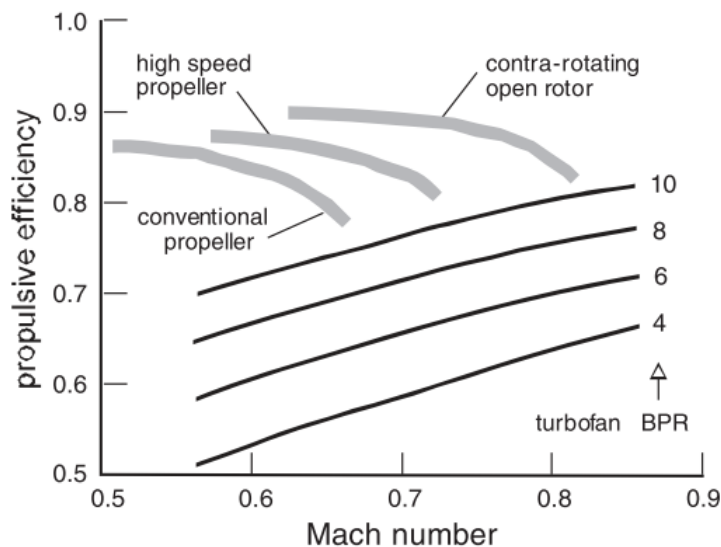


Figure 2.1: The propulsive efficiency of various aircraft propulsion, adapted from Torenbeek [22]

2.1.2. Conceptual Propeller Aircraft Design in Literature

With the characteristics of propeller propulsion are known, it is important to analyze the current state-of-the-art literature. The focus of research of propeller aircraft can be divided into two main categories: the configuration of the aircraft and the propeller engine itself.

Regarding the aircraft configurations many different possibilities have been thought of and are possible. Most change the engine, wing and tail such that a new aircraft is designed with that configuration and are compared. A large number of these studies are within the previous mentioned AGILE 3.0 project. This project has led to multiple papers with different turboprop aircraft that have different wing, tail and engine placement. Nicolosi et al. [26] uses the DOC for the comparison between the different aircraft configurations. The high-wing and T-tail configuration with the two engines mounted on the wing is chosen as the threshold for the other configurations. These configurations include a low-wing and conventional tail configuration with tail mounted turboprop engines and a canard configuration. Overall the performance of the canard configuration with horizontal tail mounted engines came out as the best, but the canard configuration brings problems regarding stability and control, which results in a limited amount built in the current market. The tail mounted engines configuration is studied more often as seen in Van Arnhem et al. [27], Mirzoyan et al. [28], Schouten et al. [29] and Goldsmith [30]. The high center of gravity excursion, due to the aft center of gravity of the engine, causes the aircraft to be outperformed by the wing mounted engine configuration [28, 29]. In these studies the wing and tail configuration often change dependent on the engine placement. If the propeller is on the wing a high-wing configuration with a T-tail is often chosen. The ground clearance of the propeller is more easily met, because of the high-wing placement. Additionally, the T-tail ensures that the horizontal stabilizer is out of the propwash [23]. If the engines are not mounted on the wing a low-wing is often chosen.

The other aspect is the engine and propeller type itself, especially the type of propulsor used. The main type used currently is the turboprop engine, which is used in the aforementioned studies, and the open rotor. The open rotor is a concept in the 1980's by the advanced turboprop project [20]. The goal of the concept is extending the higher propulsive efficiency to higher Mach number by utilizing higher swept blades, also seen in Figure 2.1. Guynn et al. [21] studies a geared counter rotating open rotor (CROR) and compares it to a turbofan model, to see what the effects are on the performance and environment. While the environmental impact is limited to NO_x and CO_2 only, the performance indicators shown are extensive and results in a

heavier aircraft. This also results in less mission fuel needed, but this study does however not take cost into account. These are potentially lower for the CROR. The same is found by Hendricks et al. [31], with updated blade technology and the same trend is found as in Guynn et al. [21]. With the increasing interest in the CROR, it is likely that it might see a commercial application, but until now it yet to be used.

The combination of these studies show that propeller aircraft are versatile, but clearly have its advantages and disadvantages when utilized. To see how propeller aircraft are utilized and what possibilities are regarding costs saving, this is better explained in next Subsection (Subsection 2.1.3).

2.1.3. Potential Propeller Aircraft Utilization Benefits

The other Subsections made clear that different configurations have an impact on the performance of the propeller aircraft. These studies showed the design of propeller aircraft, but are not used in a scenario. This Subsection focuses on the utilization and characteristics of existing or designed propeller aircraft.

The change in the fleet by utilizing propeller aircraft is highly tied in to the higher propulsive efficiency and lower cruise Mach number. Ryerson and Hanson [32] studied the changes fuel prices and the cost benefit achieved. A part of the findings is given in Figure 2.2, which shows the comparison between a regional jet (RJ), narrow-body aircraft (NB), and a turboprop (TP) aircraft. For all ranges the turboprop is more cost friendly for all distances, if the fuel price is high enough. When a lower fuel price is assumed ($\approx 3\$$), the narrow-body aircraft is cheaper and thus the logical choice. this benefit is partly caused by the lower block time, which reduces the crew costs for the mission. Note that this benefit is for one aircraft mission only and does not take into account versatility of the different aircraft types.

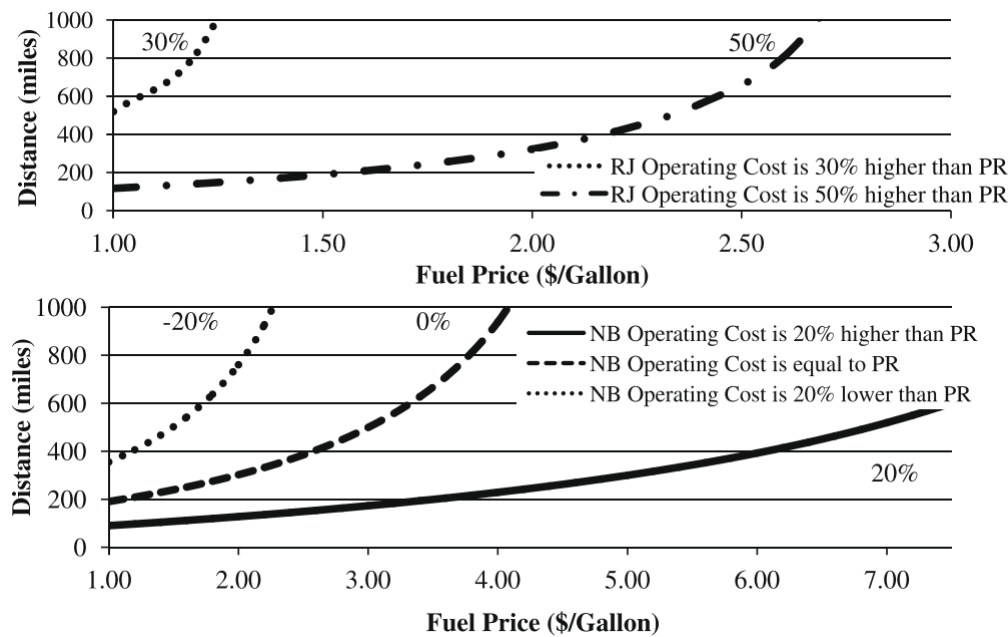


Figure 2.2: Comparison of direct operating costs for a narrow body (NB), a regional jet (RJ) and a turboprop (PR) aircraft, obtained from Ryerson and Hansen [32].

Overall the versatility, the block time, and the costs per mission are intertwined and determine the type of aircraft is used on which route. This gives an potential problem that might be encountered when flying longer distances. Even though the propulsive efficiency is higher for the propeller aircraft, the lower cruise speeds might increase the costs of the aircraft. The turboprop aircraft however uses more fuel and has a lower block time. This results in more mission performed in less time and thus much more versatile in its utilization. Even when the costs of the propeller aircraft per mission are lower, the increase in block time could potentially make less money for the airliner itself. This dilemma is strengthened by Mahieu [33], which found that the turboprop is cost-wise beneficial for the certain range as the block time or the mission range plays less of an issue.

Furthermore, it of interest to see the potential of utilizing turboprops in reducing the climate impact of aviation. A turboprop fleet that could be utilized in China could reduce the costs and environmental impact

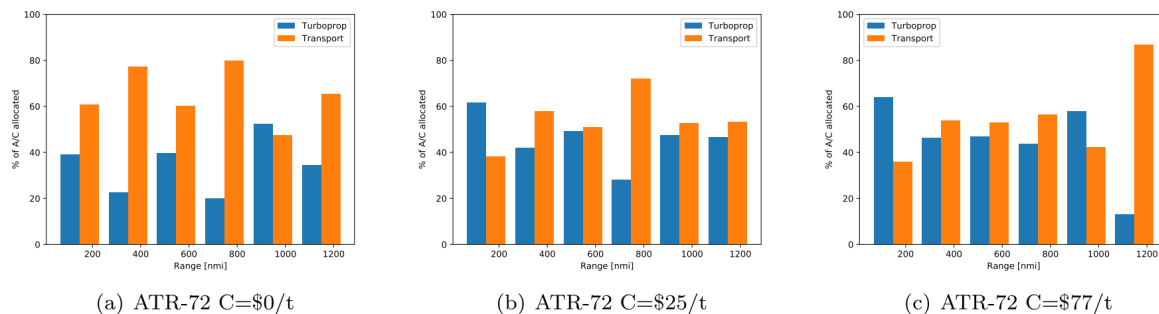


Figure 2.3: Change in aircraft allocated with increasing carbon pricing for the ATR 72, obtained from Reid et al. [35]

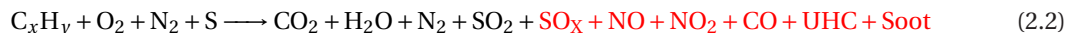
in China, at a cost of increasing travel time (block hours). This was the conclusion of Ryerson and Ge [34], with a note that this gain could potentially not limit itself to China. Research on the same topic, but with different approach, is performed by Reid et al. [35]. In the study various amounts of carbon pricing are imposed on the fuel costs to see its effect on the utilization of both turbofan and turboprop aircraft. The shift in utilization is shown in Figure 2.3. This figure shows that with the increase in carbon pricing the usage of turboprops start to increase, due to the lower fuel consumption of the turboprop aircraft. This ties in with the findings of both Ryerson and Hanson [32], and Mahieu [33]. Another way to read the data is that when CO₂ emissions become more important, the shift to propeller aircraft is sensible.

2.2. Aircraft Climate Impact and Metrics

To gain insights in the aircraft climate impact inner workings a short recap of the different emissions types and their origin are discussed. Also summarized is the approaches that can be taken to measure the aircraft climate impact and how that is done in current literature.

2.2.1. Aircraft Emissions

Overall the type of species by an aircraft is the same, as most aircraft use the same type of fuel. The burned fuel is used to generate power or thrust that is needed to propel the aircraft. Currently, kerosene is used for aircraft, which is a hydrocarbon fossil fuel. The chemical reaction within the combustor, with the added heat and oxygen, results in the formation of the chemical products that cause a climate impact. In an stoichiometric or ideal combustion process this would result in carbon dioxide (CO₂) and water vapor (H₂O), but the addition of sulfur in the fuel, it also leads to production of sulfur dioxide (SO₂) [1, 8]. In a realistic combustion process, which is non-stoichiometric, more reaction products are formed. Examples of this are the nitrogen oxides (NO + NO₂), soot and unburned hydrocarbons (UHC's) [36]. The combustion process for both types is summarized in Equation 2.2. Here the reaction products in black are the products in stoichiometric combustion, while the red are extra in a non-stoichiometric combustion process. Do note that this chemical reaction is just for illustration purposes and shows the reaction process in a simple manor. Furthermore, there are no mole ratios shown in the reaction and thus the chemical reaction is incomplete [1, 8].



Not all reaction products or aircraft emissions have an impact on the climate. Directly or indirectly CO₂, H₂O, the nitrogen oxides often summarized as NO_x, soot and sulfur oxides SO_x have a noticeable climate impact. For the sulfur oxides this is caused by the formation of sulfate (SO₄). Additionally, due to the emitted water vapor AIC can form behind the aircraft and when these in the form of persistent contrails they can have a large impact on the climate [11, 37].

The mentioned emissions all have either a positive or negative effect on the climate, or in other words a global warming or global cooling effect respectively. The effects of these species are often summarized by their radiative forcing (RF). It is defined as "The perturbation (in W/m^2) of the planetary energy balance by a climate change mechanism" [19]. Technically it is a metric for the climate impact itself, but it is often used to denote the warming or cooling effect of an emission type [38]. A positive value thus indicates a global warming effect, while a negative is a global cooling effect. An overview of the RF of the species mentioned is shown in Figure 2.4.

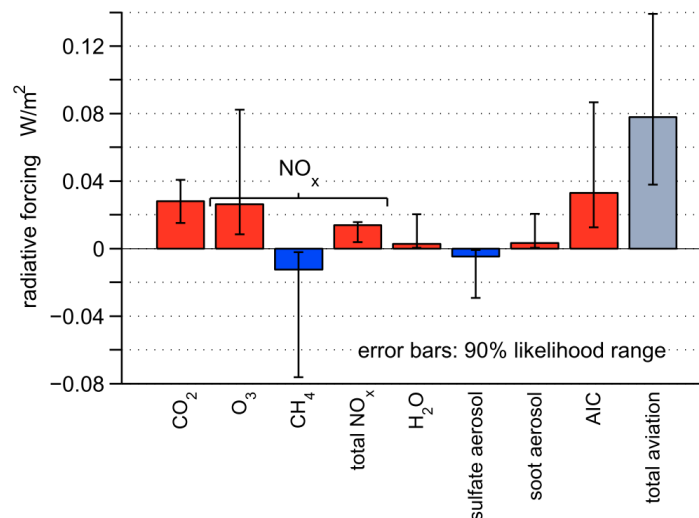


Figure 2.4: The difference in radiative forcing for aircraft emissions in 2005, obtained from Schwartz [9]

In the figure the RF of each species and their cooling or warming effects are seen. For NO_x the effects are subdivided in the global cooling effect for the destruction of methane and the global warming effect for the formation of ozone (O₃). In total NO_x has a positive RF. Additionally, the emitted sulfur oxides form sulfate, which has a small negative RF, as shown in Figure 2.4. Technically aircraft induced clouds (AIC) is not an emission, but still have a high RF. More information about the species themselves and their properties please refer the Brasseur et al. [8], Lee et al. [3], and Sausen and Schumann [39].

2.2.2. Aircraft Climate Impact Modelling

In Figure 2.4 the RF of the emissions is shown, but this is not the only way to measure the climate impact of an aircraft. Different climate metrics exist and are used for different studies. Dependent on the study or problem a different climate metric might be favorable. Guidelines posed by Grewe and Dahlmann [16] could be adhered to, in order to choose a suitable climate metric for the question or problem present. To get an idea of the metric used in previous studies various metrics discussed with their advantages and disadvantages.

The climate metrics that are elaborated upon are the amount of kilograms emitted, the RF, the global warming potential (GWP), the global temperature potential (GTP) and the average temperature response (ATR).

Kilograms of Gas Emitted

The amount of kilograms of emission emitted is a basic metric to measure the climate impact, due to the aircraft emissions. This metric is applicable for various scenarios. One mission can be chosen or a whole fleet can be summed in this metric. Often it is used for the emissions of CO₂ and LTO NO_x, as the effects of these type of emissions are well established [8, 40]. This also leads to the downside of this metric. The level of scientific understanding (LOSU) for sulfate and soot is not as high as that for CO₂ and NO_x and thus it is hard base the climate impact purely on the amount emitted. Additionally, AIC is not an emission type and is thus completely disregarded in this metric. For that reason it is often used in early conceptual studies and older climate impact studies, like Antoine and Kroo [13] and Henderson et al. [14].

Radiative Forcing

Radiative forcing was already mentioned when discussing the climate impact of the aircraft emissions itself, there it was used as a sort of measure for each emission. Officially called "The Radiative Forcing of Climate Change", this metric is backwards looking. This indicates that it is based on pre-industrial times and does not provide enough information on the impact of the gasses in the future [41]. It is useful as altitude variation is taken into account if wanted. The application itself is more as an intermediate value or climate impact indication, as done earlier, than a climate metric itself. Better metrics are available with insignificant extra computation power required [19].

Concluding, the RF is limited in its use, but is great for the climate impact indication. This makes its usage as a metric for comparisons reasons only [3, 19].

Global Warming Potential

The first metric that is more widely used in climate studies is the global warming potential. This metric is defined as the integrated RF, due to a pulse emission of unit mass divided by the integrated RF of a unit mass of CO₂ over the same time horizon. This is expressed in mathematical terms in Equation 2.3. The concept of GWP is based on the assumption that the integrated RF is a valid measure of climate change or the climate impact of all the gasses. Note that the division by CO₂ helps relating the potential of each emission to the value of CO₂, which has a high LOSU [38]. Note that the integrated radiative forcing over a specified time horizon is often denoted as the absolute global warming potential (AGWP) [42].

$$GWP = \frac{\int_0^H RF_i(t) dt}{\int_0^H RF_{CO_2}(t) dt} = \frac{AGWP_i}{AGWP_{CO_2}} \quad (2.3)$$

The main advantage of using of GWP is that the time dependencies of each emitted gas like CO₂ and NO_x are taken into account, given that the time horizon is chosen adequately. In climate studies a time horizon of 100 years is often chosen [9, 38]. The downside is the assumed linearity behavior for specific climate effects. These effects can be non-linear, resulting in an over- or underestimation of the climate impact. Additionally, the metric itself is not that easy for policy makers. What kind of number would be high or would be low, this is hard to grasp when no direct comparison is given. Generally speaking, the GWP is an improvement on the RF, but lacks clarity in the aspects mentioned [19, 42].

Overall the use of GWP in literature regarding climate studies is high, however it is not often used in aircraft conceptual design studies and thus its usage is limited. Della Vecchia et al. [18] and Stingo et al. [17] are one of the few to use it. The calculation for it lacks insight, as it is hard to reproduce.

Global Temperature Potential

The global temperature potential (GTP) was proposed in 2005, with the goal of being an extension to GWP. On contrary to GWP and RF, GTP represents the response of the global-mean surface temperature. This is calculated with similar inputs as the GWP, meaning that it is attractive for studies, even though this means a higher uncertainty. [38]. Additionally, it is an end-point metric, indicating a particular temperature change at a particular time, rather than the integrated time. This is an advantage over GWP, as it includes climate sensitivities for the different emissions and the thermal inertia of the atmosphere [42]. The relation of Equation 2.3 is also to calculate the GTP, but the AGWP is substituted with AGTP, which is seen in Equation 2.4 [38]. The denominator is also replaced with the response of CO₂, according to the equation below.

$$AGTP(H) = \int_0^H RF(t) \cdot R(H-t) dt \quad (2.4)$$

As the climate sensitivities are taken into account the chosen time horizon becomes more important. The main disadvantage of GTP is that only a snapshot is made at the specified time, and the time varying temperature potential is not known and cannot be plotted. No change over time before or after the time horizon is considered [7, 9, 19, 42]. GTP is mentioned by Koch [42], but does not use it in its final climate calculation.

Average Temperature Response

The last metric discussed is the ATR, as proposed by Schwartz in 2011 [9]. The goal of the ATR is to have a tangible and measurable metric for the aircraft emissions climate impact that is flexible to use with a relatively low uncertainty. This is performed by including both the effects and perturbation of the aircraft emissions, long after they have been emitted. In other words both short-lived and long-lived emissions are modeled. As this is a temperature based metric, it is easy to understand for policy-makers and non-specialists [9].

The calculation of the ATR is a combination of the integrated temperature change of GWP with the temporal weighting of RF. The main equation to calculate the ATR is shown in Equation 2.5, where H is the chosen time horizon and $\Delta T(t)$ is the global mean sea-level temperature change caused by the emissions at time t [9]. A more in depth calculation methodology is found in Section 5.1.

$$ATR_H = \frac{1}{H} \int_0^H \Delta T(t) dt \quad (2.5)$$

In essence the representation of ATR is different. The lifetimes of the radiative gasses, and the inertia of the atmosphere are both taken into account. While GTP only calculates the end-point value of the time horizon, the sea-level temperature change over the time horizon is known. For the ATR metric a time horizon the chosen time horizon for ATR is usually 100 years to take into account the longevity of most radiative gasses,

causing to be less dependent on the temporal evolution of emissions and the chosen time horizon [9]

Despite being relatively new the usage of ATR in aircraft climate studies is evident. Proesmans and Vos [15] and Koch [42] are two of those. Logically Schwartz uses the metric in its own research as well [36].

2.3. Aircraft Climate Impact Optimization

Optimizing aircraft for a certain objective is not new and extensive work has been performed on reducing the fuel or costs of aircraft. Optimizing the aircraft for climate impact however is relatively new. One of the first to focus on the climate impact is Antoine [43] and Antoine and Kroo [13]. Both studies focus on the multi-objective optimization an aircraft minimum cost, minimum fuel, minimum LTO NO_x and minimum noise. These objectives tend to have conflicting aircraft designs. Figure 2.5 shows this exact mismatch in objectives with an overview. Note that this this is not exactly the best measure for the climate impact, but the contrast between objectives can be identified.

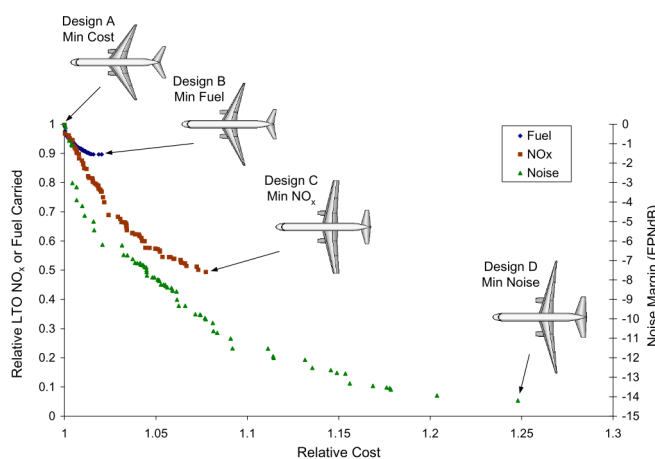


Figure 2.5: Pareto front showing different aircraft design for different objectives, relating to costs, noise LTO NO_x and fuel carried, obtained from Antoine [43]


The trend in the figure clearly demonstrates how much the noise optimized aircraft would cost, relative to the other objectives. The same is true for the other objectives. Logically the minimum cost aircraft is the cheapest one, followed by the optimum fuel, minimum LTO NO_x and the minimum noise. It thus shows how costly a certain minimum objective in comparison the cost optimum. For example, to minimize the noise as much as possible, 25% more costs would be involved with flying the aircraft. Another perspective that can be obtained is how much noise reduction can be achieved for little costs. Where for a 5% increase in costs only 40% of the noise is achieved. The last several reductions in the values for each objective is often expensive. Thus not incorporating the full objective optimized design variables aircraft can still reduce the objective significantly, which is seen for the noise objective.

The aircraft designed by Antoine [43] are not in a fleet and only fly a singular mission. This is fine for the current climate metrics used, but leaves things to be desired in the climate impact. The step to a multi-aircraft scenario is, with the aircraft already designed, a small one.

Improving on the emission scenario mentioned, is the study by Schwartz [9]. The study uses the fundamentals laid by Antoine and builds upon them. The study focuses on the climate impact objective, measured in ATR. Additionally, aircraft are designed for minimum fuel mass and minimum NO_x as well. For these objectives different technologies are employed, e.g. AIC avoidance technology, the open rotor propulsion, and bio-fuel is used to see the effect on the climate impact. The optimal turbofan aircraft designed in the study are shown in Table 2.1, where aircraft parameters and characteristics are given [9].

The difference between the objectives with the cost objective is the most apparent when looking at the geometry. As a result of the higher cruise Mach number the critical Mach number is postponed to avoid sonic velocities over the wing and thus a sweep angle applied. This is in contrast to the ATR optimal aircraft, which sees little to no sweep in its wing, due to the opposite reason for the cost optimal aircraft. The relatively low cruise altitude for the ATR optimal aircraft is to reduce the climate impact by NO_x the prevention of the for-

Table 2.1: Table showing design variables and aircraft characteristics for different objective functions, obtained from Schwartz [9]



	min cost	min fuel	min NO _x	min ATR _{$\tau=0$}	min ATR _{$\tau=3$}
Maximum TOW [lbs]	161,600	163,400	184,500	165,000	166,400
Typical mission TOW [lbs]	140,600	146,200	162,000	146,700	147,300
Wing area [ft ²]	1520	1640	1620	1470	1470
Wing aspect ratio	8.9	19.3	20.2	20.3	20.6
Wing sweep [degrees]	34.0	8.6	8.0	5.8	5.5
Cruise Mach number	0.835	0.573	0.475	0.493	0.469
Initial cruise altitude [ft]	38,600	32,400	30,000	21,500	17,000
Final cruise altitude [ft]	39,800	36,200	31,500	21,500	20,100
SLS thrust [lbs]	23,200	19,600	32,300	20,400	20,600
Engine bypass ratio	8.4	17.9	10.4	17.3	17.0

mation of persistent contrails. This leads to a higher fuel consumption and thus more CO₂ emitted, but the avoidance of contrails is more important. Within the study it is also shown that the major climate reductions are achieved for a 4% increase and all climate reductions are obtained with a 10% increase. While a 10% increase in costs is significant it is interesting to see that a major of the climate impact can be reduced with a small fractional increase in the costs.

The results from Schwartz [9] regarding the aircraft parameters and geometry are supported by the results by Henderson et al. [14] and Proesmans and Vos [15]. For both studies the aircraft tends to fly at a cruise Mach number of approximately 0.6, with a lower cruise altitude as well, when optimized for the climate metric. This being the ATR or the LTO NO_x. This clearly indicates the impact of the design variables, especially mission design variables, on the climate. Note that the results shown in Table 2.1 are for a single aircraft and are not utilized in a route or fleet. For that reason the climate impact is hard to compare, but the design trends are clear.

An expansion on the single mission optimizations are to put the aircraft in a fleet for the future climate impact. Proesmans and Vos [15] use a singular standard mission in a future fleet scenario to measure the climate impact. In the study an additional insight is made that for the change in cruise Mach number the block time between the objectives changes and thus two different scenarios were thought of: a constant fleet size and a constant productivity scenario. The former will result in a change in productivity, while the latter results in difference in fleet size [15]. This is visualized in Figure 2.6, where the left side is the constant fleet size scenario and the right side the constant productivity scenario. Within the figure the change in fleet productivity (bottom left) and the change in fleet size (top right) are clearly seen. The two scenarios assumed are a good first estimate how the aircraft and climate impact change between the objectives and for the future. This is however not the best scenario, as difference in mission length and routes is desired. A route network, similar to Koch [42], would be ideal. The combination of both Proesmans and Vos and Koch would be ideal, as this creates a realistic scenario with great climate impact simulation.

The clear definition of the emission scenario and climate metric in Koch [42], Schwartz [44], Proesmans and Vos [15], and Egelhofer [41] is greatly desired. This results in clear and easy to understand studies.

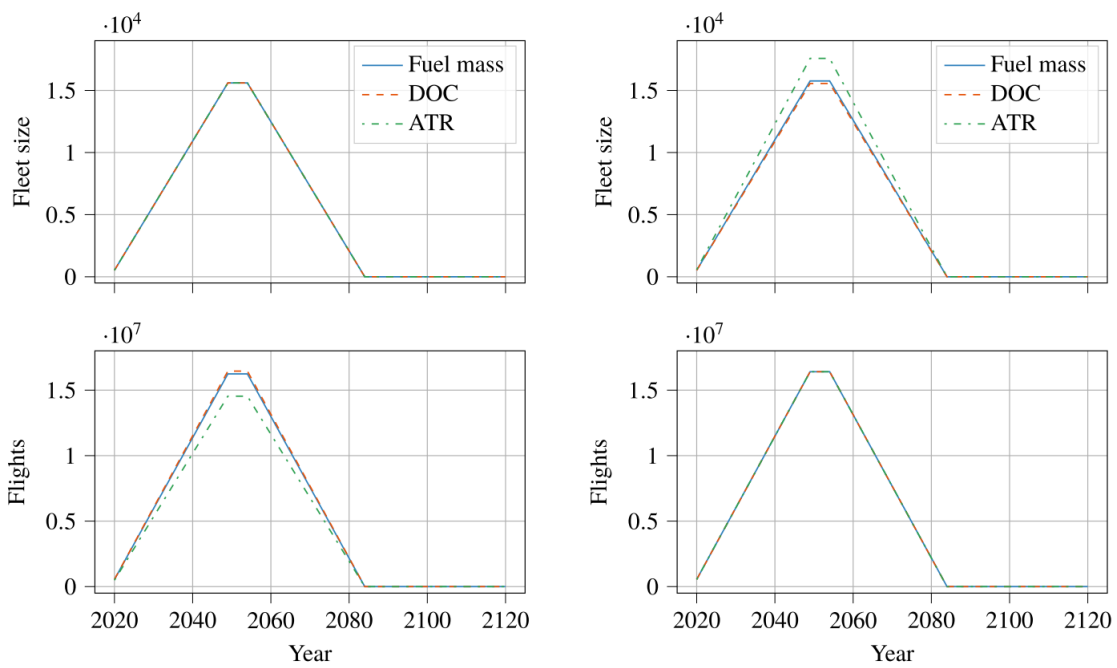


Figure 2.6: Constant fleet scenario (left) and constant productivity (right) scenario visualized, obtained from Proesmans and Vos [15]

3

Optimization & Design Methodology

To shape the optimization problem for the aircraft, it is necessary to clearly define the optimization problem, the objectives, and create a clear overview. The overview gives the flow of the design variables for the aircraft design. This is all discussed in this Chapter.

Within this Chapter, Section 3.1 describes the optimization problem, including the design variables, constraints, and aircraft designed in the optimization. Section 3.2 then shows the extended design structure matrix (XDSM) for the optimization problem

3.1. optimization Problem

When optimizing for an objective it is important to have a clear definition of the objective and the design variables used. Especially for aircraft design, where a lot of design variables and parameters are possible to steer the design. Regarding the objective it chosen for this study to optimize for minimum fuel mass (FM), minimum direct operating costs (DOC) and minimum climate impact. These objectives are identical to that of Proesmans and Vos [15] in order to have a well defined comparison between that study as well.

The fuel mass and DOC objective are straightforward and are often used in aircraft conceptual design studies. The fuel mass is the combination of the mission fuel and the reserve fuel. The DOC objective is quantified in US\$ in the year 2030, while the climate impact is measured in the average temperature response (ATR). The time horizon chosen to be 100 years (ATR₁₀₀). While noise is an important factor for propeller aircraft, it is out of the scope of this study.

The choice of using the ATR as the climate metric is determined with the guidelines from Grewe and Dahlmann [16]. The underlying question of the problem with the guidelines seen in the study helped choose the climate metric. The ATR metric is easy to understand for policymakers and easy to quantify, thus great for a conceptual aircraft study. Other metrics are considered, but deemed unfeasible for this study. The choice of the time horizon of 100 years to take into account the effects of both short-lived and long-lived emissions.

Next to the three objectives mentioned, other were thought of, like minimum block time and minimum maximum takeoff mass (MTOM). Both are valid options, but to keep the study focused these are discarded. Note that the optimization performed is a single-objective and thus per optimization the aircraft design variables are only optimized for one objectively only.

The optimization for the three objectives is executed for both a medium-range design case and a regional design case, since turbofan aircraft dominate the medium-range route, while propeller aircraft are present on the regional routes. The design requirements for both design cases is discussed in Chapter 7, including the emission scenario that the aircraft is subjected to. To guide the aircraft design for the objectives chosen, six design variables are selected. All of these have a direct impact on the designed aircraft and its characteristics in a different way. The list of design variables are shown in Table 3.1.

The six design variables listed can be sub-divided into airframe (A , W/S), engine ($\Pi_{\text{compressor}}$, TIT), and mission (h_{cruise} , M_{cruise}). This choice is based on the premise that these are generally high level aircraft parameters and thus will show enough of a trend in the aircraft design to draw a conclusion from. Additionally, the list is kept fairly short to keep the overview, unlike Henderson et al. [14]. The design variable list in this study is large and the impact of the design variables on the aircraft design is easily lost. The maximum lift coeffi-

Table 3.1: optimization Design Variables, including the initial values and the bounds

Design Variable	Symbol	Variable Type	Lower Bound	Initial Value	Upper Bound
Aspect Ratio [-]	A	Airframe	7	10	17
Wing Loading [kN/m ²]	W/S	Airframe	2000	3.0	7.0
Compressor pressure ratio [-]	$\Pi_{\text{compressor}}$	Engine	5	10	25
Turbine Inlet Temperature [K]	TIT	Engine	1100	1350	1650
Cruise Altitude [km]	h_{cruise}	Mission	3.0	6.0	10.0
Cruise Mach [-]	M_{cruise}	Mission	0.25	0.6	0.8

cient was purposely not chosen to be a design variable, as it tends to go to the upper bound for all objectives in a previous study [15].

Both the aspect ratio and the wing-loading govern the airframe design of the aircraft, especially the wing. The compressor pressure ratio ($\Pi_{\text{compressor}}$) and turbine inlet temperature (TIT) size the internal engine size and performance. Lastly, the cruise altitude and cruise Mach number shape the mission flown by the aircraft for the different objectives set. For each design variables an initial value and bounds have been set. The overview is shown in Table 3.1. The bounds were chosen such that technological advancements are taken into account. Additionally, it is preferred that the design variables are rather limited by the bounds than de constraints set. An example of the bounds is for the compressor pressure ratio. The upper bound is set to 25 as one of the most powerful turboprop uses this ratio ¹and the TIT of 1650 K [45].

3.1.1. Constraints

The constraint applied to the optimization problem, limit certain characteristics and parameters of the aircraft. The inequality constraints are not to be exceeded and guide the aircraft design to adhere to the regulations or restrictions in place.

The constraints regarding the airframe structure are the maximum span, the propeller ground clearance and the propeller fuselage clearance. The maximum span is limited by the airport category. Narrow-body aircraft are often typed for a category C airport and must be able to function at those airports². The maximum span is for that reason set to 36 m. The propeller ground clearance and propeller fuselage clearance is obtained from regulations. These clearances are set to 18 cm and 25 mm respectively [46].

The other constraints are the limitation on the turbine inlet temperature (TIT) at takeoff, the wing loading, and the cruise lift coefficient. The TIT at takeoff is restricted by the engine properties, because the high temperature can damage the internal engine, limiting the TIT during takeoff to 2000 K [45]. The wing loading is restricted by the approach velocity of the aircraft, which depends on the aircraft approach category³. This is dependent on the aircraft itself. For example a medium-range aircraft will have an approach speed of 70 m/s [15]. The maximum cruise lift coefficient is based on the buffet onset of the aircraft ($C_{L,\text{buffet}}$). When the buffet onset lift coefficient is achieved, the aircraft starts unwanted vibrations that could damage the wing and the aircraft. The maximum cruise lift coefficient is purely dependent on the mach number, as it is expected that the aircraft will have little to no sweep. The relation is obtained from polynomial analyses based on data from Vos and Farokhi [47]. The polynomial used to calculate the maximum lift coefficient is given in Equation 3.1. This equation is illustrated in Figure 3.1, for the normal and the maneuver lift coefficient. The latter is used in this study.

$$C_{L,\text{buffet}} = -0.3624M^2 - 1.8905M + 2.0536 \quad (3.1)$$

¹Pressure Ratio data: obtained on 23-11-2021 from <http://www.europrop-int.com/the-tp400-d6/>

²Obtained on 13-10-2021, from https://www.skybrary.aero/index.php/ICAO_Aerodrome_Reference_Code

³ Aircraft Approach Category: Obtained on 2-11-2021 from https://www.skybrary.aero/index.php/Approach_Speed_Categorisation

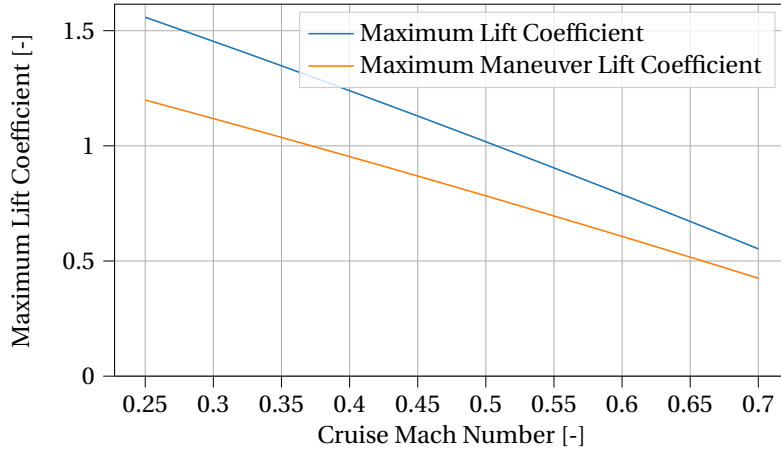


Figure 3.1: Buffet onset lift coefficient with changing mach number for normal and maneuver operation

3.1.2. Aircraft & Engine Configuration

The aircraft employed designed in the optimization is an important factor. The type of aircraft influences the performance and the characteristics during the mission. The mentioned configuration is employed on both the medium-range design case and the regional design case. The configuration is divided into the aircraft configuration and engine configuration

The aircraft configuration chosen is similar to that of the ATR 72. This aircraft has a high-wing configuration and a T-tail. The high-wing placement allows for easier ground clearance with the ground, resulting in an under-wing exhaust. The under-wing exhaust decreases the weight of the wing and engine [48]. The T-tail, with the high-wing configuration, ensures that the horizontal stabilizer is out of the wake of the propeller (propwash) to maximize the effectiveness of the component [23, 49]. For high-wing configuration the landing gear is often stowed in either the nacelle or in the fuselage. For this study the latter is chosen to avoid a long and heavy landing gear.

For the engine it is chosen to have two wing-mounted turboprops to keep the study applicable with current technology. The CROR is an interesting concept that tries to extend the propeller efficiency benefit for propeller aircraft in higher Mach numbers, but the lack of commercial application does not make it favorable for this study. Lastly, wing-mounted engines are chosen, because they outperform tail-mounted engines [28]. Fuselage mounted engines are not chosen, as it is expected to cause too much noise in the cabin.

3.1.3. Overview

The optimization problem for a specific design case with the design variables, bounds and constraints is summarized below:

$$\begin{aligned}
 & \underset{\mathbf{x}}{\text{minimize}} && F(\mathbf{x}) = \text{ATR}_{100}(\mathbf{x}), \text{DOC}(\mathbf{x}) \text{ or } m_{\text{fuel}}(\mathbf{x}) \\
 & \text{Subject to:} && W/S_{TO} \leq \frac{1}{2} \rho \cdot \left(\frac{V_{app}}{1.23} \right)^2 \cdot C_{L,\max} \\
 & && b \leq b_{\max} = 36 \\
 & && TIT_{TO} \leq TIT_{TO,\max} = 2000 \text{ K} \\
 & && C_{L,\text{cruise}} \leq \frac{C_{L,\text{buffet}}}{1.3} \\
 & && D_{\text{prop-fus}} \leq 0.035 \text{ m} \\
 & && D_{\text{prop-ground}} \leq 0.18 \text{ m} \\
 & && \mathbf{x}^L \leq \mathbf{x} \leq \mathbf{x}^U
 \end{aligned}$$

3.2. XDSM Diagram and Approach

The description of the optimization problem given with the design variables, bounds and constraints gives the full picture of the optimization problem. The structure of the optimization is shown with the help of an extended design structure matrix (XDSM), to help see the flow of the multidisciplinary problem. The XDSM diagram is illustrated in Figure 3.2, where the full scope of the optimization structure can be seen. The flow is

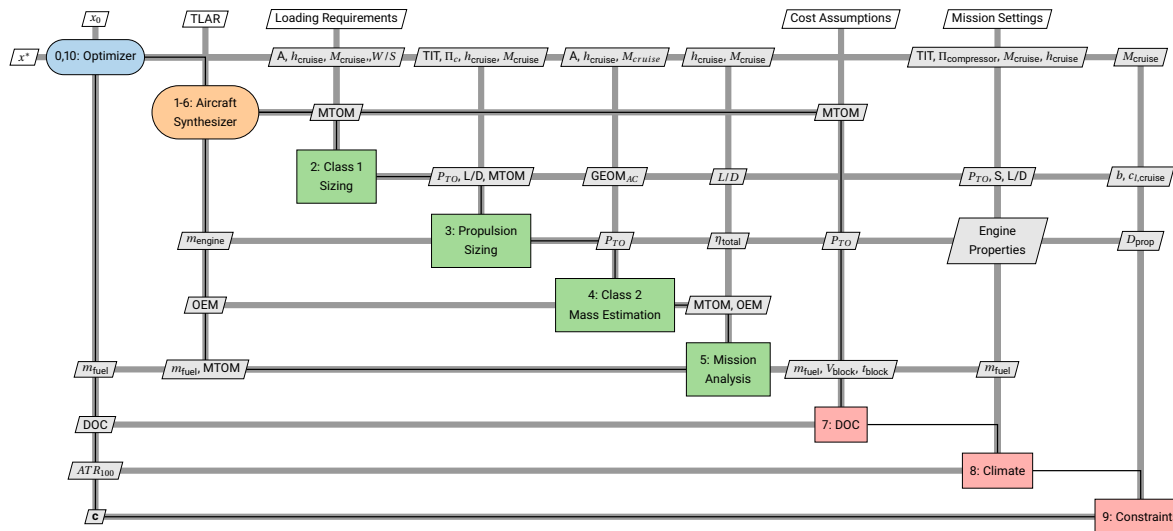


Figure 3.2: Full XDSM Diagram for the optimization, adapted from Proesmans and Vos [15]

of the optimization is given by the number order and the solid black line.

The optimization performed is in a multidisciplinary feasible (MDF) architecture with a Gauss-Seidel analysis. This is a fixed point iteration, which is often employed in a MDF architecture. The MDF architecture indicates that the different function blocks and calculations are performed in sequential order. The optimization does converge slower, but with the relatively slow design loop it is suitable. Another advantage is that for every iteration a feasible design is made, and no infeasible aircraft designs are made for the overall analysis. This is helpful if any problems during the optimization might occur [50].

The XDSM in Figure 3.2, consists of 3 main segments that together comprise the full architecture. The first is the optimizer, which steers the optimization variables in the correct direction to optimize them for the objective function. Secondly, the aircraft design loop, or aircraft synthesizer, designs the aircraft for the given design variables. The aircraft synthesizer consists of multiple functions that are, as mentioned, performed in sequential order to design the aircraft. The last distinct parts are the separate module (pink blocks), which are performed after the aircraft has been design in the aircraft synthesizer. These are the cost estimation, the climate impact estimation and the constraints evaluation. Note that the climate function is not run every loop for the FM and DOC objective, but only at the end.

The next Subsections discuss the aircraft synthesizer modules (green blocks) in more detail. More insight is gained when these are more zoomed in, as the flow of parameters becomes more clear.

3.2.1. Aircraft Sizing Module

The aircraft sizing in this study is important, it helps design the aircraft that will eventually fly the dedicated mission. This module is the largest part of the aircraft synthesizer and helps sizing the characteristics, geometry and aerodynamic properties of the aircraft. Overall the aircraft sizing module consists of three functional blocks, which can be subdivided into 5 blocks. These are the Class 1 weight estimation, the power-loading diagram, the conceptual geometry determination, the aerodynamic update, the class II weight estimation, and the mission analysis. A summary of this is shown in Figure 3.3. Note that the propulsion module is also included, as the class II weight estimation and mission analysis are performed after the propulsion module. The flow of specific parameters is also shown.

Each of the different modules are important to the aircraft sizing and the total aircraft synthesizer. From the figure the flow is clear and helps in understanding the overall approach taken for the aircraft sizing module.

3.2.2. Propulsion Module

Another important part is the propulsion module. The propulsion is an important of this study, as the propeller propulsion type is a major part that sets this study apart. The propulsion module consists of the para-

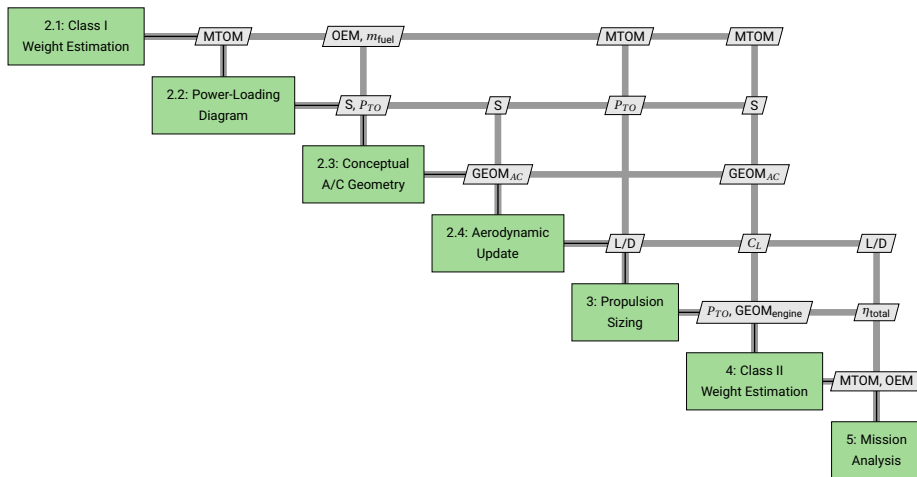


Figure 3.3: Workflow of the aircraft sizing module (step 2, 4, and 5 in Figure 3.2)

metric or on-design point analysis, the performance or off-design point analysis, the engine sizing, and the mass estimation. The zoomed in part of the XDSM diagram is shown in Figure 3.4.

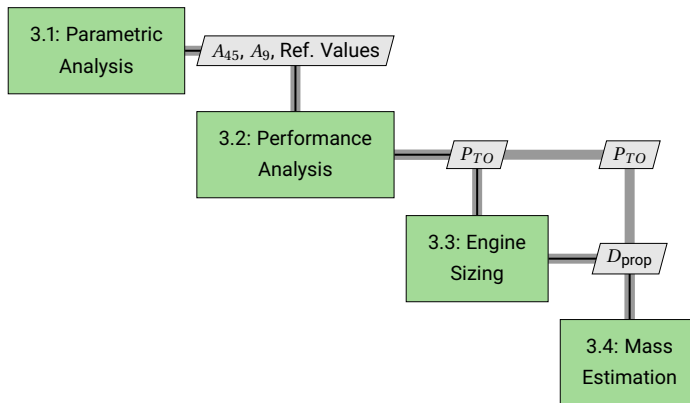


Figure 3.4: Workflow of the propulsion sizing module (step 3 in Figure 3.2)

4

Aircraft Design Methodology

In the previous Chapter the XDSM diagram for the optimization problem is shown. Here the aircraft sizing module, the propulsion module and the cost module are shown. The methods employed within these three different modules are elaborated upon and their inner workings are explained. Subsection 4.1.1 discusses the aircraft sizing module including the class I weight estimation, the class II weight estimation, and the mission analysis. Section 4.2 discusses the propulsion module and finally Section 4.3 discusses the cost estimation employed for the separate cost module.

4.1. Aircraft Sizing Module

The aircraft sizing module designs the aircraft by using the design variables as input. The sizing modules exist of five sub-modules that each help to size and design the aircraft. These are in operational order: the class I weight estimation, the power-loading diagram generation, the conceptual aircraft geometry determination, the aerodynamic update, and the class II weight estimation. Even though the class II weight estimation is performed after the propulsion module it is part of the aircraft sizing module.

4.1.1. Class I Weight Estimation

The purpose of the class I weight estimation is to estimate the main three aircraft masses: the maximum takeoff mass (MTOM), the operative empty mass (OEM) and the fuel mass. Summing the OEM with the fuel mass and payload mass leads to the first estimation of the MTOM of the aircraft. This summation is shown in Equation 4.1. Where the goal is to obtain the fuel mass and OEM as a function of the MTOM.

$$MTOM = OEM + m_{\text{payload}} + m_{\text{fuel}} \quad (4.1)$$

As little is known about the aircraft structure and size, a statistical approach is taken for the first estimation of the OEM. From reference aircraft a database is made from where the MTOM and OEM of the aircraft is listed. These aircraft are all propeller aircraft flying similar missions and categorized based on the number of engines as well. Aircraft that can be thought are the ATR 72 or the DHC Dash-8.

From the statistical MTOM and OEM a linear relationship will be created to get the OEM and a function of MTOM. An example of the relation is shown in Equation 4.2, which is illustrated in Figure 4.1.

$$OEM = 0.563 \cdot MTOM + 1243.14 \quad (4.2)$$

The equation and linear fit shown are not unique. This linear fit will change when aircraft are added or deleted from the database. It is thus dependent on the scale of the database and the approach taken. Statistical relations are also researched in Vouvakos et al. [51], Ibrahim [52], and Marinus and Quodbach [53]. The latter has an extensive number of statistical relations that could be used in conceptual design. Still, it is decided that to use the own database, as it easily expandable in the future.

The fuel mass estimation is also statistical and the well-established weight fraction method is used for the estimation. This method used statistical weight fractions to estimate the fuel consumed during the aircraft missions segments, with the exception of the cruise and loiter segments. For these segments the Breguet

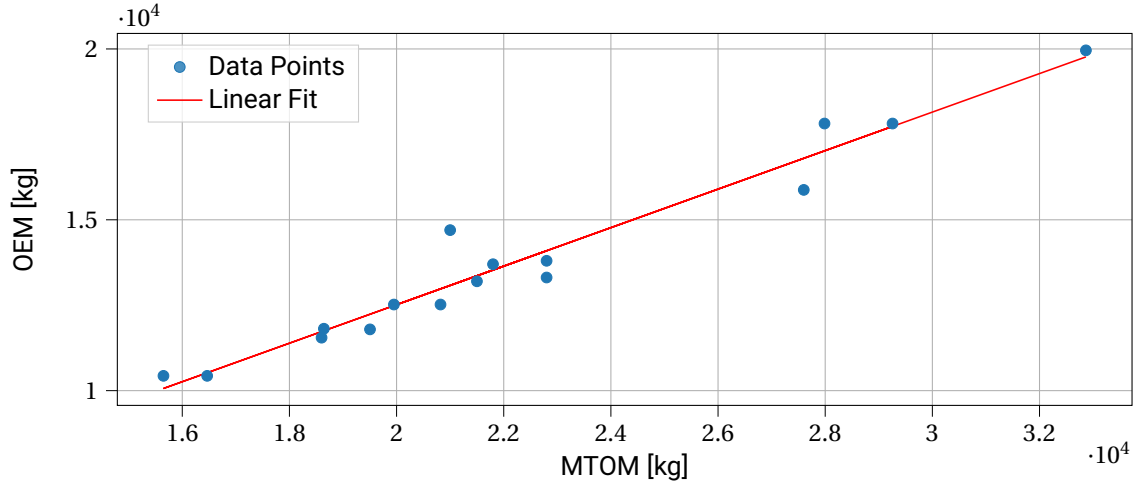


Figure 4.1: Statistical relation between the OEM and MTOM for turboprop aircraft with wing mounted engines

range equation and the Breguet endurance equation are used for propeller aircraft. These are shown in Equation 4.3 and Equation 4.4 respectively.

$$R = \left(\frac{\eta_{\text{prop}}}{g_0 \cdot c_p} \right)_{\text{cruise}} \cdot \left(\frac{C_L}{C_D} \right)_{\text{cruise}} \cdot \ln \left(\frac{W_{\text{begin}}}{W_{\text{end}}} \right) \quad (4.3)$$

$$E = \frac{\eta_{\text{prop}}}{V \cdot g_0 \cdot c_p} \cdot \left(\frac{L}{D} \right) \cdot \ln \left(\frac{W_{\text{begin}}}{W_{\text{end}}} \right) \quad (4.4)$$

In the equations the range (R) and endurance (E) are obtained from the requirements, while fuel fraction ($W_{\text{begin}}/W_{\text{end}}$) is wanted to obtain the fuel mass. The specific fuel consumption (c_p), lift coefficient (C_L), drag coefficient (C_D), propeller efficiency (η_{prop}) are obtained from statistics as this is early in the conceptual design stage.

Using both the estimated fuel mass and OEM the MTOM is calculated, which is used to calculate the OEM and fuel mass as well.

4.1.2. Loading Diagram

The loading diagram, in this case a power-loading diagram, is applied to determine the wing area (S) and the takeoff power (P_{TO}) of the aircraft. Using performance requirements set by either regulations or by the top-level aircraft requirements (TLAR), the wing area and takeoff power are sized accordingly. The use of a power-loading diagram is different from a turbofan powered aircraft as these tend to be sized for thrust, instead of power [23, 48].

The loading diagram is constructed for the different requirements, which either can limit the wing-loading (W/S) or the power-loading (W/P). Then for this study the approach will be taken that the maximum W/P will be chosen for the set wing-loading to minimize the engine size. Many requirements can be set, like the takeoff length, landing length, and the climb rate. This could be come a long list, however to keep it simple the following have been chosen to be implemented as these will most likely be sizing:

- Sizing for approach speed (W/S)
- Sizing for takeoff length (W/P)
- Sizing for cruise performance (W/P)
- Sizing for climb rate in OEI condition (W/P)
- Sizing for climb gradient for approach and takeoff OEI condition (W/P)

The wing-loading or power-loading in brackets indicates what it restricts for the aircraft. Indicating that the only limitation on the wing-loading is the approach speed. For the climb rate and gradient the one engine inoperative (OEI) it is expected that that value is sizing over the normal climb rate and gradient requirements.

An example of a power-loading diagram is illustrated in Figure 4.2. The wing area and takeoff power are then obtained with the estimated MTOM.

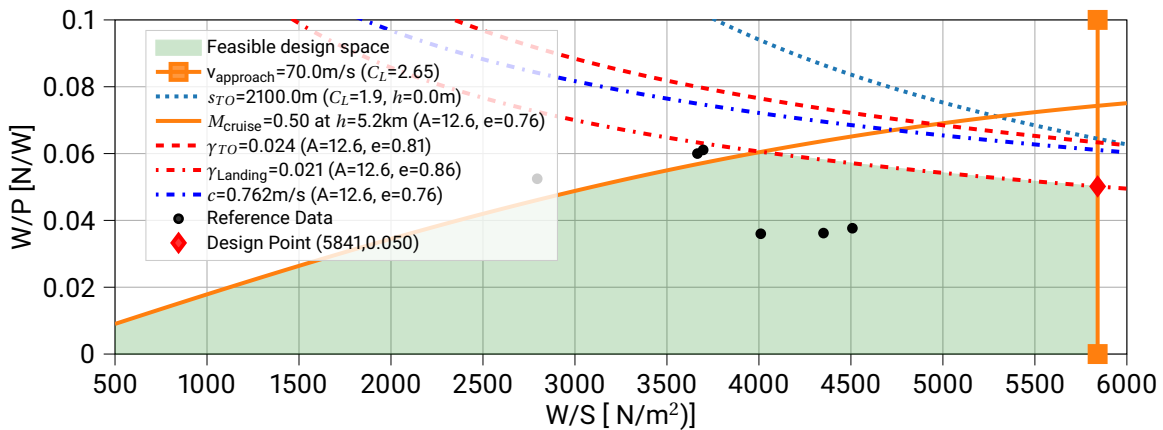


Figure 4.2: Power-loading diagram example including the performance requirements, reference data, and the design point

4.1.3. Geometry Layout Generation

With the wing area and takeoff power determined, a simple conceptual geometry of the aircraft is made. This basic geometry helps to judge the outlook of the aircraft and compare how the optimal designed aircraft differ between the objectives. Additionally, basic aircraft geometry is needed for the class II weight estimation.

The geometry determination is divided into several parts, which are all sized according to different rules and statistical relations. The geometry of the fuselage, wing, and stabilizers are part of this module, while the engine and propeller are sized final in the propulsion module. Still an estimation with the takeoff power obtained from the loading diagram is made, but is updated later. The guidelines and relations obtained are from Torenbeek [48] and Raymer [23]. An example of conceptual aircraft geometry is shown in Figure 4.3, with the quarter chord line, mean aerodynamic chord (MAC) and aerodynamic center (AC) highlighted.

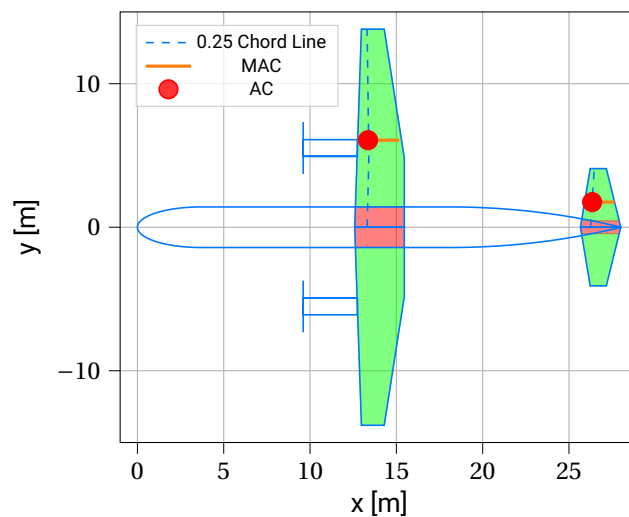


Figure 4.3: Top-view geometry example for the aircraft configuration used

The fuselage geometry is created from assuming constant cockpit length of 4 meters. The cabin length is dependent on the number of passengers and the seat pitch assumed. This is multiplied with a constant factor length to take into account any toiletry and room for the flight attendants. The tail length is obtained from a constant fineness ratio, which relates the tail length to the fuselage diameter.

The wing geometry is determined from the known aspect ratio, with the wing area obtained from the loading diagram. The wing placement however is more intricate, where on the wing the AC is assumed to be

on 25% of the MAC. Then the center of gravity is assumed with the statistical aircraft group weights, and the wing is placed according to stability and control. This approach is summarized in Equation 4.5, where x_{cg} is the x location of the center of gravity of either the wing group (wg) or the fuselage group (fg). Additionally m is the mass and c is the chord.

$$x_{le,mac} = x_{cg,fg} \cdot c_{MAC} \cdot \left(\frac{x_{cg,wg}}{c_{MAC}} \cdot \frac{m_{wg}}{m_{fg}} - 0.25 \cdot \left(1 + \frac{m_{wg}}{m_{fg}} \right) \right) \quad (4.5)$$

Lastly, the horizontal and vertical tail size are obtained with a constant volume approach. Ideally, a scissor or x-plot is made, but this causes more uncertainties at the conceptual design level. The placement of the horizontal tail is assumed on a fixed location on the fuselage length. The stabilizer area is calculated by applying Equation 4.6. The same equation is applied for the vertical tail, but the span of the wing is used rather than the MAC. The constant tail volume of the horizontal and vertical tail are 1.14 and 0.085 respectively. The vertical tail volume coefficient is smaller than that for a low-wing configuration due end-plate effect [23].

$$S_h = S_{wing} \cdot V_h \cdot \frac{c_{wing,MAC}}{l_{h,arm}} \quad (4.6)$$

4.1.4. Aerodynamic Update

The conceptual geometry determined for the aircraft is in this part used to update the aerodynamic values that were previously assumed from statistics. For aerodynamic update the estimation from Obert [54] are employed to update the drag coefficient (C_D) and the Oswald efficiency factor (e). The latter is calculated with Equation 4.8. For the drag polar a quadratic relation is assumed as shown in Equation 4.7, where the zero-lift drag coefficient ($C_{D,0}$) is unknown.

$$C_D = C_{D,0} + \frac{C_L^2}{\pi \cdot A \cdot e} \quad (4.7)$$

$$e = \frac{1}{1.05 + 0.007 \cdot \pi \cdot A} \quad (4.8)$$

To estimate the zero-lift drag coefficient of the whole aircraft, the aircraft itself is divided into multiple elements. Each element is taken as its own entity to calculate that elements zero-lift drag coefficient and are summed add the end.

First, for each element the flat plate skin friction coefficient is estimated using statistical data for the corresponding Reynolds number, assuming turbulent flow. This skin friction coefficient is used in Equation 4.9 to take any compressibility factors into account, due to the effect of the Mach number on the skin friction coefficient [54].

$$c_{f,compress} = c_{f,flat} * (1 - 0.12 \cdot M^2) \quad (4.9)$$

Secondly, the calculated skin friction coefficient is multiplied with the shape factor (λ). The shape takes the shape, or geometry, of an aircraft element into account and differs for each element type the aircraft is divided in. Examples are the body type element or the wing type element. The shape factors for body type element and the wing type element are given in Equation 4.10 and Equation 4.11.

$$\lambda_{body} = 1 + 1.5 \cdot \left(\frac{D_{max}}{l} \right)^{1.5} + 7 \cdot \left(\frac{D}{l} \right)^3 \quad (4.10)$$

$$\lambda_{wing} = 1 + 2 \cdot \frac{(t/c)}{\sqrt{1-M^2}} + 100 \left(\frac{(t/c)}{\sqrt{1-M^2}} \right)^4 \quad (4.11)$$

Here the effects of the shape of the element, being body or wing type, are clearly shown. For example, the body type element changes with maximum diameter (D_{max}), while the wing type element changes with thickness to chord ratio (t/c). The stabilizers are both of the wing type, while the nacelle is of the body type.

The second to last step is to combine the shape factor with the compressibility skin friction coefficient and multiply that with the reference area, as explained by Obert [54]. These are all summed and results in the zero-lift drag coefficient for each aircraft element, which is shown in Equation 4.12. Where the subscript e is the element and subscript n is the number of elements. The last step is to add the excrescence drag coefficient, accounts for all deviations from a smooth surface. In other words the drag, due to the roughness or protrusions over the aircraft skin, is added. The aircraft size independent excrescence drag coefficient is

1.5% of the minimum profile drag, while aircraft dependent excrescence drag coefficient is taken to be 0.0035 of the reference wetted area [15, 54].

$$C_{D_0} = \sum_e^n (C_{D,f_e} \cdot \lambda_e \cdot \left(\frac{S_{wet}}{S_{ref}}\right)_e) + C_{D,E_I} + C_{D,E_{II}} \cdot \frac{S_{wet}}{S_{ref}} \quad (4.12)$$

4.1.5. Class II Weight Estimation

The aircraft geometry created is used to update the OEM of the aircraft. While the class I weight estimation estimated the MTOM, OEM and fuel mass, the class II weight estimation only estimated the OEM, but with more detail, by accounting for the aircraft size and design choices. The class II weight estimation gives more insight into the weight distribution between aircraft groups and thus the OEM weight breakdown. The new calculated OEM can then be used to update the MTOM of the aircraft.

In order to update the OEM, the aircraft is subdivided into groups, where the mass for each group is estimated. These groups are the fuselage group, the empennage group, the undercarriage group and the propulsion group. Equations for these groups are obtained and documented in Raymer [23], Torenbeek [48] and Roskam Part V [55]. The focus of this Subsection are the specific changes needed to incorporate the propeller aircraft and both the wing and tail configuration. The mass for the propulsion group is explained in Subsection 4.2.4, with the exception of the nacelle weight.

Fuselage and Undercarriage Mass

The fuselage weight is calculated with the approach taken from Torenbeek [48], where the full methodology is explained. The general changes needed are for the different chosen high-wing configuration. This choice adds weight fuselage-wing connection and the landing gear.

The fuselage-wing connection for a low-wing configuration is often a continuous torque box that goes through the lower part of the fuselage. A high-wing configuration also has a continuous torque box, but a weight penalty of two-thirds of a low-wing configuration is added [48]. The equation with the extra weight penalty is given in Equation 4.13.

$$W_{fus-wing, connec} = \frac{5}{2} (20.4 + 0.907 \cdot 10^{-3} \cdot n_{ult} \cdot MTOM) \quad (4.13)$$

As the landing gear is stowed in the fuselage rather than in the wing, an belly fairing is added that facilitates the stowage. A choice similar to that of the ATR 72. The need for a belly fairing adds 7% of the original fuselage weight [48]. The addition of the belly fairing adds extra wetted area for the aircraft, but this is not accounted for in the zero-lift drag coefficient estimation that is discussed in Subsection 4.1.4

Nacelle Mass

A turboprop engine has a different nacelle size, than the currently integrated turbofan nacelle size estimation, as mentioned in Subsection 4.2.4. The nacelle weight depends on the design choices made for the aircraft and the propulsion system. As the landing gear is stowed in the fuselage the nacelle weight does not have to increase. Additionally, the option for an over-wing exhaust could potentially add weight to the nacelle [48]. This type of exhaust is often seen for turboprop aircraft with a low-wing configuration. Applying Equation 4.14 determines the nacelle weight around the turboprop engine.

$$W_{nacelle} = (0.0635 + k_1 + k_2) \cdot P_{TO} \quad (4.14)$$

Where k_1 and k_2 are for landing gear stowage in the nacelle and for an over-wing exhaust applied respectively. These are set to zero for this study, but are 0.018 and 0.05 respectively if applicable.

4.1.6. Mission Analysis

The last main part of the aircraft sizing module is the mission analysis. Where the class II weight estimation updates the OEM of the aircraft, this function block updates the mission fuel mass, including the reserve mission fuel. The fuel mass estimation made in Subsection 4.1.1 is highly statistical, as the fuel fractions are used. The method used here is an improvement on the fuel fractions, however it is still a method best used for the conceptual design. The method used is the Lost-Range method as described by Torenbeek [56]. This method is great for the early design stages, as no long numerical mission analysis is needed. An overview of the conceptual mission flown and assumed is illustrated in Table 4.4 with the mission numbering given in Table 4.1.

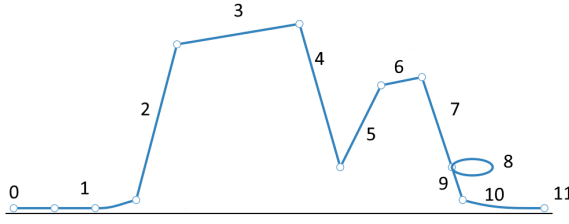


Figure 4.4: Normal and reserve aircraft mission, adapted from Proesmans and Vos [15]

Table 4.1: Mission segments numbering

Number	Part	Number	Part
0	Start-up & Taxi	6	Cruise 2
1	Takeoff	7	Descent 2
2	Climb	8	Loiter
3	Cruise 1	9	Descent 3
4	Descent 1	10	Landing
5	Climb 2	11	Taxi & Shutdown

The equations employed for this method hold for different propulsion types and is thus applicable for jet, turbofan and propeller powered aircraft, as long as the internal engine is a gas turbine. Based on the Breguet range equation, this method makes use of the non-dimensional range parameter (P_r), which is an indication of the cruise performance of the aircraft. Additionally, the energy height is used, which is a measure of the geopotential and geometric altitude that can be obtained if all kinetic energy is traded for potential energy [57]. The definition of the range parameter and equivalent energy height are given in Equation 4.15 and Equation 4.16 [56].

$$P_r = \eta_{\text{total}} \cdot \frac{L}{D} \quad (4.15)$$

$$h = h + \frac{V^2}{2 \cdot g_0} \quad (4.16)$$

The introduced range parameter and equivalent energy height are then used to obtain the mission fuel mass as a fraction of the MTOM. The mission fuel mass estimated is divided into three main parts: the cruise or nominal mission fuel, the mission fuel for the takeoff and climb segments, and the mission fuel for the for possible maneuvers during the flight. These three parts are easily distinguished in Equation 4.17 [15, 56]. Note that the 0.7 for the second part is the assumed total engine efficiency during the climb and takeoff segment.

$$\frac{m_{\text{fuel,mission}}}{\text{MTOM}} = \frac{R_{\text{mission}}/R_H}{P + 0.5 \cdot R_{\text{mission}} \cdot R_H} + \frac{h_{e,\text{cruise}}}{0.7 \cdot \eta_{\text{total,cruise}} \cdot R_H} + \frac{0.0025}{\eta_{\text{total,cruise}}} \quad (4.17)$$

Equation 4.17 is easy to implement in the optimization and gives accurate results for the conceptual design phase. The reserve mission fuel needed for the loiter and diversion are obtained from the same method and shown Equation 4.18 and Equation 4.19 respectively. Note that reserve mission fuel are given as a fraction of the nominal mission fuel.

$$\frac{\Delta m_{\text{fuel,diversion}}}{m_{\text{fuel,mission}}} = 1.2 \cdot \frac{R_{\text{diversion}}}{R_{\text{mission}}} \quad (4.18)$$

$$\frac{\Delta m_{\text{fuel,hold}}}{m_{\text{fuel,mission}}} = 0.2 \cdot t_{\text{hold}} \cdot \frac{R_H}{R_{\text{mission}}} \cdot \left(1 - \frac{m_{\text{fuel,mission}}}{\text{MTOM}}\right) \quad (4.19)$$

In the aircraft synthesizer, the mission is flown according the conceptual method explained above. For the climate impact analysis the nominal mission is flown numerically. The nominal missions consists of the takeoff, climb, cruise, descent, and landing segments, or number 1 to 4 and 10 in Table 4.1. The approach taken for the numerical mission analysis and the segments itself is discussed in Section 5.2.

4.2. Propulsion Module

The propulsion module is an important part of the aircraft synthesizer as it directly affects the aircraft performance, design and geometry. This section focuses on explaining the internal engine architecture, the thermodynamic analysis, the size estimation, the mass estimation of the engine. These are discussed sequentially in Subsection 4.2.1 to 4.2.3.

4.2.1. Internal Engine Architecture

The internal layout, also called architecture, of the engine determines the performance and thermodynamic cycle of the engine. Different layouts are possible and have different characteristics and advantages. The

internal engine itself is for a turboprop a gas turbine, where one of the turbines drives the gearbox and thus indirectly the propeller. The turbine driving the gearbox is often a free power turbine, as it is only linked to the propeller or gearbox and not a compressor. The internal layout chosen for this study is a 2-spool turboprop with a separate free power turbine, resulting in three spools total. This is similar to the architecture of the PW127, which is used on the ATR 72. The current 3-spool engine however is modeled as a 2-spool engine for a simple reason. The high pressure turbine (HPC) only drives high pressure turbine (HPT), the same is true for the low pressure components. There is no extra inlet fan and thus the high and low spool components can be modeled as one spool for both with the extra free power turbine. The modeled 2-spool engine is illustrated in Table 4.5 with the station numbering shown in Table 4.2 [45, 58, 59].

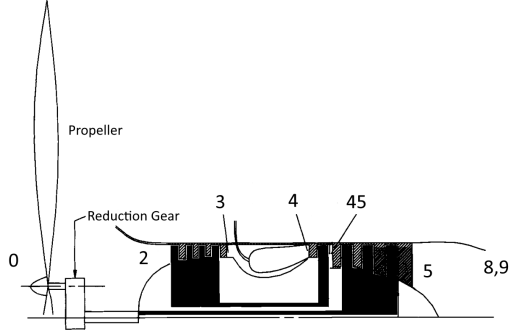


Figure 4.5: Turboprop engine architecture, adapted from Mattingly et al. [45]

Table 4.2: Engine station numberings [45]

Station Number	Location
0	Free stream
2	Compressor entry
3	Compressor exit
4	Combustor exit
45	HPT entry
5	LPT exit
8	Core exhaust entry
9	Core exhaust exit

The station numbering shows are according to Mattingly et al. [45]. The station numbers used for cooling flow and power off-take are omitted in both the figure and the table, because both are assumed zero in this study. The positioning of the free power turbine causes it to be denoted as the low pressure turbine (LPT) in this architecture. The numbering is used for both the on-design point and off-design point analysis.

4.2.2. Propulsion Design Analysis

It was stated for the loading diagram that turbofan aircraft are often sized for thrust, while the propeller aircraft are sized for power. This applies to the current engine analysis as well. Before discussing the on-design point and off-design point methodology of the engine it is necessary to introduce the work interaction coefficient (C). The work interaction coefficient is defined as the ratio between the total power interaction with the vehicle divided and core the mass flow, which is again divided by the free stream static enthalpy (h_0). As both the core and propeller produce thrust, the work interaction coefficient is split into a propeller component (C_{prop}) and a core (C_{core}). The combination of both gives the total work interaction coefficient (C_{total}). The definitions for the three work interaction coefficients are shown in Equation 4.20, 4.21, and 4.22.

$$C_{\text{prop}} = \frac{P_{\text{prop}} \cdot \eta_{\text{prop}}}{\dot{m}_0 \cdot h_0} = \frac{F_{\text{prop}} \cdot V_0}{\dot{m}_0 \cdot h_0} \quad (4.20)$$

$$C_{\text{core}} = \frac{F_{\text{core}} \cdot V_0}{\dot{m}_0 \cdot h_{s,0}} \quad (4.21)$$

$$C_{\text{total}} = C_{\text{prop}} + C_{\text{core}} \quad (4.22)$$

The work interaction coefficient is the fundamental parameter for both the on-design and off-design performance of the engine. These are called the parametric and performance analysis respectively. The parametric analysis forms the basis of the engine and sizes the internal geometry. The performance analysis uses the sized engine and calculates the off-design performance of the engine. The methods employed for both the parametric analysis and performance analysis are obtained from Mattingly [60] and Mattingly et al. [45]. Note that during both the parametric and performance analysis the variable specific heat model by Walsh and Fletcher is used [61].

Parametric analysis

The thermodynamic cycle for the parametric analysis does not differ much from a normal gas turbine cycle calculation. The added propeller does add different steps and minor differences that need to be accounted.

The design point chosen for the parametric analysis is cruise phase of the mission. The variables impacting the performance of the engine are directly or indirectly incorporated in the design variables. The cruise Mach number and cruise altitude dictate the atmospheric conditions, while the TIT and compressor pressure dictate the internal engine. The option for the total turbine enthalpy ratio as a design variable is also an option, however the use in an optimization study is undesirable.

Up until the HPT the parametric analysis is similar to that of any gas turbine with no inlet fan present. The cruise altitude dictates the static pressure and temperature before the inlet, which directly influences the pressure and temperature after the combustor. Using the pressure ratios for the compressor inlet and combustor, which are all known, the total pressure at the HPT entry is obtained ($p_{t,4}$). Equation 4.23 shows the equation. Note that no losses between the engine stages are assumed unless stated otherwise Π indicates the pressure ratio of specific engine component.

$$p_{t,4} = p_{t,0} \cdot \Pi_{\text{inlet}} \cdot \Pi_{\text{compressor}} \cdot \Pi_{\text{combustor}} \quad (4.23)$$

The transition of the static to the total values for the pressure and temperature is performed by employing the TASOPT methods by Drela [62]. This method calculates the total pressure (p_t), total temperature (T_t), and total specific enthalpy (h_t) for a certain for is the change in pressure or total temperature is known.

The amount of fuel injected at the combustor is dependent on the efficiency and the specific total enthalpy before and after the combustor. The fuel-to-air ratio (f_m). Iteration is required, which uses Equation 4.24 to calculate the new fuel-to-air ratio. Then $h_{t,4}$ is updated and the new ratio is again calculated until it converges. The core mass flow is then updated, due to the added fuel.

$$f_m = \frac{h_{t,4} - h_{t,3}}{\eta_{\text{combustor}} \cdot LHV - h_{t,4}} \quad (4.24)$$

The low heating value (LHV) and $\eta_{\text{combustor}}$ are assumed constant and known. The calculation for the specific total enthalpy is done with the TIT and the method from TASOPT by Drela [62]. THE

From the power balance between the HPT and compressor, the HPT enthalpy ratio (τ_{tH}), which is shown in Equation 4.25 [45].

$$\tau_{tH} = 1 - \frac{\tau_{\text{inlet}} \cdot (\tau_{\text{compressor}} - 1)}{\eta_{\text{mech,HPT}} \cdot \tau_{\text{inlet}} \cdot \tau_{\text{compressor}} \cdot (1 + f)} \quad (4.25)$$

Where in Equation 4.25 $\eta_{\text{mech,HPT}}$ is the mechanical efficiency of the HPT and τ is the enthalpy ratio for the specific engine components. This ratio is used to obtain the specific total enthalpy after the HPT, which subsequently leads to the total pressure and total temperature [62].

At the LPT the free power turbine is reached and the analysis takes a different approach. For the analysis the total turbine enthalpy ratio (τ_t) is used. The total turbine enthalpy ratio has a great influence on the downstream conditions and the performance of the engine. In other words, it determines how much power is extracted from the flow in total by the HPT and LPT. Selection of this parameter is not straightforward. Too large and an excessive amount of energy is taken out of the flow and the total pressure ratio at the exit is smaller than one, leading to infeasible exit conditions. Too small and the engine operates at a non-optimal condition. Additionally, the choice is heavily dependent on the TIT and the compressor pressure ratio and thus a constant value is undesirable for the optimization routine [45].

For that reason it is decided that for every combination of the TIT and compressor pressure ratio the optimal total turbine enthalpy ratio is used. For the conditions between the HPT and LPT a small optimization routine is used to determine the optimal value. In other words this maximizes total work interaction coefficient. The routine determines the minimum allowable value of τ_t , based on the given that the outlet total pressure must be bigger than one. The value is then selected that gives the highest total work interaction coefficient. The initial guess for the value is based on the equation provided by Mattingly [60].

With both the total enthalpy ratio and the HPT enthalpy ratio the LPT enthalpy ratio is obtained by applying Equation 4.26. The values downstream are obtained in a similar manner to that of the HPT [45].

$$\tau_{tL} = \frac{\tau_t}{\tau_{tH}} \quad (4.26)$$

With the power extracted by the LPT the last calculation of the parametric analysis is the exhaust. The calculations for the exhaust are dependent on whether the flow is choked or unchoked, which is determined by

the exit Mach number and the total to static pressure ratio. If $M \geq 1.0$ obtained with Equation 4.27 the flow is choked, while if $M < 1.0$ the flow is unchoked [45].

$$M = \sqrt{\frac{2}{\gamma_9 - 1} \cdot \left(\frac{p_{t,9}}{p_{s,0}}\right)^{\frac{\gamma_9 - 1}{\gamma_9}} - 1} \quad (4.27)$$

For unchoked flow the outlet static pressure is equal to the ambient pressure, which is most of the case for turboprop aircraft.

From the outlet conditions the work coefficient of both the propeller and core are obtained. Using the power-balance for the LPT the propeller work interaction coefficient is calculated, the core work interaction coefficient is obtained by the jet thrust and pressure thrust from the core. Both equations within Mattingly et al. [45] for the propeller coefficients and parameters contained mistakes and a separate derivation was performed to obtain Equation 4.28 and Equation 4.29 for the propeller and core respectively. These equations were double checked to ensure their correctness.

$$C_{prop} = (1 + f) \cdot \eta_{gearbox} \cdot \eta_{prop} \cdot (\eta_{mech,LPT} \cdot \tau_{compressor} \cdot \tau_{inlet} \cdot \tau_{tH} \cdot (1 - \tau_{tL})) \quad (4.28)$$

$$C_{core} = \frac{V_0}{h_{s,0}} \cdot \left((1 + f) \cdot V_9 - V_0 + (1 + f) \cdot T_{s,9} \cdot \frac{R_9}{V_9} \cdot \left(1 - \frac{p_{s,0}}{p_{t,9}}\right) \right) \quad (4.29)$$

The work interaction coefficient is summed to get the total value, which is used for the determination of the engine performance parameters. For example the specific power (P/\dot{m}) and specific thrust (F/\dot{m}) are obtained from the definition of the work interaction coefficient.

Other parameters of interest are the thermal efficiency, the propulsive efficiency and the thrust specific fuel consumption (TSFC). Equation 4.30, 4.31, and 4.32 show the equations respectively for all three. The total efficiency is then obtained by multiplying the thermal with the propulsive efficiency. Again, the equations from the parametric analysis routine source were wrong and the equations below have been derived from their definitions.

$$\eta_{thermal} = \frac{C_{total}}{f \cdot LHV} \cdot h_{s,0} \quad (4.30)$$

$$\eta_{propulsive} = \frac{C_{total} \cdot h_{s,0}}{h_{s,0} \cdot \frac{C_{prop}}{\eta_{prop}} + ((1 + f) \cdot V_9^2 - V_0^2)} \quad (4.31)$$

$$TSFC = \frac{f \cdot V_0}{C_{total} \cdot h_{s,0}} \quad (4.32)$$

Performance analysis

The performance analysis is of great importance for this study. It is used to update the takeoff power, which is used to determine the size and mass of the propulsion system. Additionally, this routine is called during the numerically flown mission during the various mission segments.

The performance analysis takes a slightly different approach in comparison to the parametric analysis. Where the compressor pressure ratio is an input for the parametric analysis, this is not the case for the performance analysis. The Mach number, atmospheric conditions, and TIT are still inputs however. The TIT for the off-design is also seen as the engine throttle setting. Regarding the cycle analysis, the main difference is the iterative procedure. In the analysis both the exit Mach number (M_9) and the core air mass flow (\dot{m}_0) are iterated upon [45].

For both turbines a specific subroutine are employed, namely the TURB is used [45]. The subroutine uses the inlet and reference outlet values and iterates upon the latter. This is applied to both the HPT and LPT. The total pressure and total specific enthalpy are then obtained using the methods from TASOPT [62]. This is all due to the iteration of the Mach number and core mass flow. These are assumed known, and thus a slightly backwards approach is necessary. When the Mach number and core air mass flow have converged the work interaction coefficients and the engine characteristics can be calculated using the same equations shown earlier (Equation 4.21-4.32). For the full performance analysis please refer to Mattingly et al. [45].

The implemented performance analysis is numerically unstable for the convergence of the exit Mach number. The final result would not convergence and a numerical stabilizer is added to the performance

analysis. The numerical stabilizer implemented is a simple equation that slows down the convergence rate by making it more gradual. This makes it the analysis numerically stable, but also more computationally heavy. The stabilizer uses both the calculated exit Mach number ($M_{9,\text{calculated}}$) and the exit Mach number from an iteration earlier ($M_{9,\text{prev}}$) to calculate the new value. Linear proportional gains are applied (k_1, k_2), which slow down or fasten up the calculation dependent on their values. The implemented numerical stabilizer is shown in Equation 4.33

$$M_{9,\text{new}} = k_1 \cdot M_{9,\text{calculated}} + k_2 \cdot M_{9,\text{prev}} \quad (4.33)$$

The propeller model incorporated for the performance analysis is purely dependent on the free stream Mach number. A propeller map would ideally be used, but this increases the computational effort greatly [63]. Additionally, the extra accuracy obtained in the already highly uncertain conceptual design is contradictory. This means that the rotations per minute (RPM) and propeller diameter have no influence on the performance of the propeller. The change of the propeller efficiency with the Mach number relation is obtained from Mattingly et al. [45]. This relation however tends to overestimate the propeller efficiency for Mach number up until 0.1, after comparison using the GasTurb program. For that reason a small change is made to the existing model. The model used in the study is shown in Equation 4.34 to 4.37.

$$\eta_{\text{prop}} = 6.5 \cdot M_0 \cdot \eta_{\text{prop,max}} \quad M_0 \leq 0.1 \quad (4.34)$$

$$\eta_{\text{prop}} = 7 \cdot \eta_{\text{prop,max}} \cdot (M_0 - 0.1) + \eta_{\text{prop},M=0.1} \quad 0.1 < M_0 \leq 0.15 \quad (4.35)$$

$$\eta_{\text{prop}} = \eta_{\text{prop,max}} \quad 0.15 < M_0 \leq 0.7 \quad (4.36)$$

$$\eta_{\text{prop}} = \left(1 - \frac{M_0 - 0.7}{3}\right) \cdot \eta_{\text{prop,max}} \quad 0.7 < M_0 \leq 0.85 \quad (4.37)$$

The value for the maximum propeller efficiency ($\eta_{\text{prop,max}}$) is taken as 88% or 0.88. This is above the current estimates, which are between 80-85%. The 88% thus takes into account technological advancements made for propeller efficiency in the future [23, 64].

In the normal aircraft synthesizer design loop the performance analysis is used to determine the takeoff power more accurately and determine the TIT for the set constraint. During the numerically flown mission the performance analysis is used to determine the engine performance parameters.

4.2.3. Engine, Propeller & Nacelle Size Estimation

The size estimation sizes the engine envelope, the nacelle and the propeller diameter. Even though the propeller diameter has no direct influence on the performance, the size gives an indication and determines if the clearance requirements are met.

The first step is to determine the engine size, also called the engine envelope. These are diameter and length of the engine. These are sized based on the takeoff power obtained from the performance analysis. The geometry of the engine is assumed constant, while the size changes with the change in takeoff power. The engine diameter and length are determined with Equation 4.38 and Equation 4.39, where the takeoff power (P_{TO}) is for both engines and N_{engine} is the number of engines [23, 65].

$$D_{\text{engine}} = 0.2 \cdot \left(\frac{P_{TO}}{1000 \cdot N_{\text{engine}}}\right)^{0.18} \quad (4.38)$$

$$l_{\text{engine}} = 0.1 \cdot \left(\frac{P_{TO}}{1000 \cdot N_{\text{engine}}}\right)^{0.4} \quad (4.39)$$

The diameter and length of the engine form the actual size of the engine. As the nacelle needs to be fitted around the engine, a larger engine results in a larger nacelle. This to have sufficient room for a support structure and to encompass the larger engine. The gearbox is allowed for in the engine diameter and thus a smaller width margin is applied. The nacelle size is determined with Equation 4.40 - 4.42 [33, 65].

$$l_{\text{nacelle}} = \frac{3.3}{2.12} l_{\text{engine}} \quad (4.40)$$

$$h_{\text{nacelle}} = 1.5 \cdot D_{\text{engine}} \quad (4.41)$$

$$w_{\text{nacelle}} = 1.1 \cdot D_{\text{engine}} \quad (4.42)$$

The size of the propeller is also determined with the takeoff power. Different bladed propellers often lead to different sizes. The method employed is indifferent for the number of blades, however it best used for high

bladed propellers, e.g. 4 minimum. The original equation is obtained from Raymer [23], but has been adapted for more modern propeller diameters [65]. Equation 4.43 shows the equation employed for the propeller diameter.

$$D_{\text{prop}} = 0.55 \cdot \left(\frac{P_{TO}}{1000 \cdot N_{\text{engine}}} \right)^{1/4} \quad (4.43)$$

4.2.4. Propulsion Mass Estimation

The size of the engine and nacelle have a great influence on the mass, which directly affects the mass of the aircraft. For the mass estimation different methods exist. This study employs the mass subcategories made by Roskam Part V [55], while the methods within that distinction are varied from different sources.

The propulsion mass is divided into three categories: the power-plant mass, the nacelle mass, and the propeller mass. Each category is discussed in order.

Power-plant Mass

The power-plant mass is everything that is included with the engine, with the exception of the propeller mass and nacelle mass. The propeller could potentially be seen as power-plant mass, but a distinction is made within this study. The power-plant mass itself is for this study subdivided into the engine mass, the fuel system mass and the propulsion system mass. Together the three make up the power-plant mass. This summation is shown in Equation 4.44, where m_{fs} is the fuel system mass and m_{ps} is the propulsion system mass.

$$m_{\text{power-plant}} = m_{\text{engine}} + m_{fs} + m_{ps} \quad (4.44)$$

The engine mass is purely the engine itself that is bought of the shelf and also called the dry engine. Normally this is bought from the manufacturer itself, and the mass of the dry engine is precisely known. Since this study is performed in the conceptual design, a different approach is taken. A simple relation from Roskam Part V [55] could be used, however the relation is outdated. A regression analysis performed by Teeuwen [64] for the PW100 series engine, which the current engine is modeled after, is employed. The regression analysis is only dependent on the takeoff power per engine and is shown in Equation 4.45. More information about the regression analysis is found in Teeuwen [64].

$$m_{\text{engine}} = 10 \cdot P_{TO}^{0.266} \quad (4.45)$$

The fuel system mass fuel injection system and all other fuel related systems in the engine. The Torenbeek method found in Roskam Part V is used and is dependent on the fuel mass and the fuel density. The relation obtained is shown in Equation 4.46. Note that m_{fuel} is in lbs and ρ_{fuel} is in lbs/USgal[48, 55].

$$m_{fs} = 3.2 \cdot \left(\frac{m_{\text{fuel}}}{\rho_{\text{fuel}}} \right)^{0.727} \quad (4.46)$$

The last part is the propulsion system weight mass. This entails the engine control mass (m_{ec}), the engine starting system mass (m_{ess}), the propeller control mass (m_{pc}) and the oil system mass (m_{osc}). The fuel injection mass is of In order Equation 4.47 -4.50 are used to calculate, which all are in imperial units. The length are in ft, while the power is in hp.

$$m_{ec} = 56.84 \cdot \left(\frac{(l_{\text{fuselage}} + b) \cdot N_{\text{engine}}}{100} \right)^{0.514} \quad (4.47)$$

$$m_{\text{ess}} = 12.05 \cdot \frac{m_{\text{engine}}^{1.458}}{1000} \quad (4.48)$$

$$m_{pc} = 0.322 \cdot (N_{\text{blades}}^{0.589}) \cdot \left(\frac{D_{\text{prop}} \cdot P_{TO}}{1000} \right)^{1.178} \quad (4.49)$$

$$m_{osc} = 0.07 \cdot m_{\text{engine}} \quad (4.50)$$

Nacelle Mass

The nacelle mass could be seen as part of the wing weight, but since the nacelle sizing was seen as part of the engine the mass estimation is also part of this module. The method used for the nacelle mass is straightforward. The nacelle weight is based on the takeoff power of the engine, as shown in Equation 4.51. As the engine is also dependent on the takeoff power this is a logical approach. The takeoff power is again in hp [48].

$$m_{nacelle} = c \cdot \frac{P_{TO}}{N_{engine}} \quad (4.51)$$

The simple method is dependent on the constant c . normally c takes the value of 0.0635, but increases with 0.05 when an over-wing exhaust is used and by 0.018 when the landing gear retracts in the nacelle. Other methods for the nacelle mass require reference data, which is not available [33].

Propeller mass

The propeller mass can be a significant percentage of the total propulsion system mass, and an accurate estimation is wanted [64]. For that reason different mass estimation exist for different type of aircraft. The Torenbeek method and Nicolai Method are well established, easy to implement, and require only basic knowledge to estimate the propeller mass [48, 66]. For this study an adapted version of the Torenbeek is used. Teeuwen [64] analyzed modern propellers to update the method in a similar way performed for the engine mass. The updated method shows great compliance, with a standard error of 1.73 %, with verification from more recent propeller masses. The inputs are all known as the amount of propeller blades, the propeller diameter and the takeoff power are used. The relation is shown in Equation 4.52.

$$m_{propeller} = 1.1 \cdot (D_{prop} \cdot P_{TO} \cdot \sqrt{N_{blades}})^{0.52} \quad (4.52)$$

4.3. Direct Operating Cost Estimation

The DOC are an important characteristic of the aircraft. In the current aviation industry it is one of the main drivers of airlines, as the minimizing costs, results in maximum profit. The aircraft with the lowest costs is thus highly wanted and often chosen. Since only the aircraft mission is analyzed, the indirect operating costs (IOC) will not be taken into account. The DOC can be given in different metrics, e.g. \$, \$ per hour or \$/seat-nm. The latter is chosen as this allows a better comparison between different aircraft sizes and ranges [67].

The DOC consists of five different types of costs: the flight costs, the maintenance costs, the depreciation costs, the fee costs and the financing costs. Together they make up the total DOC of the aircraft (Equation 4.53). Each category consists of different type of costs themselves, which are discussed shortly. The cost estimation employed is by Roskam [67] and is an adaptation of the ATA-method developed decades ago [68]. Note that all costs are in US\$ and a in the optimization are extrapolated to the year 2030 with a 2% inflation rate.

$$DOC_{total} = DOC_{flight} + DOC_{maintenance} + DOC_{depreciation} + DOC_{fees} + DOC_{finance} \quad (4.53)$$

4.3.1. Flight Costs

The flight costs are, as the name implies, the costs made from performing the aircraft mission. This includes the costs made from the crew salaries, the fuel & oil costs, and the insurance costs.

The crew costs are dependent on the type of crew members, the amount of crew members and the duration of the flight. The crew for the aircraft is assumed to consist of a pilot, a co-pilot and flight attendants. The number of crew members is aircraft size dependent. For example, one cabin attendant is often used per 35 passengers [69]. Each crew member has a maximum of hourly rate per year of 1000 flight hours and thus extra crew members might be necessary, which leads to extra costs. The salaries are obtained from online databases^{1 2}.

The fuel and oil costs per flight are dependent on how fuel and oil efficient the aircraft is. The fuel price taken in 2.71 US\$ per US gallon, while the oil costs are 73 US\$ per US gallon. Note that these are the current prices and are extrapolated to the year 2030.

The insurance costs depend on the aircraft price itself. The estimation of an aircraft price is not easy and depends on the current market, the aircraft size and utilization of the aircraft. For the medium-range aircraft

¹Pilot and Co-pilot salary obtained from: <https://epicflightacademy.com/airline-pilot-salary/>

²Cabin attendant salary obtained from: <https://www.indeed.com/cmp/American-Airlines/salaries/Flight-Attendant>

Equation 4.54 is used, while Equation 4.55 is used for the regional aircraft [15, 67]. The 2.23 factor in the latter is to go from 1989 US\$ to 2021 US\$

$$P_{AC,2021,medium} = 0.0052 \cdot 10^6 \cdot OEM^{0.927} \quad (4.54)$$

$$P_{AC,2021,regional} = 2.23 \cdot 10^{1.1846+1.2625 \cdot \log_{10}(MTOM)} \quad (4.55)$$

Maintenance Costs

The maintenance costs are comprised of the labor costs and the material costs for both the engine and the airframe. The summation of both the engine maintenance and airframe determines the total maintenance costs. For the airframe labor and material costs, relations and assumptions made obtained from Roskam [67] are employed. The aircraft price previously shown is also needed. The engine maintenance costs require the engine price which is estimated using Equation 4.56.

$$P_{engine,2021} = 3.32 \cdot 2160000 \cdot (0.533 \cdot sf + 0.467) \quad (4.56)$$

Similar for the regional aircraft price the 3.32 is to go from 1980 US\$ to 2021 US\$, while sf is the scaling factor which helps incorporate engine of different sizes for the equation [67]. Combining the maintenance costs for both the engine and airframe results in the total maintenance costs.

Depreciation, Fee, and Financing Costs

The last three types are summarized together, which are the depreciation, fee and financing costs. The depreciation costs assume a linear relation for the airframe, engine, and propeller over a certain period of time. The spare parts included. The depreciation time for the airframe and engine is set to 20 years, while the depreciation time for the propeller is set to 7 years. The propeller for this depreciation is estimated using Equation 4.57. Again the 3.32 is for the inflation between 1980 and 2021 US\$ price.

$$P_{prop,2021} = 3.32 \cdot 10^{(0.7746+1.1432 \cdot \log(P_{TO}))} \quad (4.57)$$

The landing fee and taxes costs are assumed to a certain percentage of the total DOC and vary with MTOM of the aircraft, as stated by Roskam [67]. The financing costs are taken as a constant percentage of the total DOC, and is set to 7%.

5

Aircraft Climate Impact & Mission Modeling

To accurately model the climate impact, a methodology is needed to calculate the emissions and obtain the ATR. This Chapter focuses on the determination of the ATR and the numerically flown mission. The climate impact modeling is discussed in Section 5.1, while the numerical mission modeling is elaborated upon in Section 5.2.

5.1. Aircraft Climate Impact & Emission Modeling

To correctly estimate the ATR, caused by the aircraft emissions, it is important to accurately model the amount emitted for a specific mission. The different type of emissions take different approaches. The radiative forcing of each emission is discussed in Section 2.2.

The estimation of the ATR in this study includes the climate effects of CO₂, NO_x, H₂O, sulfate, and soot. Additionally, the effect caused by the formation of persistent contrails are accounted for. The approach taken for the amount emitted for each species is discussed in Subsection 5.1.1, which is followed by the discussion on the calculation of the ATR in Subsection 5.1.2

5.1.1. Aircraft Emission Modeling

For the calculation of the amount emitted for the different species, the emission index (EI) is used. The EI is the ratio between an emissions species with the amount of fuel consumed. In other words, how much kg is emitted per kg of fuel. The value has thus a direct consequence on the climate and a correct value of the emission index is desired. The definition for the emission index is shown in Equation 5.1.

$$EI = \frac{\dot{m}_i}{\dot{m}_{\text{fuel}}} \quad (5.1)$$

Various approaches to the obtain the emission index exist. For some a constant value approach is highly accurate, while for other a more detailed method is needed. For CO₂, H₂O, and sulfate a constant EI is assumed. Their emission is directly proportional to the amount of fuel consumed and the constant value approach is valid. For the soot aerosol and NO_x a different approach is needed. The EI changes dependent on the internal engine conditions. It is expected that the climate impact of soot is relatively small to that of NO_x, CO₂ and potentially that of the formed persistent contrails and for that reason a constant emission index is employed for soot as well.

For NO_x this approach cannot be taken, because it has potentially a large impact on the ATR. This impact is altitude dependent and has both short-term and long-term effects. The main two methods to calculate the EI of NO_x are the fuel-flow method and the p3-T3 method. The fuel-flow method uses reference data from similar aircraft to link the fuel-flow to the amount NO_x emitted and make an empirical relation between the two [35]. Reference data is not available and thus the p3-T3 method is utilized. This method uses the compressor outlet temperature ($p_{t,3}$) and temperature ($T_{t,3}$) to calculate the emission index of NO_x. The combination of the pressure and temperature simulates the conditions in the combustor. Equation 5.2 shows the relation for an internal gas turbine [9], where H_0 is the specific humidity.

$$EI_{NO_x} = 0.0986 \cdot \left(\frac{p_{t,3}}{101325} \right)^{0.4} \cdot \exp \left(\frac{T_{t,3}}{194.4} - \frac{H_0}{53.2} \right) \quad (5.2)$$

With the emission index the kg of each species is calculated using the fuel flow of the aircraft at that point in time. An overview of all the emission indices for the species is shown in Table 5.1. Note that AIC or contrails are not an emission type or species itself, thus it does not have an EI. Still the effects of AIC are taken into account for the total aircraft climate impact.

Table 5.1: Overview of the EI for the various emitted gasses [15]

Species	EI [kg/kg]
CO ₂	3.16
NO _x	See Equation 5.2
H ₂ O	1.26
SO ₄	$2.0 \cdot 10^{-4}$
Soot Aerosol	$4.0 \cdot 10^{-5}$

5.1.2. Aircraft Climate Impact

As mentioned earlier, the ATR metric is easy to understand for policymakers and has a relatively low uncertainty. The metric is chosen according to the guidelines by Grewe and Dahlmann [16]. The calculation of the ATR, however, is non-trivial and requires several steps to go from the emissions itself to the actual ATR. Equation 5.3 shows the general equation and definition of the ATR, which in other words is the integrated temperature change over time divided by the time horizon (H).

$$ATR_H = \frac{1}{H} \int_0^H \Delta T(t) dt \quad (5.3)$$

The time horizon is set to 100 years to account for both the long-lived and short-lived emissions and their lasting perturbation after the species is emitted.. In other words this the full impact of a species for the time horizon is modeled for the ATR and the temperature change over the upcoming 100 years. As the time horizon is chosen the main goal is to calculate the temperature change (ΔT) that is integrated over time. To obtain the temperature change the different temperature changes for the different emissions are summed to obtain the final ATR value.

To obtain the temperature change at a specific time, due to the emissions of the aircraft, the radiative forcing (RF) is used. The radiative forcing, also seen in Figure 2.4, is calculated for each emission type, including AIC. The obtained radiative forcing for all is normalized to obtain the normalized radiative forcing (RF*). The normalized RF of a species is based on the efficacy (f) of the species and is divided by the RF of CO₂ that is obtained from a doubling in atmospheric CO₂. This is better shown in Equation 5.4 [3].

$$RF_i^* = f_i \cdot \frac{RF_i}{RF_{2 \times CO_2}} \quad (5.4)$$

Where subscript i is for the different emission types (CO₂, H₂O etc.) including AIC and $RF_{2 \times CO_2}$ is the mentioned RF that is obtained from a doubling in atmospheric CO₂. The efficacy in Equation 5.4 is a dimensionless parameter that relates the impact of the different emission types with the impact of CO₂. Logically, the efficacy of CO₂ is equal to one. The efficacies are obtained using known climate effects and inventories of aircraft emissions [36]. The efficacy used in this study is independent of altitude, which are summarized in Table 5.2. Note that the efficacy of NO_x is split into the methane and ozone effects. The usage of normalized RF is regular in climate impact studies, as the value helps relate the impact of certain species to the impact of CO₂, which has a high level of scientific understanding (LOSU) [3, 15].

The obtained normalized RF is subsequently used to calculate the temperature change by applying Equation 5.5, with G_T given in Equation 5.6 [39]. The first equation is the convolution integral, which calculates the temperature change based on the normalized radiative forcing. The second equation is Green's function or response function, which is used to model the temperature response caused by the emissions.

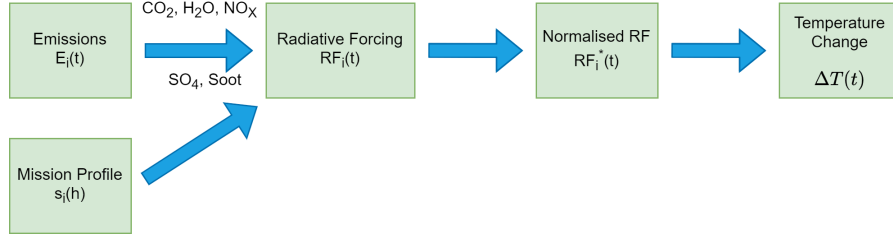


Figure 5.1: Workflow for determining sea-level temperature change, adapted from Dallara Schwartz [44]

$$\Delta T(t) = \int_0^t G_T(t-\tau) \left[\sum_i^{\text{all species}} RF_i^*(\tau) \right] d\tau \quad (5.5)$$

$$G_T = \alpha_T \cdot e^{-t/\tau_T} \quad (5.6)$$

Where in Equation 5.6 α_T and τ_T are both constant parameters and equal to 2.246/36.8 K/year and 36.8 years respectively. In Equation 5.5 the summation of the normalized RF and the impact on the temperature is clearly shown. The summation over all species is indicated. Furthermore, the calculation steps with the RF is summarized in Figure 5.1 [44]. Note that AIC are not shown in this figure, but follow a similar procedure.

The current method assumes a known RF for the different climate effects. The determination of the RF for the climate effects are discussed in the next Subsection. The climate effects discussed are CO₂, NO_x, H₂O, SO₄, Soot and the effects of contrails.

Table 5.2: Efficacy of the different climate impact species [44]

Species	Efficacy [-]
CO ₂	1.0
H ₂ O	1.14
O ₃	1.37
CH ₄	1.18
Soot	0.7
SO ₄	0.9
AIC	0.59

Table 5.3: Coefficients for the impulse response function for CO₂ concentration, used in Equation 5.8 [39]

j	α_j	τ_j
1	0.067	∞
2	0.1135	313.8
3	0.152	79.8
4	0.0970	18.8
5	0.041	1.7

Carbon Dioxide (CO₂)

CO₂ is likely the most well-known greenhouse gas (GHG) and the effects are well understood, resulting in a high LOSU. The gas itself has a long lifetime and can stay in the atmosphere for up to 100 years. The effects from the emitted amount of CO₂ is still noticeable in the far future and for that reason the effects are independent of the altitude it is emitted at [39]. The total amount of CO₂ put into the air by the aircraft is easily calculated and the RF follows from this value.

To determine the RF of the extra emitted CO₂ into the atmosphere the new concentration of atmospheric CO₂ needs to be determined. The change of atmospheric CO₂ ($\Delta\chi_{\text{CO}_2}$) is dependent on the amount emitted by the aircraft. A similar convolution integral and response function to that of the temperature change is adopted (Equation 5.5). The equation, shown in Equation 5.7, uses the amount emitted (E_{CO_2}) and the response function (G_T) given in Equation 5.8.

$$\Delta\chi_{\text{CO}_2} = \int_{t_0}^t G_{\text{CO}_2}(t-\tau) \cdot E_{\text{CO}_2}(\tau) d\tau \quad (5.7)$$

$$G_{\text{CO}_2} = \sum_{j=1}^5 \alpha_j \cdot e^{-t/\tau_j} \quad (5.8)$$

The response function represents the decay of RF caused by a pulse emission of CO₂ in W/m² per kg of CO₂ [9]. The values for α_j and τ_j for the response function are given in Table 5.3.

With the change in atmospheric CO₂, the new atmospheric CO₂ concentration (χ_{CO_2}) can be obtained by adding the change of concentration obtained. To obtain the normalized RF for CO₂, Equation 5.9 is applied. The background atmospheric CO₂ is assumed to be 380 ppmv [15]. In the equation a d, a doubling of atmospheric CO₂ is thus equal to one, as mentioned earlier.

$$RF^* = \frac{\ln((\chi_{CO_2} + \Delta\chi_{CO_2}) / \chi_{CO_2})}{\ln 2} \quad (5.9)$$

As can be seen in the equation for the normalized RF, well-mixed CO₂ is roughly proportional to the natural logarithm of its concentration. The proportionality chosen approximates the saturation of the atmosphere, as additional CO₂ has a smaller effect on the RF and normalized RF [39].

Nitrogen Oxides (NO_x)

In contrast to CO₂, the effects of NO_x are less straightforward. Three main effects by NO_x on the climate are distinguished: the reduction of methane (CH₄), the formation of short-term ozone (O₃), and the reduction of long-term ozone. Different methods are employed for the three effects and a summation gives the total RF, due to emitted NO_x.

The depletion of methane and the long-term ozone, also shortened as O_{3L}, take the same approach. While for CO₂ the methods by Sausen and Schumann are used, for NO_x a similar approach is employed by Schwartz [44]. The response function, G_k , is used to model the response of both the methane and the long-term ozone reduction caused by a pulse emission of NO_x. Equation 5.10 shows the response function, where the subscript k indicates the response of either for CH₄ or O_{3L} [9].

$$G_k(t) = A_k \cdot e^{-t/\tau_k} \quad (5.10)$$

Within the equation A_k takes the value of $-5.16 \cdot 10^{-13} (W/m^2)/kg_{NO_x}$ and $-1.21 \cdot 10^{-13} (W/m^2)/kg_{NO_x}$ for the response of methane and long-lived ozone respectively. Additionally, the time constant τ_k is set to 12 years [9]. The response function with the values for both methane and long-lived ozone reduction is used in a linear response system to obtain the RF for both effect caused by NO_x. Applying Equation 5.11 results then in the RF for both the methane reduction and the long-term ozone reduction effect [9], with the altitude dependent forcing factor $s_k(h)$ included. Note that Equation 5.11 assumes a steady-state, while in reality a more transient response is true for the methane reduction [70].

$$RF_k(t, h) = s_k(h) \int_{t_0}^t G_k(t - \tau) \cdot E_{NO_x}(\tau) d\tau \quad (5.11)$$

As the effects of NO_x are highly altitude dependent, the forcing factor accounts for that. Generally, the higher altitude the altitude the higher the climate impact ascribed to NO_x [39]. The variation of the forcing factor with altitude is illustrated in Figure 5.2 [36]

Both the methane and and long-term effects are global cooling effects, while the short-term ozone formation is a global warming effect. This is the most prominent effect that generally has the highest absolute radiative forcing, due to the emission of NO_x (Figure 2.4). The RF of the short-term ozone formation, shortened as O_{3s}, takes a simpler approach than the linear response systems seen earlier. Reference data from the intergovernmental panel on climate change (IPCC) on the RF per mission caused by this climate impact is stored. This data normalized with the amount of NO_x emitted for the IPCC reference mission. Equation 5.12 shows the equation for determining the RF for the short-term ozone formation for the emission of NO_x [9].

$$RF_{O_{3s}} = s_{O_{3s}}(h) \cdot \left(\frac{RF_{ref}}{E_{ref}} \right)_{NO_x} \cdot E_{O_{3s}}(t) \quad (5.12)$$

Again for this effect an altitude dependent forcing factor is applied. The altitude dependency is different than the methane and long-term ozone reduction and is indicated by the blue color in Figure 5.2. The reference RF over the amount emitted in Equation 5.12 is equal to $1.01 \cdot 10^{-11} (W/m^2)/kg_{NO_x}$.

Summing the three RF for all effects will give the total RF, due to the emitted NO_x.

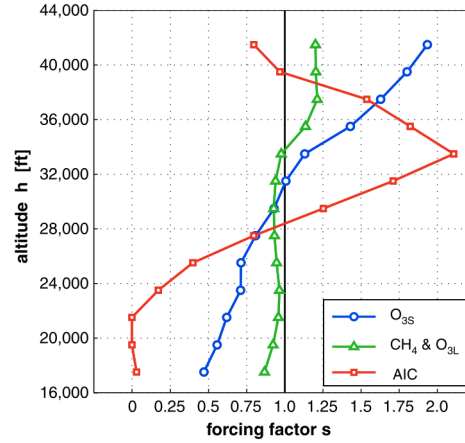


Figure 5.2: The forcing factor for the NO_x climate effects and AIC, obtained from Dallara Swartz et al. [44]

Water Vapor (H₂O), Sulfate (SO₄), and Soot

The effect of these short-lived emissions, as the name indicates, is short-term and for all these emissions a constant EI is set for this study (Table 5.1) [3, 38]. Similar to the short-term ozone formation, reference data is obtained for all three emission types and applied in a similar manner. This leads to Equation 5.13, where i is one of the three short-lived emissions [9, 15].

$$RF_i(t) = \left(\frac{RF_{ref}}{E_{ref}} \right)_i \cdot E_i(t) \quad (5.13)$$

The reference RF over the amount emitted are equal to $7.43 \cdot 10^{-15} \text{ (W/m}^2\text{)/kg}_{\text{H}_2\text{O}}$, $-1.0 \cdot 10^{-10} \text{ (W/m}^2\text{)/kg}_{\text{SO}_4}$, and $5.0 \cdot 10^{-10} \text{ (W/m}^2\text{)/kg}_{\text{soot}}$ for H₂O, SO₄, and soot respectively. There is no forcing factor as the altitude dependency of the effect of these emissions is negligible. Only at supersonic cruise altitudes does the altitude dependency of water vapor become more apparent [2, 71].

Aircraft Induced Clouds

Aircraft induced cloudiness (AIC) or often called contrails are not an emission of its own, but should not be overlooked as their impact can be substantial [72]. Not only is the RF of the contrails important, but the criterion for the formation of the contrails themselves is also of importance, which are both are discussed.

Different types of AIC exist and can form behind the aircraft, caused by the emission of water vapor, e.g. cirrus clouds, non-persistent contrails and persistent contrails. Of these types only persistent contrails have a clear impact on the climate. These types of AIC can span for kilometers and last up to several hours after forming. This is contrary to non-persistent contrails which could only last for minutes [11, 73]. Both types of contrails form when the ambient air is cold enough. In more detail, contrails are formed when the relative humidity is below the saturation pressure over an surface of ice such that the ice particles can evaporate. This evaporation of the ice particles is then seen as contrails in the air [74], which is true for both non-persistent and persistent contrails. The persistent type only forms when the ambient air is supersaturated (more saturation than normally possible) with ice [11, 74].

To model the formation of contrails the Schmidt-Appleman criterion is employed. This criterion checks if contrails are formed and whether these are of the persistent or non-persistent types [75]. The geometrical analysis of the criterion is illustrated in Figure 5.3, with the water saturation pressure and ice saturation pressure in green.

The blue line and the red line within the figure are called the critical mixing line and the mixing line respectively. The critical mixing line determines the threshold for the formation of contrails. If the mixing line is above critical mixing line contrails or cirrus can form, while if it is below no type of AIC are formed. The critical mixing line is tangent to the water saturation pressure and has the same slope as the real mixing line. The slope of both mixing lines are calculated by applying Equation 5.14 [44].

$$G = EI_{\text{H}_2\text{O}} \cdot \frac{c_p \cdot p_{s,0}}{\epsilon \cdot Q \cdot (1 - \eta_{\text{total}})} \quad (5.14)$$

In Equation 5.14, c_p is the specific heat value at constant pressure, $p_{s,0}$ is the ambient static pressure in, ϵ is the ratio of molar masses of water vapor and air, η_{total} it the total engine efficiency, and Q is the specific

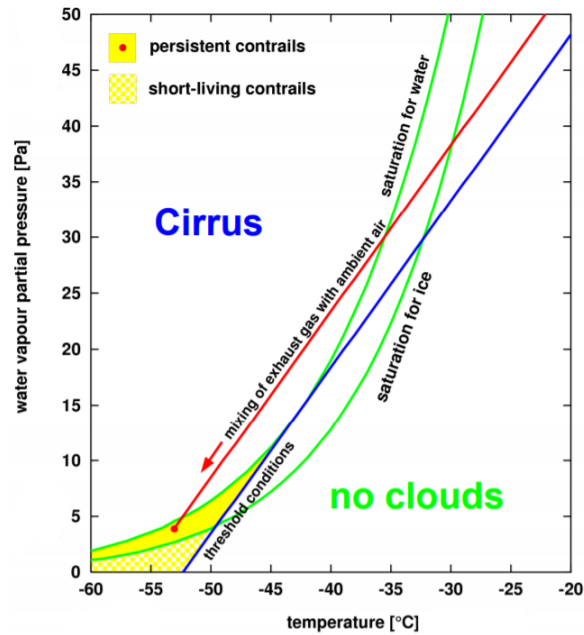


Figure 5.3: Geometrical analysis of contrail, based on the Schmidt-Appleman criterion [76]

combustion heat. From the equations an observation can be made that a higher EI_{H_2O} and a higher total engine efficiency both lead a higher slope and easier contrail formation.

With the slope known the endpoint of the real mixing lines determines the type of AIC that is formed. The real mixing line goes from the engine conditions, which are not seen in Figure 5.3, to the ambient conditions, indicated by the red dot. If the ambient conditions are beneficial for contrail forming, the red dot is either in the dark yellow or light yellow area, which is limited by the critical mixing line. The forming area, between the water saturation pressure line and ice saturation pressure line is where persistent contrails are formed, while below the ice saturation pressure line the non-persistent type is formed [75, 76].

If the engine conditions and atmospheric are beneficial for the formation of persistent contrails, reference data is used to estimate the RF due to the formation of the contrails. The reference RF divided by a certain reference length is used to help calculate the final RF caused by the formation of persistent contrails. This shown in Equation 5.15, with the reference RF over the length shown and is equal to $2.2 \cdot 10^{-12} (W/m^2)/nm$.

$$RF_{AIC}(t, h) = S_{AIC}(h) \cdot \left(\frac{RF_{ref}}{L_{ref}} \right)_{AIC} \cdot L_{pers,contrails} \quad (5.15)$$

Within Equation 5.15, $L_{pers,contrails}$ is the total summed length of the persistent contrails and $S_{AIC}(h)$ is the altitude dependent forcing factor. The change in forcing factor with altitude for the AIC is also illustrated in Figure 5.2. The total length is obtained by checking the Schmidt-Appleman criterion repeatedly during the numerical mission analysis. The current model applied is great simplification of the real RF from the formation of AIC. Ideally, the ambient conditions of difference in geographical location, time of day and season are all taken into account. The current detail is enough for the conceptual design and thus implemented [9, 15, 42].

5.2. Numerical Aircraft Mission Modeling

The knowledge of the different climate effect and models implemented help the determination of the climate impact. The climate impact is, in contrast to the fuel mass, determined by flying the aircraft missions numerically, as mentioned in Subsection 4.1.6. The numerical mission uses mission approaches taken of flight performance books like Ruijgrok [57] or Sadraey [25]. In summary, the mission flows consists of the takeoff, climb, cruise descent and landing segment. The reserve mission is not flown numerically as the frequency of these is approximately 0.15%¹.

¹ Diversion statistics: Obtained on 5-10-2021 from:

<https://www.bustle.com/articles/124628-are-planes-diverted-often-the-air-france-flights-werent-the-only-ones-rerouted>

At the start of the mission a state is made with all necessary parameters and emissions that are for every time-step of the mission. Examples are the velocity, height, and the amount of kg CO₂ emitted. The state is updated each time-step for a specific segment. The propulsion module is then called once every time-step, as little difference is observed between every time-step. For example once every simulated 60 seconds, while the time-step is 5 seconds. The power, total engine efficiency, and TSFC obtained from the engine analysis, determine how the aircraft performs and the emissions. The latter is performed with the emission indices mentioned in Subsection 5.1.1. The emission index for NO_x is also updated at the same time the engine performance is updated. The same is true for the Schmidt-Appleman criterion for the contrail formation. An example flowchart for the cruise segment of the numerical mission analysis is illustrated in Figure 5.4.

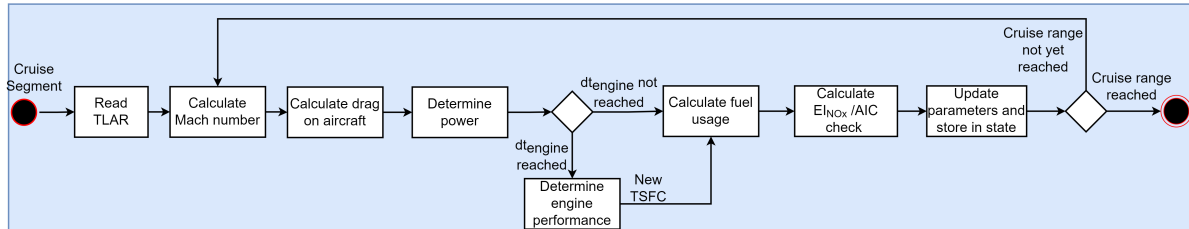


Figure 5.4: Numerical missions analysis workflow for the cruise segment, including the engine analysis time-step (dt_{engine})

Within Figure 5.4 the logical steps can be identified. With reading the TLAR and the previous state, the cruise Mach number is calculated, which determines the power needed. For the first time-step and when the time-step has reached a certain value, named dt_{engine} , the engine performance function is called. This is indicated by the diamond within the figure. Then, as explained, the emissions and data are stored after the calculation of EI_{NO_x} and the contrail check. If the cruise range is reached the descent will start.

The following Subsections discuss the approach taken for each segment in sequential order for the numerical mission.

5.2.1. Takeoff Segment

The takeoff segment serves as the starting point of the mission and has the goal to enough velocity and lift to get the aircraft off the ground to start climbing. The takeoff segment consists of the ground phase the rotation phase and the airborne phase. Each having its own equations of motion (EoM) that are obtained from Ruijgrok [57]. For the takeoff segment all engines are set to full power. This will give maximum acceleration and also the shortest takeoff length. The performance for the engine module however is off for low Mach number ($M < 0.08$) and for that reason the thrust, or static thrust is approximated with the help of the actuator disc theory. The static thrust is approximated with Equation 5.16 [64].

$$F_{static} = P_{TO}^{2/3} \cdot \left(2\rho \cdot \pi \cdot \left(\frac{D_{prop}}{2} \right)^2 \right)^{1/3} \quad (5.16)$$

Once the 35 ft screen height has been reached the takeoff segment transitions to the climb segment. The values for the velocity and more are passed on to that segment.

5.2.2. Climb & Descent Segment

The goal of the climb segment is to reach the cruise altitude with the correct cruise Mach number. So that no acceleration is needed during horizontal flight. The climb approach is that the aircraft climbs at a constant equivalent airspeed (EAS) until the cruise Mach number is reached. From that point the cruise Mach number is maintained until the cruise altitude is reached [57]. Other climb approaches are possible, like the minimum time to climb or the minimum fuel climb. These are rarely used in normal aircraft operation and thus not applicable for this study. For the climate the minimum fuel climb could be of interest, but is not used within this study.

The descent segment takes a similar approach is taken to that of climb. A constant mach number is held during descent until a particular operating speed is reached, after which a constant equivalent airspeed is being maintained until the approach or landing segment [25, 57].

5.2.3. Cruise Segment

The cruise segment is the most straightforward segment. The aircraft flies at the cruise Mach number until the mission range has been and the descent is initiated. The height and Mach number are updated throughout the segment, as the lift and weight are not in equal equilibrium and the aircraft gains height during the cruise phase [25, 57].

5.2.4. Landing Segment

When the aircraft has descended to the screen height of 35ft, the landing segment start. From the screen height the aircraft descends further, rotate, and hit the runway where the velocity will reach zero. During the ground phase a brake force is applied, which is directly proportional to the normal force of the ground on the landing gear of the aircraft. Equation 5.17 shows the equation applied.

$$F_{brake} = \mu_{brake} \cdot N_{aircraft} \quad (5.17)$$

6

Verification & Validation

This chapter discusses the verification performed for the thermodynamic analysis of the engine and the validation of the total aircraft synthesizer. Section 6.1 discusses both the GasTurb and paper verification, while Section 6.2 discusses the aircraft synthesizer validation.

6.1. Propulsion Module Verification

The propulsion module needs to be verified for both the parametric and performance analysis. The parametric analyses is verified using two different sources. One of them is the paper by Ali Dinç [77], the other being a gas turbine program called GasTurb 14. The latter is developed by GasTurb GmbH, which for many engine configurations can calculate the on-design point and the off-design performance. The GasTurb is also used for the performance analysis verification.

6.1.1. Parametric analyses verification

The first step is the parametric analyses verification with the paper by Ali Dinç [77]. In this paper, Dinç analyses a unmanned aerial vehicle (UAV) turboprop for ten different flight conditions, which are all taken as the on-design point. The on-design points are analyzed according to the same methodology as specified in Section 4.2. The same engine layout is also used in this paper and thus great for verification purposes. Additionally, the paper itself is also verified with the GasTurb program. The only downside of this verification is that the paper is unclear with some input parameters, especially the input of the cooling air is ambiguous. Still the paper is used for verification of the parametric analysis.

From the paper three main missions were chosen to discuss in this Subsection. In total all missions simulate the engine condition in various flight segments. From these ten on-design missions, two are shown here. The main input parameters for these are shown in Table 6.1.

Table 6.1: Input parameters for three on-design point missions, obtained from Dinc [77]

Input Parameter	Mission #3	Mission #5
$\Pi_{\text{compressor}}$ [-]	10.37	10.37
TIT [K]	1368.7	1368.7
M_0 [-]	0.568	0.339
$p_{s,0}$ [kPa]	45.56	30.08
$T_{s,0}$ [K]	248.5	248.5
Altitude [km]	6.1	9.1

The basic input parameters obtained from the paper vary between the missions, while some are kept constant. For example the compressor pressure ratio and the turbine inlet temperature are kept constant over all missions. The two missions shown show the comparison between the values from the paper and the program. The missions chosen have no extra implication. The result is shown in Table 6.2.

Table 6.2: Paper and propulsion module parametric analysis comparison [77]

Parameter	Mission #3			Mission #5		
	Parameter Code	Value Paper	Perc Difference	Value Code	Value Paper	Perc Difference
$T_{t,3}$ [10^3 K]	0.58	0.59	-0.01%	0.54	0.54	+0.02%
$T_{t,5}$ [10^3 K]	0.83	0.81	+3.3%	0.83	0.80	+3.9%
$p_{t,3}$ [kPa]	493	492	+0.2%	328	328	+0.2%
$p_{t,5}$ [kPa]	48.6	48.0	+1.2%	31.9	31.0	+2.7%
TSFC [$g/kN \cdot s$]	8.5	8.2	+3.3%	9.5	9.4	+4.0%
F_{total} [kN]	5.0	4.4	+2.5%	3.2	2.8	+1.8%

Looking at the values in the table, it is clear that the values of the parametric analysis of the two missions show great compliance. The absolute values of some parameters do have some difference, e.g. the turbine outlet temperature ($T_{t,5}$) can vary for mission #5 around 30 K. Looking at the percentage difference however, the analysis is accurate with 3.9% difference for $T_{t,5}$. The maximum percentage difference is the 4.0 % for the thrust specific fuel consumption (TSFC) for the same mission. In total the maximum percentage difference, positive or negative, for all missions the percentage difference lie between -2% and +5%, which is deemed acceptable for the conceptual stage this study is performed in. It has to be said that part of the difference can be allocated to the ambiguity of the input values of the paper. Some input values could not be found and had to be estimated, but still affect the final result. Even with the ambiguity the values match well and is used as a verification step in this study. A full list of the input parameters for all ten missions is listed in Appendix A. The full verification for all ten missions, including the percentage differences, is also shown in the appendix.

Because of the ambiguity in the research paper by Dinç [77], it is decided to add an extra step of verification for the parametric analyses. A singular on-design point analysis is performed with the GasTurb program. The design point is taken in a cruise condition with a Mach number of 0.6 and a cruise altitude of 6.0 km, which are similar to the cruise conditions of the DHC Dash 8-400. The other input variables are shown in the second column of Table 6.3.

Table 6.3: Input parameters for the Gasturb parametric and the two performance analysis verification

Input Parameter	On-Design	Off-Design #1	Off-Design #2
$\Pi_{compressor}$ [-]	15	N.A	N.A
M_0 [-]	0.6	0.1	0.3
TIT [K]	1450	1450	1500
Altitude [km]	6.0	0.0	3.0
$p_{s,0}$ [kPa]	47.1	101.3	70.1
$T_{s,0}$ [K]	249	288	269

Putting the input parameters into the parametric analysis results in the values shown in Table 6.4. Here the comparison between the parametric analysis, as explained in Subsection 4.2.2, and the GasTurb program. Overall the absolute values of the percentage differences lie between -0.78% and 2.4% for the TSFC and core thrust respectively. The latter is in absolute only a few newtons of force, which makes a small difference. A full list of the input parameters for the GasTurb parametric analysis is listed in Appendix A.

In contrast to the paper verification, the GasTurb verification has relatively low absolute percentage difference and indicates the correct workings of the parametric analysis. The parametric analysis is with the combination of both the paper and GasTurb program deemed verified.

6.1.2. Performance Analyses

As the parametric analysis is verified, the next step is to verify the performance analysis. For the verification of the off-design performance of the engine, the engine designed using the GasTurb program in the parametric analysis verification is used. In other words the previous mentioned designed engine is used as the on-design

Table 6.4: GasTurb and propulsion module parametric analysis comparison

Parameter	Code Value	GasTurb Value	Percentage Difference
$T_{t,45}$ [$10^3 K$]	1.1	1.1	+0.1%
$T_{t,5}$ [$10^3 K$]	0.81	0.81	+0.14%
$p_{t,45}$ [kPa]	265	265	+0.15%
$p_{t,5}$ [kPa]	54.8	54.2	+1.0%
TSFC [$g/kN \cdot s$]	12.7	12.6	-0.78%
F_{core} [kN]	019	0.19	+2.4%
F_{prop} [kN]	5.7	5.7	-0.88%

point for the current off-design point analysis.

The methods, as explained in Mattingly et al. [45], for the performance analysis are put into two different off-design conditions. One at a smaller Mach number and the same TIT, while the other has lower Mach number and higher TIT. The overview of the input parameters for both off-design analyses are shown in the third and fourth column of Table 6.3. Here the lower Mach number for both missions, the change in TIT and the different altitude becomes clear from the input parameters.

Using the mentioned on-design point to size the engine and the input parameters for both off-design analyses, results in the value comparison in Table 6.5. More parameters are shown due to the importance of the performance analysis.

Table 6.5: GasTurb and propulsion module performance analysis comparison

Parameter	Off-design #1			Off-design #2		
	Value Program	Value GasTurb	Percentage Difference	Value program	Value Gasturb	Perc. Difference
$T_{t,3}$ [$10^3 K$]	0.64	0.640	+0.93%	0.64	0.64	-0.01%
$T_{t,5}$ [$10^3 K$]	0.87	0.86	+1.01%	0.870	0.86	+0.77%
$p_{t,3}$ [kPa]	1320	1320	+0.17%	1130	1130	-0.06%
$p_{t,5}$ [kPa]	110	110	+0.94%	78.9	78.6	0.43%
\dot{m}_0 [kg/s]	4.52	4.51	+0.13%	3.79	3.79	-0.17%
TSFC [$g/kN \cdot s$]	4.14	4.01	+3.2%	7.12	6.9	+2.8%
F_{core} [kN]	0.70	0.68	+2.6%	0.49	0.48	+2.2%
F_{prop} [kN]	25.3	26.7	-2.9%	13.1	13.5	-2.4%

Analyzing the results it overall indicates that the combustor inlet pressure ($p_{t,3}$) and combustor inlet temperature ($T_{t,3}$) are accurately calculated with little percentage difference. The same conclusion is drawn regarding the total pressure and temperature. The compressor pressure ratio is thus closely estimated, which is also true for the core mass flow (\dot{m}_0), which has a less than 1% percentage difference for both off-design cases. This is not true for the TSFC, which shows the biggest percentage difference 3.2% for off-design #1 and 2.8% for off-design #2. The thrust calculation differs around the 2.5% for both analyses. This difference is due to the usage of a propeller map by the GasTurb program, while the current propeller model only accounts for the Mach number. The map is more accurate than the current method employed, however the change is still minimal.

Even with the differences in place for the thrust, FAR and TSFC the comparison does show great compliance with GasTurb. Additionally it has to be taken into account that the propulsion design is still in the conceptual phase and a percentage difference in the order of 5% is normal. Especially in a conceptual design study.

6.2. Aircraft Synthesizer Verification

The propulsion module is a important module to verify and validate, because an accurate model is needed for an accurate climate impact. Additionally the internal engine conditions have direct influence on the fuel use and the climate impact of the aircraft. The engine propels the aircraft forward, it is important to verify the aircraft synthesizer as well. Two different propeller aircraft are chosen in order to validate the size, per-

formance and mass of the aircraft synthesizer. The two aircraft chosen are the ATR 72-600 and the DHC Dash 8-400. These are the most employed turboprop aircraft today and indicate the regional propeller market.

Listing all input parameters is impossible due to the large list of assumptions made for the validating. The main TLAR for the current validation for both aircraft are listed in Table 6.6. This list gives an indication of the main inputs parameters used to design and size the aircraft. Overall the harmonic range and maximum structural payload are similar, while the cruise mach number does varies considerably. The same can be said about the cruise altitude and wing-loading at takeoff. These input parameters are then used to design the aircraft^{1 2}.

Table 6.6: Aircraft synthesizer verification input parameters

Parameter	ATR 72	Dash 8
Harmonic Range [km]	987	955
Maximum Structural Payload [kg]	7500	7800
Cruise mach number [-]	0.44	0.53
Cruise altitude [m]	5180	7620
Takeoff length [m]	1278	1268
Aspect Ratio [-]	12	12.8
W/S_{TO} [N/m ²]	3697	4351

The landing gear placement is also an extra input parameter for both aircraft. The ATR 72 stows the landing gear in the fuselage, while the DHC Dash 8-400 stows the landing gear in the nacelle. The latter causes a larger nacelle and higher landing gear weight. The fuselage weight however is reduced. Using the input parameters results in the value comparison shown in Table 6.7. Here the outputs of the aircraft synthesizer are compared to the real value of the aircraft. The table includes the basic mass estimation and some basic geometrical dimensions of the aircraft. The combination gives a good indication of the correct workings of the aircraft synthesizer and thus for the optimization performed.

Before discussing the results it is important to note that for the DHC Dash 8-400 an extra five meters is added to the fuselage of the aircraft. Analyzing the geometry of the cabin showed approximately five meters of length that is not present in aircraft of similar types. In the airport planning manual [78], a cabin length of 18.8 meters was found, which compared to the ATR 72-600 of only 14.1 meters is considerably larger. With a similar cabin layout and passenger count it was decided to add the five meters to have an accurate fuselage length.

Table 6.7: Aircraft synthesizer validation with the ATR-72 and the DHC Dash 8-400

Parameter	ATR 72 ¹			DHC Dash 8-400 ²		
	Synthesizer	Reference	Percentage Difference	Synthesizer	Reference	Percentage Difference
MTOM [Metric tonnes]	23.6	2.30	+2.6%	27.5	27.6	-0.3%
OEM [Metric tonnes]	13.9	13.3	+4.3%	17.1	17.1	+0.15%
Fuel mass [Metric tonnes]	2.2	2.19	+1.5%	2.6	2.61	-1.3%
Wing Area [m ²]	62.7	61.0	+3.5%	62.1	63.1	-1.5%
Fuselage Length [m]	28.0	27.2	+3.1%	33.4	32.8	+1.6%
Fuselage diameter [m]	2.82	2.9	-2.4%	2.74	2.69	+1.46%

The aircraft synthesizer takes seven iterations for the ATR 72-600 and six for the DHC Dash 8-400, which in total takes approximately one minute in total to develop the full aircraft design. Analyzing the values within Table 6.7 it shows that for the ATR 72 the relative differences lie between -2.4% and +4.3% for the MTOM and the fuselage diameter respectively. For the DHC Dash 8 the differences are smaller and lie between -1.5% and

¹ ATR 72 data: Obtained on 21-09-2021 from <https://customer.janes.com/JAWADevelopmentProduction/Display/JAWA0440-JAWA>

² DHC Dash 8-400 data: Obtained on 21-09-2021 from <https://customer.janes.com/JAWADevelopmentProduction/Display/JAWA0096-JAWA>

+1.6%, for the wing area and fuselage length respectively. Generally speaking for both aircraft the percentage differences lie below the 5% and the results are accurate for the conceptual design phase. The over- and underestimation of the aircraft parameters can be allocated to the conceptual methods that are used in the aircraft synthesizer. For example a constant volume approach is taken for the stabilizer area, while in reality a scissor or x-plot is more accurate in determining the necessary tail area for stability and control.

The last aspect to check is the performance of the aircraft with the help of the payload-range diagram. For this the maximum fuel mass is set to 5000 kg for the ATR 72 and 5390 kg for the Dash 8. Both aircraft are compared to their respective payload-range diagram. Figure 6.1 and Figure 6.2 show the payload-range diagram for the ATR 72 and Dash 8 respectively [78, 79]. The correspondence for both payload-range diagrams is overall satisfactory, with no real major differences found, still there are some minor differences in both payload-range diagrams. Especially the ATR 72 has great compliance up until the point where payload mass is reduced with the maximum fuel mass reached. The gradient after that is underestimated leading to a higher maximum mission range.

The harmonic range for the Dash 8 (Figure 6.2) is well estimated. The gradient is then slightly overestimated resulting in lower mission range with maximum payload and mission fuel. The final mission range with zero payload however is accurate and compensates for the previous underestimation. The over and underestimations of these sections are most likely due to the difference in total engine efficiency and the lift-to-drag ratio when not at maximum payload.

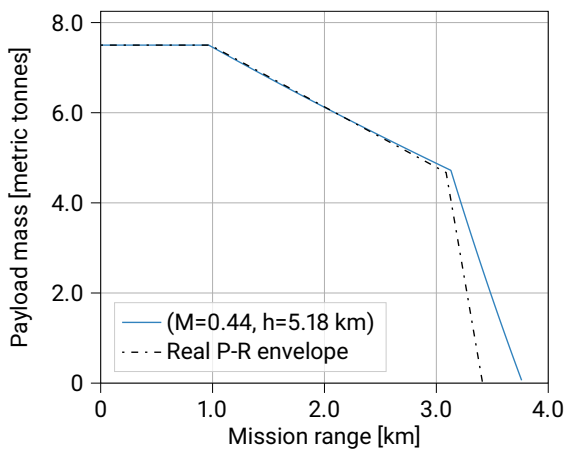


Figure 6.1: Payload-Range diagram comparison for the ATR 72

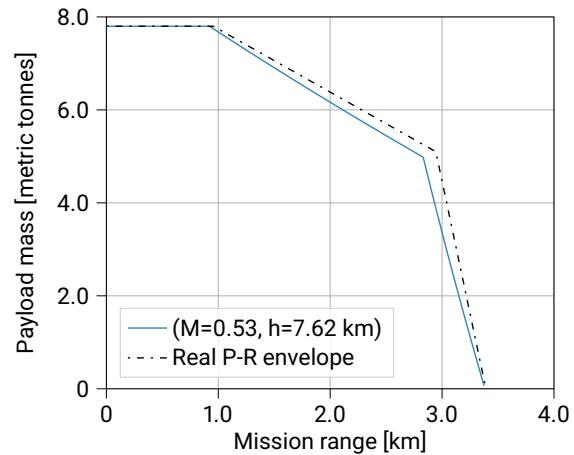


Figure 6.2: Payload-range diagram comparison for the Dash 8

7

Aircraft Design Cases & Emission Scenario

As the design methodology, climate impact and optimization problem are known and identified, the next step is to discuss the specific scenario regarding the aircraft mission and the potential fleet. Section 7.1 discusses the regional and medium-range design cases and the design requirements for each design case, while Section 7.2 elaborates on the two future fleet scenarios, or emission scenario, that are both design cases are subjected to.

7.1. Aircraft Design Cases

As mentioned in Subsection 3.1.2, the aircraft and engine configuration is the same for both the regional and medium-range design case. The regional design case is the design case where the current aircraft type and configuration are often employed. The medium-range is the range where turbofan aircraft are mostly employed, because of their lower block time and lower costs [32, 80]. The medium-range design case thus allows for a direct comparison with the turbofan aircraft. Compared to the medium-range design case the regional design case is characterized by a shorter range and a lower passenger capacity. The design requirements and mission requirement change dependent on the aircraft design case (ADC).

An overview of the design requirements for both ADC is shown in Table 7.1, including the scenario variables, which are discussed in Section 7.2. The top level aircraft requirements (TLAR) for both design cases is shortly discussed in the following Subsections.

7.1.1. Regional Design Case

The regional design case has a harmonic range of 1000 km, a maximum passenger capacity of 78 and a take-off distance requirement of 1200 meters, as shown in Table 7.1. The maximum passenger capacity leads to a maximum structural payload of 7800 kg, cause 100 kg is assumed per passenger. The regional aircraft is assumed have a category B in the International Civil Aviation Organization (ICAO) aircraft approach category¹, where approach speed requirement is set to 57 m/s.

Where the aircraft design requirement help design the total aircraft, the mission design requirement are the requirements specifically for the mission that the designed aircraft flies. These differ for the reason that an aircraft rarely flies with full capacity and its harmonic range. The mission range for this design case is kept equal to the harmonic range, while the passenger capacity is lowered to 68 passengers or a payload of 6800 kg. This is a capacity often flown by regional aircraft [80].

7.1.2. medium-range Design Case

The medium-range design case uses the same configuration, but for a complete new set of design requirements. The requirements for the medium-range design case are equal to that of the turbofan aircraft in the study by Proesmans and Vos [15]. This allows for a direct comparison between aircraft designed for the same design requirements. Logically, the mission design requirements are also equal.

While propeller aircraft tend to have shorter takeoff distances, the takeoff distance is still set equal to the turbofan aircraft. Otherwise the comparison is not equal, due to the more stringent takeoff requirement.

¹ Aircraft Approach Category: Obtained on 2-11-2021 from https://www.skybrary.aero/index.php/Approach_Speed_Categorisation

This could result in a sizing and the higher takeoff requirement might be sizing for the power-loading of the aircraft. The approach speed is set to 70 m/s, because of the approach speed category of the medium-range aircraft (category C) [15]. Lastly, the difference in harmonic range and payload between the design and mission requirements is for the reason that narrow-body aircraft often operate near this payload-range combination [80].

Table 7.1: Aircraft design requirements and both mission- and future fleet scenario variables

Aircraft Design Requirement	Regional Design Case	medium-range Design Case
Passenger capacity [#]	78	180
Maximum structural payload [kg]	7800	18200
Harmonic Range [km]	1000	3200
Approach speed [m/s]	57	70
Takeoff distance (h=0) [m]	1200	2100
Mission Design Requirements	Regional Design Case	medium-range Design Case
Passengers [#]	68	130
Payload [kg]	6800	13000
Mission range [km]	1000	1852
Scenario Variables	Regional Design Case	medium-range Design Case
Yearly utilization [hrs/year]	2665	3900
Productivity ₂₀₅₀₋₂₀₅₅ [RPK]	$1.31 \cdot 10^{11}$	$3.95 \cdot 10^{12}$
Fleet size ₂₀₅₀₋₂₀₅₅ [#]	3020	15600
Aircraft lifetime [years]	35	35

7.2. Future Fleet Scenarios

An important in determining the climate impact of an aircraft is to determine what kind of mission and scenario the aircraft is subjected to after it has been designed. For this study this is done with both design cases, mentioned above. The scenario determines how often the aircraft are utilized and how many are needed in the current scenario. Using the insights of Proesmans and Vos [15], two main future fleet scenarios are investigated. The first scenario is the constant fleet size scenario, which keeps the fleet size for the three objectives (FM, DOC, ATR₁₀₀) constant and changes the number of flights flown. The second scenario keeps the number of flights constant, which results in a change in fleet size to maintain the productivity for all objectives. The changes in either fleet size or productivity is caused by the expected change in block time between the objectives. For both scenarios the maximum fleet size and productivity is achieved in the years 2050-2055. The regional design case and medium-range design case are both subjected to the two future fleet scenarios. The constant fleet size and productivity achieved in the years 2050-2055 are listed under the scenario variables in Table 7.1.

For the constant fleet size scenario, the effect of the change in block time on the missions performed per year is calculated by applying Equation 7.1 [15].

$$N_{\text{flight/year}} = N_{AC, \text{year}_i} \cdot \frac{U_{\text{annual}}}{t_{\text{block}}} \quad (7.1)$$

Where in Equation 7.1, U_{annual} is the constant yearly utilization, N_{AC, year_i} is the fleet size at year i and $N_{\text{flight/year}}$ is the mission flown for that fleet size with the given block time. A lower block time results in more mission performed with the same fleet size

The change in fleet size for the constant productivity is found in a similar manner. The productivity in the year 2050 is taken and with the block time and yearly utilization, the required fleet size in the year 2050 is obtained by using Equation 7.2.

$$N_{AC, 2050} = \frac{\text{Productivity}_{2050}}{N_{\text{passengers/flight}} \cdot R_{\text{block}}} \cdot \frac{t_{\text{block}}}{U_{\text{annual}}} \quad (7.2)$$

In Equation 7.2, $N_{\text{passengers/flight}}$ is the number of passengers per flight, R_{block} is the block range, and $N_{\text{AC},2050}$ is the resulting fleet size in the year 2050. In this equation a larger block time would lead to a higher fleet size, due to the constant yearly utilization.

The yearly utilization, the productivity and the fleet size varies between the regional design case and medium-range design case. The scenario variables for the medium-range design are equal to that of Proesmans and Vos [15]. For the regional design case, the yearly utilization is based on the daily utilization (7.3 hrs) of current turboprop aircraft, which is extrapolated to full year². The productivity in the year 2050 is based on the productivity found on regional routes in China with a 3% growth factor applied for each year, resulting in $1.31 \cdot 10^{11}$ RPK³. The fleet size is obtained from the ATR market forecast [81]. Lastly, an operational aircraft lifetime of 35 years is assumed for both design cases [82].

The overview of the scenario variables for both the regional and medium-range design case, as mentioned, is shown in Table 7.1. Additionally Figure 7.1 shows the different design cases, the scenarios within the design cases and the objectives. This shows that both design cases are subjected to the two scenarios and the objectives are optimised within that scenario.

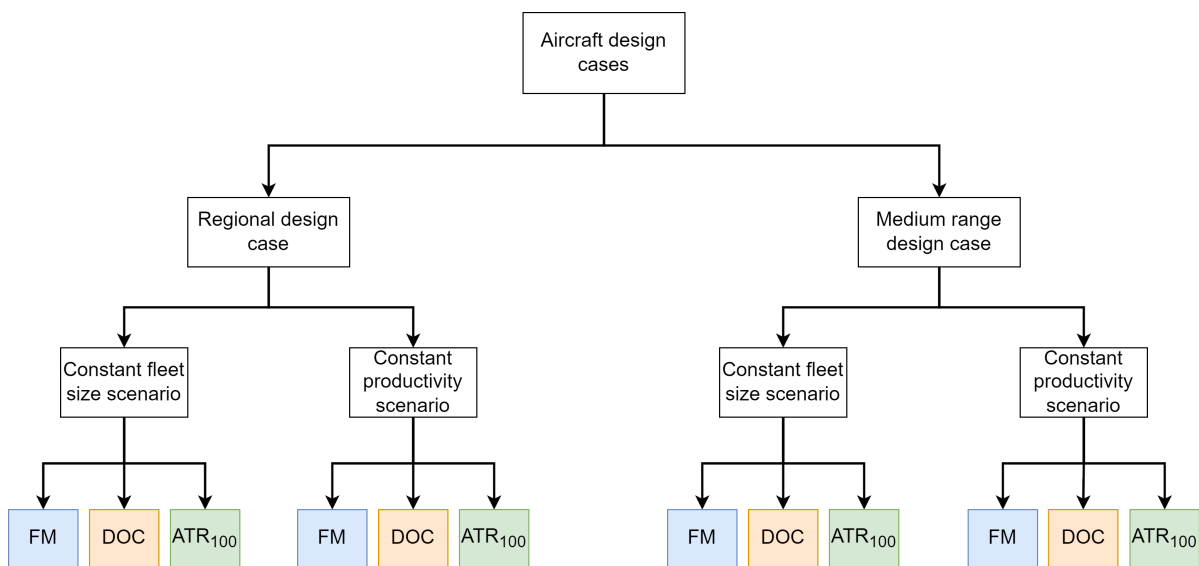


Figure 7.1: Overview of the air craft design cases, objectives and future fleet scenarios

² Daily turboprop utilization: Obtained on 20-10-2021 from https://www.planestats.com/bhsr_2019jun

³RPK data obtained from: Obtained on 1-11-2021 <https://www.ceicdata.com/en/china/air-air-china/air-china-revenue-passenger-kilometre-regional>

8

Aircraft Design Case Results

The results for both design cases and the scenarios they are subjected to are the focus of this Chapter. Throughout the chapter the constant fleet is characterized by solid lines, while the constant productivity scenario is characterized by dashed or dotted line unless specified otherwise. Additionally, throughout the discussion the fuel mass objective is denoted by FM, the cost objective with DOC, and the ATR_{100} objective is denoted by ATR_{100}^* .

The Chapter is separated into three Sections. Section 8.1 and Section 8.2 discuss the results for both design cases respectively. Section 8.3 summarizes the trends found in the scenarios and design cases.

8.1. medium-range Design Case

As shown in Table 7.1, the medium-range design case is characterized by a passenger capacity, range, and approach speed belonging to a narrow-body aircraft. The two different future fleet scenarios are both discussed separately (Section 7.2). The combination of both scenarios for the design case shows the complete picture for the medium-range design case. For the constant productivity scenario a direct comparison with the turbofan aircraft is made.

8.1.1. Constant Fleet Size Scenario

The constant fleet size scenario for the medium-range design case has a fixed fleet of 15600 aircraft between the years 2050-2055. These aircraft perform a certain amount of flights during scenario with the change in block time. Together they shape the utilization and productivity for the three objectives.

Setting the objectives and performing the optimization for the medium-range design case, while assuming a constant fleet size, results in the objective values shown in Table 8.1. From the table it can be concluded that for the different objectives conflicting values are obtained. Each objective, as expected, leads to the minimum value for its respective objective. The differences between them is more interesting. For example, shifting from the ATR_{100}^* objective to the DOC objective results in an 66% increase in ATR_{100} , while the costs are reduced by 24%. The shift from the DOC objective to the FM objective is potentially more realistic than the shift to ATR_{100}^* objective, because the costs are lower.

Table 8.1: Objective function values for the medium-range design case, assuming constant fleet size

Objective	Numerical Value			Relative difference		
	m_{fuel} [kg]	DOC [\$/seat-nm]	ATR_{100} [mK]	m_{fuel}	DOC	ATR_{100}
FM	$4.9 \cdot 10^2$	0.23	5.2	N.A	+21%	+4.6%
DOC	$5.8 \cdot 10^2$	0.19	8.3	+18%	N.A	+66%
ATR_{100}^*	$5.2 \cdot 10^2$	0.25	5.0	+6.1%	+32%	N.A

The reason for the difference in ATR_{100} between the objectives, becomes clearer by plotting the scenario over the set time horizon. Figure 8.1 shows the constant fleet size on the left side (Figure 8.1a) and the number of flights performed on the right side (Figure 8.1b). The fleet size over the next 100 years is logically constant

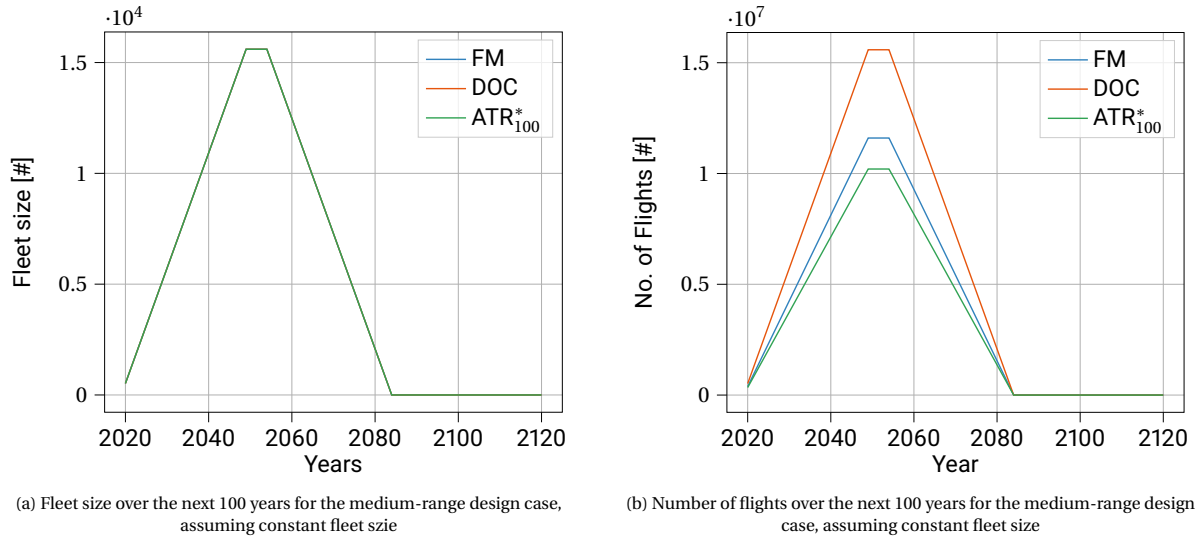


Figure 8.1: Fleet size and number of flights performed for the medium-range design case, assuming constant fleet size

for all objectives, while the productivity, measured in number of flights performed, varies between the objectives. The different designed aircraft have different block times for each mission, resulting in this change. With the constant yearly utilization thus leads to less flights performed, as calculated with Equation 7.1. The difference in flight performed makes the climate impact comparison unfair. The DOC objective performs more than 50% the amount of flight in comparison to the ATR₁₀₀* objective. This leads to a higher ATR₁₀₀, because a higher amount is emitted. The low ATR₁₀₀ by the ATR₁₀₀* objective is thus somewhat caused by lower amount of flights performed. Seen from another perspective, shifting from the DOC objective to the ATR₁₀₀* or FM objective results in a loss of productivity for this scenario. If a similar productivity is required, it comes at the cost of an increase in ATR₁₀₀.

The aircraft designed for each objective are a direct consequence of the design variables chosen. Table 8.2 shows the optimal design variables for the different objectives. The wing loading for all aircraft is constrained by the approach speed, indicating that the smallest wing possible, is the best option for current requirements set. For the FM and ATR₁₀₀* objective the high wing loading and aspect ratio results in an active span constraint, which is 36 meters. An even higher aspect ratio is desired, but is not possible, due to the span constraint. A higher aspect ratio for the DOC objective would result in higher depreciation and maintenance cost for the aircraft, because the weight of the wing increases. This leads to an inactive span constraint for the DOC objective. The engine design variables all follow the same trend, with one exception. The trend is to increase the compressor pressure ratio to its upper bound, while the TIT is increases until it is constrained by the TIT at takeoff. The variable cruise TIT changes dependent on the cruise Mach number. The cruise segment is the design point of the engine and as the cruise Mach number increases, the relative throttle setting with takeoff segment is smaller and thug a higher TIT can be achieved during cruise. The pressure compressor ratio of 20 for the ATR₁₀₀* is the exception and can be allocated to the optimization cut early by the tolerance set. As the climate impact comparison is already found to be unfair, it is expected that the impact is low.

Table 8.2: Optimal design variables values for the medium-range design case, assuming constant fleet size

Design Variable	FM	DOC	ATR ₁₀₀ *
W/S [kN/m ²]	5.84	5.84	5.84
A [-]	13.9	12.1	13.8
TIT [K]	1412	1564	1340
$\Pi_{\text{compressor}}$ [-]	25	25	20
h_{cruise} [km]	4.8	7.5	4.0
M_{cruise} [-]	0.39	0.61	0.33

Table 8.3: Aircraft parameters and characteristics for the medium-range design case, assuming constant fleet size

AC Parameter	FM	DOC	ATR ₁₀₀ *
MTOM [metric tonnes]	55.2	58.1	56.3
OEM [metric tonnes]	28.6	30.1	28.6
S [m ²]	92	97	94
W/P [N/W]	0.053	0.043	0.053
TSFC _{cruise} [g/kN·s]	7.7	10.6	6.9
t_{block} [hrs]	5.2	3.9	5.9
N _{flights} [#]	$1.2 \cdot 10^7$	$1.6 \cdot 10^7$	$1.0 \cdot 10^7$

The mission design variables between the FM and ATR₁₀₀* are similar, but the ATR₁₀₀* objective flies as slow as possible while satisfying the maximum cruise lift coefficient for the buffet onset constraint. The FM is similar, but tries to fly at fuel optimal Mach number with the accompanied cruise altitude. The DOC objective takes a different route and balances the different types of costs, e.g. crew vs flight costs. The cruise altitude is then optimal for the Mach number. The higher the cruise Mach number the higher it flies, due to the lower air density. Note that the low cruise altitude for the FM and ATR₁₀₀* objective could potentially cause problems in mountainous areas, like the alps in Europe.

The characteristics and parameters for the designed aircraft, using the design variables, are shown in Table 8.3. The MTOM differs slightly between the objectives. The FM aircraft being the lightest, which also stems from the lower fuel mass, affecting both the OEM and wing area (S). A different aspect is the power-loading (W/P) shown. The wing-loading between the objectives is equal, however this does lead to different power-loading for the objectives. The DOC aircraft is limited by the cruise performance, while the FM and ATR₁₀₀* are limited by the OEI climb gradient condition during landing. The power-loading diagrams are shown in Appendix C. It is interesting to see that the TSFC for the FM aircraft is higher than that of the ATR₁₀₀ aircraft, however this is where the block time come into play. The engine might be more efficient, but if the mission takes too long, that advantage is lost. The difference in block time is, as mentioned, the cause for the difference in productivity observed. In numerical terms, the DOC aircraft can perform one and a half mission while the ATR₁₀₀ only finished one, an increase of around 50%.

The optimal geometry for the aircraft designed using the design variables are compared in Figure 8.3. The difference between the FM and ATR₁₀₀ aircraft can be identified, but are almost negligible. The DOC aircraft has a bigger horizontal tail and a smaller span. Due to the higher takeoff power the size of the nacelle and propeller are larger. No quarter chord sweep angle is applied for all aircraft, as the cruise Mach number is not high enough to cause the need to increase the critical Mach number over the wing ($M > 0.7$) [23].

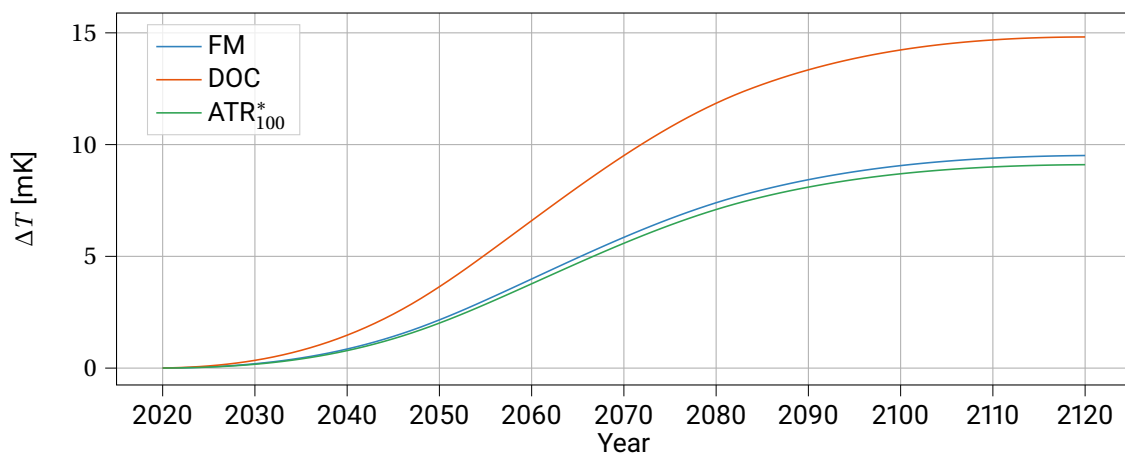


Figure 8.2: Sea-level temperature change comparison for the medium-range design case, assuming constant fleet size

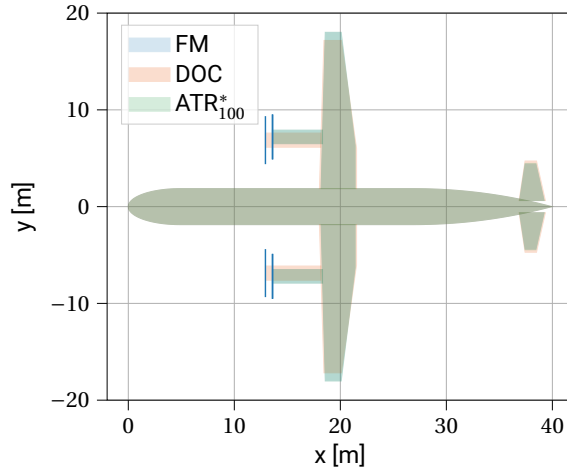


Figure 8.3: Optimal aircraft geometry comparison for the medium-range design case, assuming constant fleet size

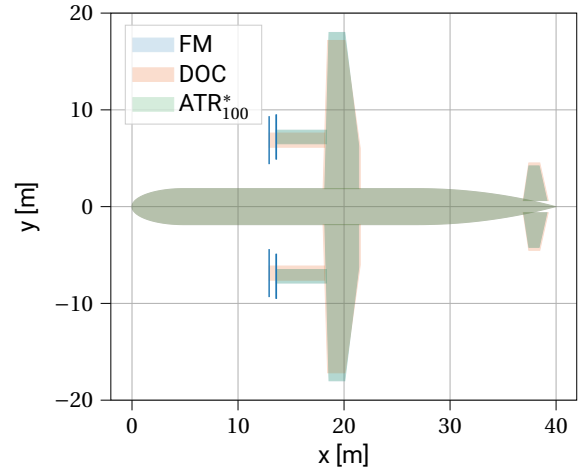


Figure 8.4: optimal aircraft geometry comparison for the medium-range design case, assuming constant productivity

The last aspect to discuss for this scenario, is the sea-level temperature change over the time horizon of 100 years, which is shown in Figure 8.2. For all objectives, the temperature increase is mainly caused by the climate effect of CO_2 . Since the emission of CO_2 is directly proportional to the fuel consumption, the temperature change is almost directly proportional to amount of fuel consumed. In this specific scenario the amount of flights performed plays also a role, as mentioned earlier. NO_x effects for the FM and ATR_{100}^* are small, as it has a lower cruise altitude and thus forcing factor. This leads, for these objectives, to a small negative ATR_{100} . For the DOC objective this is positive and explains the quick rise of the DOC line. Persistent contrails are not formed for all objectives, due to the unfavorable atmospheric conditions during the cruise phase. The ambient temperature are not favorable to make the AIC type persistent. The geometrical analysis and explanation of contrail formation is discussed in Appendix E The discussion of the climate effects will be more thoroughly discussed in Subsection 8.1.2.

8.1.2. Constant Productivity Scenario

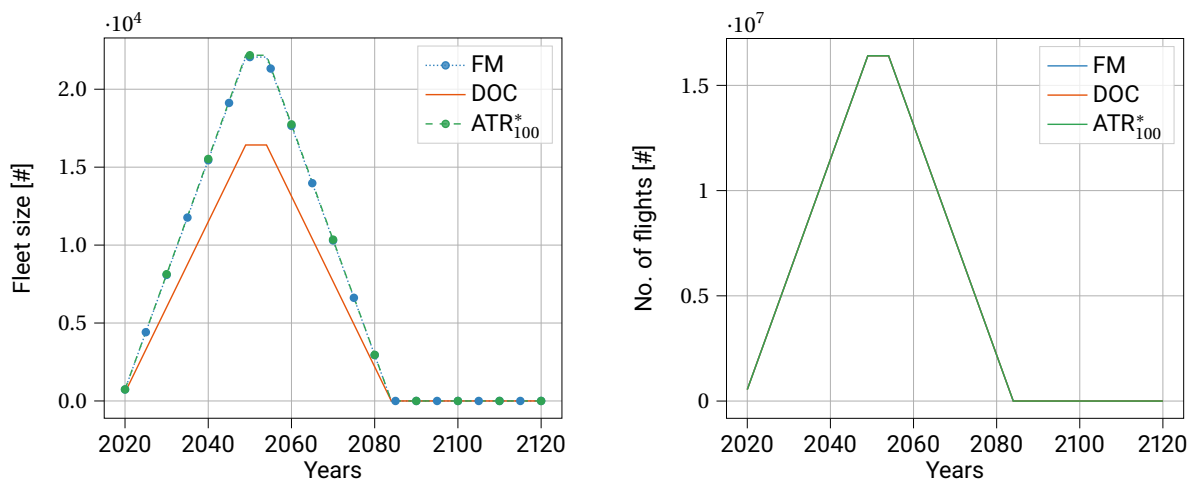
In contrast to the constant fleet scenario, the constant productivity scenario is characterized by the same number of flights performed, which is a measure of the productivity. As discussed earlier, this results in a change in fleet size between the objectives. Note that since the FM and DOC objective are design case specific and not scenario specific, the design variables an aircraft designed are identical.

Table 8.4 shows the objective values and their relative percentage difference in the constant productivity scenario. Interestingly, the difference between the ATR_{100}^* and FM objective is negligible for the objective values. The shift to the DOC objective for both objectives is thus almost equal. The shift from either the FM or ATR_{100}^* objective results in an 18% increase in ATR_{100} and a 17% decrease in costs.

Table 8.4: Objective function values for the medium-range design case, assuming constant productivity

Objective	Numerical Value			Relative difference		
	m_{fuel} [kg]	DOC [\$/seat-nm]	ATR_{100} [mK]	m_{fuel}	DOC	ATR_{100}
FM	$4.9 \cdot 10^2$	0.23	7.4	N.A	+21%	0.0%
DOC	$5.8 \cdot 10^2$	0.19	8.8	+18%	N.A	+18%
ATR_{100}^*	$4.9 \cdot 10^2$	0.23	7.4	+0.0%	+21%	N.A

Shifting between the objectives within the constant productivity scenario has a direct influence on the necessary fleet size, with the complete scenario shown in Figure 8.5. Within, Figure 8.5, Figure 8.5a shows the fleet size over the time horizon, while Figure 8.5b shows the number of flights performed over the same period. Note that markers have been added as the FM and ATR_{100}^* objective for the fleet size for clarification. The DOC objective has the again the lowest block time, resulting in the lowest required fleet size to maintain the productivity. For both scenarios the DOC objective has the highest benefit scenario wise. The FM and ATR_{100}^*



(a) Fleet size over the next 100 years for the medium-range design case, assuming constant productivity

(b) Number of flights over the next 100 years for the medium-range design case, assuming constant productivity

Figure 8.5: Fleet size and number of flights performed for the medium-range design case, assuming constant productivity

overlap closely and no clear difference is observed. The reduction in fleet size when shifting from the FM or ATR*₁₀₀ objective to the DOC objective is approximately 5600 aircraft, a reduction of 26%. To put this amount into perspective, roughly 540 Airbus A320's are build each year¹, thus the shift would take an additional 10 years to build the necessary amount of aircraft. A potential manufacturing problem could also be an issue for opting for the ATR*₁₀₀ objective. The climate impact related to the manufacturing process is also worth considering. The climate impact caused by the this process is out of the scope of this thesis, but noteworthy.

The overlap of the FM and ATR*₁₀₀ objective indicates that they are optimized for the same objective. This is strengthened by similar design variables shown in Table 8.5. The trends regarding the design variables explained in Subsection 8.1.1 still apply. The ATR*₁₀₀ objective for this scenario however are different. These design variables are similar to the FM objective and only differ slightly. The compressor pressure ratio are again all bounded, with the TIT again following the same trend as for the constant fleet size scenario. The cruise altitude differs 200 m, which can be seen as negligible. The same holds for the difference in TIT. The other design variables are near identical, which indicates the ATR*₁₀₀ and FM both optimize for minimum fuel mass. In other words, minimum ATR*₁₀₀ is obtained by reducing the fuel consumption. The exact reason is explained during the discussion for the sea-level temperature change.

With the knowledge of both scenarios it is interesting to see the compressor pressure ratio go to the upper bounds for almost all objectives in the two scenarios seen. As explained in Section 4.2, the optimum total turbine enthalpy ratio is chosen. Thus each combination of the compressor pressure ratio and the TIT operates at an optimal condition. This causes, within the bounds of the optimization, both the TIT and compressor pressure ratio to increase, resulting in an increase in engine performance. The impact on the objective values and aircraft is certain, but because this is true for all three objectives the relative difference is expected to remain.

¹A320 Production rate: Data obtained on 16-1-2022 from <https://www.airbus.com/en/newsroom/press-releases/2021-01-airbus-updates-production-rates-in-response-to-market-environment>

Table 8.5: Optimal design variables values for the medium-range design case, assuming constant productivity

Design Variable	FM	DOC	ATR ₁₀₀ *
W/S [kN/m ²]	5.84	5.84	5.84
A [-]	13.9	12.0	13.9
TIT [K]	1412	1564	1415
Π _{compressor} [-]	25	25	25
h _{cruise} [km]	4.8	7.5	5.0
M _{cruise} [-]	0.39	0.61	0.40

Table 8.6: Aircraft parameters and characteristics for the medium-range design case, assuming constant productivity

AC Parameter	FM	DOC	ATR ₁₀₀ *
MTOM [metric tonnes]	55.2	58.1	55.3
OEM [metric tonnes]	28.6	30.1	28.5
S [m ²]	92	97	93
W/P [N/W]	0.053	0.043	0.053
TSFC _{cruise} [g/kN·s]	7.7	10.6	7.6
t _{block} [hrs]	5.2	3.9	5.3
N _{ac,max} [10 ³ #]	22.0	16.4	22.1
EI _{NO_x}	0.011	0.0098	0.011

Logically similar design variables between the FM and ATR₁₀₀* objective result in similar aircraft characteristics and parameters, which shown in Table 8.6. The difference in aircraft parameters between the FM and ATR₁₀₀* is minor, e.g. the MTOM, OEM, and wing area. The block time differs slightly, which results in the difference in maximum fleet size. For the same wing-loading the higher MTOM of the DOC aircraft leads to a higher wing area. The same is true for the propeller and nacelle size. The geometry differences between the objectives, shown in Figure 8.4 is similar to that of the constant fleet size scenario. The differences are almost imperceptible.

The exact reason for the conclusion that minimum fuel mass leads to a minimum climate impact as well, is better explained with a more in depth look into the climate impact for the scenario. The sea-level for the objectives is illustrated in Figure 8.6. The overlap between the FM and ATR₁₀₀* objective is true over the time horizon set, while the DOC aircraft has a higher ATR₁₀₀ and thus also a sea-level higher temperature increase. For the former markers have been added, as seen earlier, to clarify the overlap. The temperature difference obtained between the objectives is mainly due to the amount of fuel consumed. CO₂, H₂O, and soot all have a constant EI and no altitude dependency in this study [2, 8]. A higher fuel consumption leads thus to a greater sea-level temperature for the time horizon. The difference in temperature change, caused by the extra emitted soot, sulfate and H₂O for the DOC objective, is noticeable. This however small compared to temperature change by CO₂. The climate impact of NO_x is more complex, due to the three effects mentioned in Chapter 5. The EI of NO_x during the cruise phase for the DOC is lower than that of the FM and ATR₁₀₀*, which are 0.0098 kg/kg and 0.011 kg/kg respectively. This is also shown in Table 8.6. The difference in EI is caused by the distinct atmospheric conditions that directly influences the combustor inlet pressure ($p_{t,3}$), which is altitude dependent. The total amount emitted between all objectives does not differ much, but the cruise altitude of the DOC causes a higher RF, because the cruise altitude increases the forcing factor for all NO_x effect, especially that of the short-term ozone formation (Figure 5.2) [9]. This causes an increase in sea-level temperature during the operational lifetime of the aircraft. Logically, the cooling effects are also increased. For the FM and ATR₁₀₀* objective, the lower forcing factor results in a lower RF due to the emission of NO_x. Over the complete time horizon the warming effect of the short-term ozone formation is even nullified by the two cooling effects, resulting in negative total ATR₁₀₀ due NO_x for the FM and ATR₁₀₀* objective.

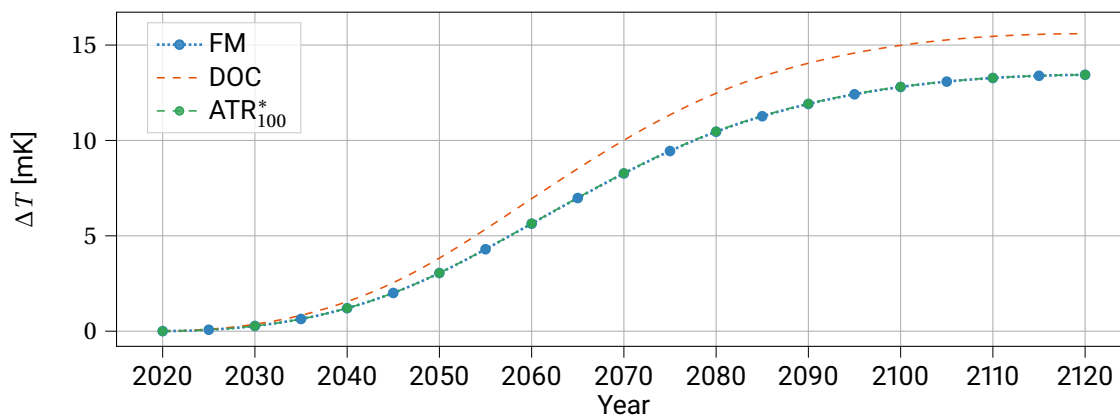


Figure 8.6: Sea-level temperature change for the medium-range design case, assuming constant productivity

The last main effect discussed is the formation of persistent contrails. As mentioned in Subsection 8.1.1, The formation of persistent contrails is hindered, due to the unfavorable atmospheric conditions. In other words the aircraft flies too low and the engine exhaust conditions are not beneficial for the formation of persistent contrails. The geometrical analysis is discussed and shown in Appendix E.

The conclusion of the NO_x effects for the FM and ATR_{100}^* objective in combination with the avoidance of persistent contrails, leads to the insight that the main contributor to the climate impact is CO_2 , with little influence of the short-lived emissions. CO_2 and the short-lived emissions are both directly proportional to the amount of fuel consumed during the mission. It can be concluded that optimizing for minimum fuel mass results in minimum ATR_{100} and are thus within the current optimization the same objective in the constant productivity scenario.

8.1.3. Turbofan Comparison

The combination of the scenarios discussed, give insight in how the current aircraft can be implemented when optimized for different objectives. The effects on the climate, fleet size and productivity are evident from the discussions in the previous Subsections. These are exclusive for the propeller aircraft, but currently a turbofan aircraft is often employed on medium-range routes. A direct comparison is made to help determine if the propeller aircraft performs better for the three objectives. The comparison made is only for the constant productivity scenario.

Table 8.7 shows the comparison in objective values for the two types of aircraft. Note that this time the objectives are in the columns instead of in the rows as in previous tables. Additionally, the block time and EI_{NO_x} are added. From the numerical values it is clear that the propeller aircraft performs better in the value the objective is minimized for. An ATR_{100} reduction of 33% is realized between both ATR_{100}^* . The reduction is lessened to 20% if the DOC turboprop objective is utilized. The fuel mass and costs are then also lower for their respective turboprop objectives. Next to the ATR_{100} benefit, the higher fuel mass is expected, due to the higher propulsive efficiency. The cost benefit between the two DOC objectives however is unanticipated. The cost estimation contradicts the current utilization of turbofan on medium-range routes, because turbofan are generally more cost friendly on these routes. The turboprop cost estimation is likely underestimated, with the current assumptions, e.g. the assumed fuel price. This indicates that the costs must be looked at critically. The cost estimation is highly range dependent and likely favors the turbofan on longer routes. Because the block time of the DOC turbofan aircraft has the lowest block time, it is the logical choice costs wise.

Table 8.7: Objective function values comparison between the turboprop and turbofan objectives, including block time and EI_{NO_x}

Value	Turboprop			Turbofan		
	FM	DOC	ATR_{100}^*	FM	DOC	ATR_{100}^*
m_{fuel} [kg]	$4.9 \cdot 10^3$	$5.8 \cdot 10^3$	$4.9 \cdot 10^3$	$7.2 \cdot 10^3$	$7.7 \cdot 10^3$	$7.7 \cdot 10^3$
DOC [\$/seat-nm]	0.23	0.19	0.23	0.22	0.20	0.23
ATR_{100} [mK]	7.4	8.8	7.4	26	26	11
t_{block} [hrs]	5.2	3.9	5.3	3.6	3.4	3.9
EI_{NO_x}	0.011	0.0098	0.011	0.025	0.011	0.017

The ATR_{100} benefit is visualized in Figure 8.7 which compares and shows the sea-level temperature change between the two aircraft types. The impact by the ATR_{100}^* turbofan objective follows a similar trend to that of the DOC turboprop objective, but amplified. The higher fuel mass leads to a higher amount of CO_2 and short-lived emissions emitted. This results in an amplification of the cooling and warming effects of these emissions. The higher EI_{NO_x} of the ATR_{100}^* turbofan objective also leads to more NO_x emitted and thus the ATR_{100} , due to NO_x is higher for the ATR_{100}^* objective. The forcing factor is similar to the DOC turboprop objective and with more NO_x emitted the temperature change is higher. The FM and DOC turbofan objective both form contrails, which increases the ATR_{100} substantially by approximately 11 mK for both objectives. The geometrical analysis for the formation of persistent contrails for the turbofan is also discussed in Appendix E. The impact is clearly seen during the operational lifetime of the aircraft. Thus the short-lived emissions and contrails dominate the temperature change during the operational lifetime for both the FM and DOC turbofan objectives. The avoidance of persistent contrails and the lower NO_x climate impact thus greatly reduced the sea-level temperature change and thus ATR_{100} between the turboprop and turbofan objectives.

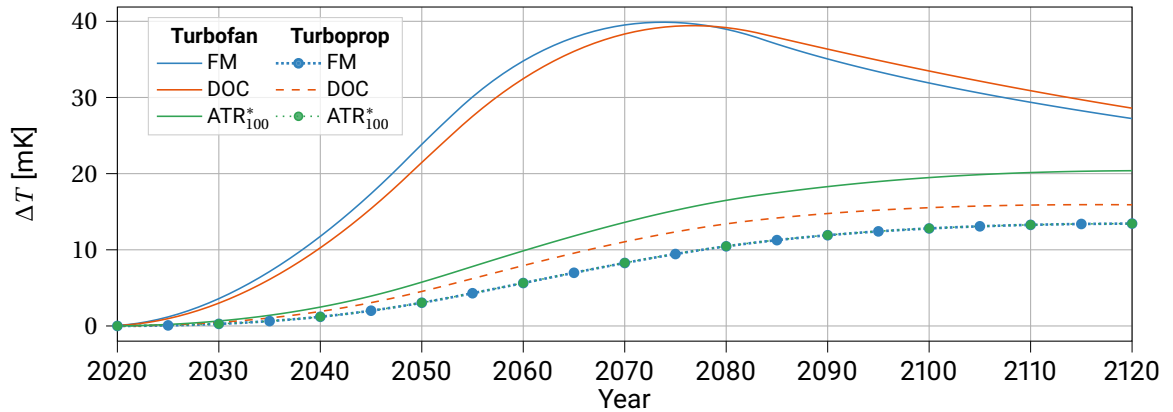


Figure 8.7: Sea-level temperature change for the turboprop and turbofan objectives for the medium-range design case, assuming constant productivity

The geometry of both ATR_{100}^* objectives, shown in Figure 8.9, follow the same design trend. The cabin layout, cabin diameter and wing span are identical for both aircraft. The differences in geometry lie in the wing and stabilizer area. As the wing-loading of both aircraft is equal, the higher MTOM of the turbofan aircraft results in a larger wing area and subsequently larger stabilizer area.

The change in block time, shown in Table 8.7, between the turbofan and turboprop ATR_{100}^* objective is 1.4 hours. This difference shows a large change in the required fleet size for the constant productivity to be maintained. This is illustrated in Figure 8.8, with Figure 8.8a and 8.8b showing the fleet size over the time horizon for the turboprop and turbofan objectives respectively. To better show the difference the y-axis range has been made equal. This shows that for the 32% reduction in ATR_{100} , approximately 5500 more aircraft are needed between the ATR_{100}^* objectives. The substantial difference results in a higher production rate, as mentioned earlier. The extra production of these aircraft also causes an increase in ATR_{100} to the production of these 5500 aircraft. Ideally the effects of the gain ATR_{100} benefit from utilizing propeller aircraft is compared to the extra ATR_{100} , as a result of the production of the extra aircraft. This is out of the scope of this thesis, but

indicates a slightly skewed comparison between the ATR_{100} objectives.

The fleet size are not comparable, due to the high difference in block time. To decrease the fleet size and block time, a block time constraint is added to the optimization for the turboprop. The maximum block time for the new optimization is set to four hours and is discussed in Subsection 8.1.4.

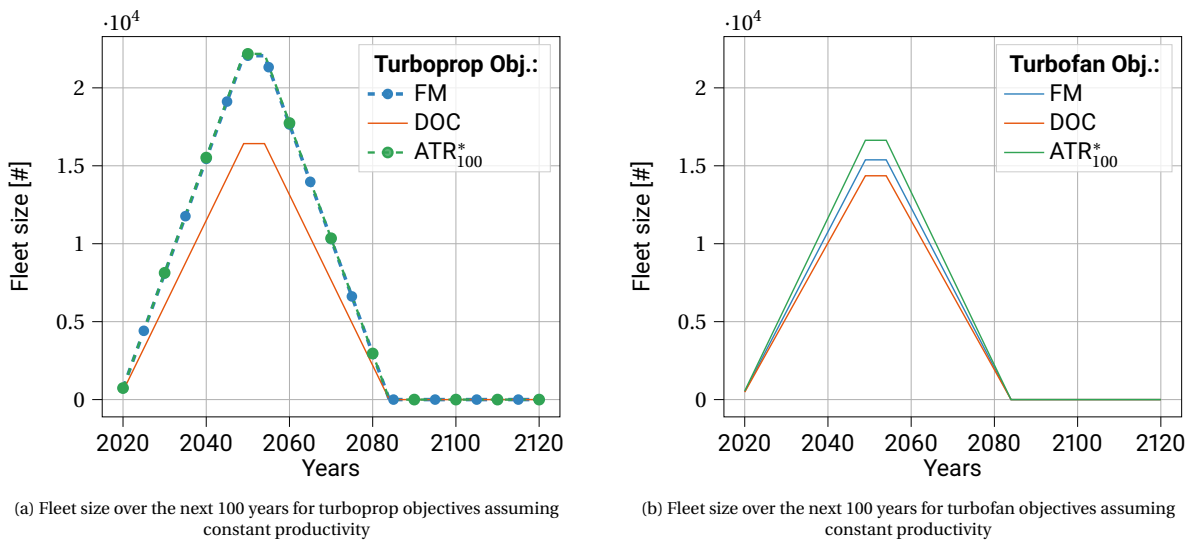


Figure 8.8: Fleet size comparison between the turboprop and turbofan aircraft, assuming constant productivity

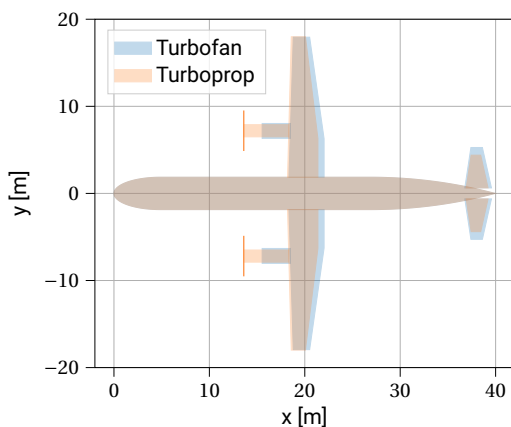


Figure 8.9: Optimal aircraft geometry comparison between the turboprop and turbofan ATR_{100}^* objective, assuming constant productivity

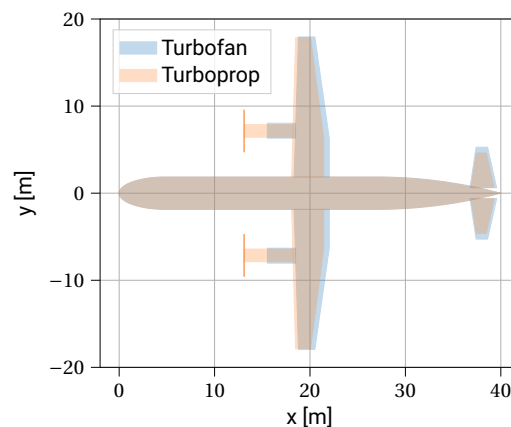


Figure 8.10: Optimal aircraft geometry for the turboprop, with the block time constraint applied, and turbofan objective ATR_{100}^* , assuming constant productivity

8.1.4. Block Time Constraint

The addition of the block time constraint partly eliminates the large difference in fleet size eminent between the different objectives, because of their different block times. The maximum allowable block time for this constraint was set to four hours and gives insight in the objectives when fleet sizes are comparable. Note that the block time for the DOC aircraft is already below four hours and thus is only applicable to the FM and ATR_{100}^* objective.

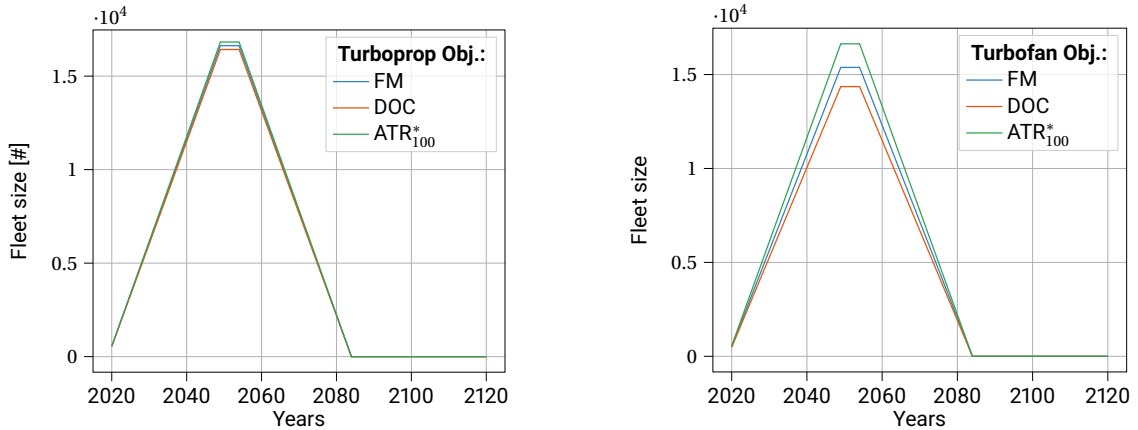
The new values for the objective values and their new block times are shown in Table 8.8. Due to the extra block time constraint, there is an observable difference in the numerical values for obtained for FM and ATR_{100}^* turboprop objective. The block time constraint decreases the block time, which results in non-optimal flying conditions for the aircraft. This causes the fuel mass for the FM and ATR_{100}^* objective to increase from $4.9 \cdot 10^3$ kg to $5.7 \cdot 10^3$ kg for both objectives. This is still significantly lower than the minimum fuel mass of $7.2 \cdot 10^3$ kg for the FM turbofan objective. The higher fuel mass results also in a higher ATR_{100} , while the lower block time reduced the costs. For all turboprop objectives the difference between the objectives becomes

smaller.

Table 8.8: Objective function values comparison between the turboprop, with the block time constraint applied, and turbofan objectives, including block time and EI_{NO_x}

Value	Turboprop			Turbofan		
	FM	DOC	ATR_{100}^*	FM	DOC	ATR_{100}^*
m_{fuel} [kg]	$5 \cdot 10^3$	$5.8 \cdot 10^3$	$5.7 \cdot 10^3$	$7.2 \cdot 10^3$	$7.3 \cdot 10^3$	$7.7 \cdot 10^3$
DOC [\$/seat-nm]	0.19	0.19	0.20	0.22	0.20	0.23
ATR_{100} [mK]	8.6	8.8	8.5	26	26	11
t_{block} [hrs]	4.0	3.9	4.0	3.6	3.4	3.9
$EI_{NO_x, cruise}$	0.0099	0.0098	0.0099	0.025	0.011	0.017

The ATR_{100} for all turboprop objectives is still lower than that of the ATR_{100}^* turbofan objective. Additionally, the cost are lower, which is logical in the current estimation, due to the decreasing block time. This indicates that for similar fleet sizes, as shown in Figure 8.11, a reduction of 22% in ATR_{100} and a 15% reduction in costs can be achieved. Note that within Figure 8.11 solid lines are used to distinguish the objectives better. The significant improvement, in comparison to the ATR_{100}^* turbofan objective, in both the costs and the climate impact is optimistic. This might imply that the overall aircraft design, including fuel mass and ATR_{100} , is underestimated, which is likely caused by the assumed cruise propeller efficiency (88%). For this reason a sensitivity analysis is performed and discussed in Chapter 9 to put the current benefits into perspective. Even though with the possible underestimation of the turboprop aircraft designed and the objectives, the rest of the Subsection focuses on the current result to show the trends by decreasing the block time in the aircraft design, design variables, geometry, and climate impact.



(a) Fleet size over the next 100 years for the turboprop objectives with the block time constraint, assuming constant productivity

(b) Fleet size over the next 100 years for the turbofan objectives assuming constant productivity

Figure 8.11: Fleet size comparison between the turboprop with the block time constraint applied and the turbofan objectives, assuming constant productivity

The primary changes to the design variables for the FM and ATR_{100}^* turboprop objectives are the cruise altitude and the cruise Mach number. The overview of design variables is shown in Table 8.9. For the FM turboprop objective the higher cruise Mach number changes the cruise altitude as well to account for the higher cruise Mach number. The lower air density is better for the faster velocity. The ATR_{100}^* objective has a lower cruise altitude to decrease the effect of NO_x . The TIT for both objectives is increased, due to the higher cruise Mach number. This causes a lower relative throttle setting with takeoff segment and thus a higher TIT. The aspect ratio is decreased as a result of the increase in wing area, because the span constraint is still active. The wing-loading and compressor pressure ratio remain unchanged.

The design variables for the optimization with the block time constraint applied, lead to the geometry for the ATR_{100}^* turboprop objective that is compared to the same turbofan objective in Figure 8.10. Overall the difference is small, but an increase in wing area and stabilizer area can be observed for the turboprop aircraft.

Table 8.9: Optimal design variables for the medium-range design case with the block time constraint applied

Design Variable	FM	DOC	ATR* ₁₀₀
W/S [kN/m ²]	5.84	5.84	5.84
A [-]	13.3	12.1	13.1
TIT [K]	1520	1564	1501
$\Pi_{\text{compressor}}$ [-]	25	25	25
h_{cruise} [km]	8.2	7.5	7.2
M_{cruise} [-]	0.60	0.61	0.58

These new design variables lead to different aircraft of which the main design characteristics are shown in Table 8.10, which are directly compared to the turbofan aircraft. Comparing the MTOM of the different aircraft it becomes clear that the turboprop aircraft is about 10 metric tonnes lighter. The difference in OEM is more around 5-6 metric tonnes between the objectives. Again, the lower MTOM for the turboprop leads to a smaller wing, as the wing-loading is constant for all. The large difference in the three aircraft parameter shown is, as mentioned earlier, partly caused by the high assumed propeller efficiency. Still the trend in increasing MTOM and OEM when compared to the normal constant productivity scenario (Table 8.6) holds even without it present. The TSFC for the turboprop objectives is similar, and significantly lower than the turbofan objectives. Showing the higher propulsive efficiency in numbers.

Table 8.10: Aircraft parameter comparison between the turboprop, with the block time constraint applied, and turbofan objectives

Aircraft Parameter	Turboprop			Turbofan		
	FM	DOC	ATR* ₁₀₀	FM	DOC	ATR* ₁₀₀
MTOM [metric tonnes]	58.2	58.1	58.6	67.2	65.8	66.3
OEM [metric tonnes]	30.9	30.1	31.1	37.2	36.0	35.5
S [m ²]	98	97	99	115	110	107
W/P or F/W [W/N or N/N]	0.040	0.043	0.040	0.30	0.30	0.32
TSFC _{cruise} [g/kN·s]	10.3	10.6	10.4	14.9	16.8	14.6

Lastly, the sea-level temperature increase comparison over the time horizon is shown in Figure 8.12. Again, blue and green are added to indicate the overlap of the FM and ATR*₁₀₀ objectives. The sea-level increase for both these objectives is now even more close to that of the DOC turboprop objective. Logically, the effects of the short-lived emissions and CO₂ have increased, due to the higher fuel consumption. The higher cruise altitude results in the higher forcing factor for the NO_x effects for the FM turboprop objective, resulting in positive total contribution to the ATR₁₀₀. The same is true for the ATR*₁₀₀ turboprop objective, but is slightly smaller. Even though the cruise altitude has increased for all turboprop objectives, especially that of the FM turboprop objective, persistent contrails still do not form. The atmospheric conditions are more favorable than the normal constant productivity scenario, but the formation of persistent contrails does still not occur. The geometrical analysis for the analysis with block time constraint is also shown in Appendix E.

It is interesting to see that the overlap of the three turboprop is seen throughout the analysis with the block time constraint applied. The numerical values obtained for each turboprop objective in Table 8.8, but also for the design variables in Table 8.9 and the aircraft parameters in Table 8.10. Even the sea-level temperature change between all three objectives differs slightly in Figure 8.12. The objectives align well if the block time constraint is added, due to the similar block time between the aircraft.

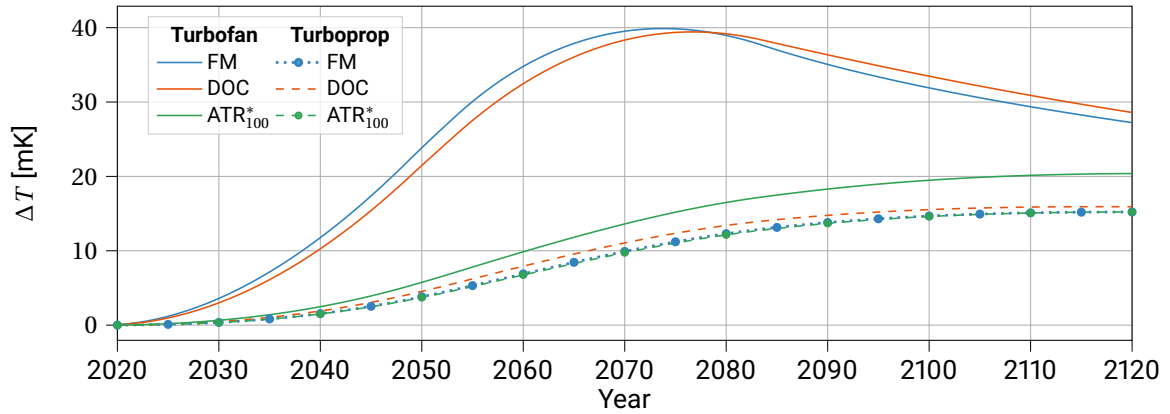


Figure 8.12: Sea-level temperature change comparison between the turboprop, with the block time constraint applied and turbofan objectives

8.2. Regional Design Case

The lower passenger capacity and harmonic range of the regional design case, helps put the trends seen in the medium-range design case into perspective. The difference in range gives insight in the importance of the range on the aircraft design variables. As the medium-range design case is the main interest of this study, the overall discussion for this design is held short.

Due to the unfair comparison of the constant fleet size scenario the discussion for that scenario is held short and confined to the objective values and the scenario comparison.

8.2.1. Constant Fleet Scenario

The constant fleet size scenario for the regional design case operates with a fleet size of 3020 aircraft and results in an unfair comparison as concluded earlier.

The numerical values shown in Table 8.11 clearly show the overall differences between the objectives. The difference in ATR_{100} between the objectives is small, due to the small fleet size assumed. Still, the relative differences are of interest. If a larger fleet size is assumed it will logically result in a larger ATR_{100} . The overall trend found in the table is comparable to that of the medium design case. The ATR_{100}^* and FM have a lower ATR_{100} , because a lower amount of missions are performed. The shift from the DOC objective to the ATR_{100}^* objective reduces the costs by 22%, while the ATR_{100} is increased by 88%. The 88% is caused by the relative increase of flights performed by the DOC objective. The ATR_{100} increase from shifting from the ATR_{100}^* to the DOC objective is comparable relative more than the medium design case, which is due to the fleet size assumed.

Table 8.11: Objective function values for the regional design case, assuming constant fleet size

Objective	Numerical Value			Relative difference		
	m_{fuel} [kg]	DOC [\$/seat-nm]	ATR_{100} [mK]	m_{fuel}	DOC	ATR_{100}
FM	$1.6 \cdot 10^2$	0.31	0.25	N.A	+26%	+5%
DOC	$2.1 \cdot 10^2$	0.25	0.45	+33%	N.A	+88%
ATR_{100}^*	$1.6 \cdot 10^2$	0.32	0.24	+0.3%	+30%	N.A

The constant fleet size scenario for the regional design case is illustrated in Figure 8.13, with Figure 8.13a and Figure 8.13b showing the fleet size and number of flights performed over the time horizon respectively. This scenario follows the same trend as the medium-range design case. The DOC objective has the lowest block time and thus the highest productivity. In comparison the DOC objective performs 49% more flights than the ATR_{100}^* objective and 43% more than FM objective. If a larger fleet size is chosen it is expected that this gap in productivity becomes more apparent. The effect of the larger fleet size on the ATR_{100} is especially noticeable with the pronounced difference in productivity.

The design variables for the constant fleet size scenario and the sea-level temperature change are both found and discussed in Appendix B.

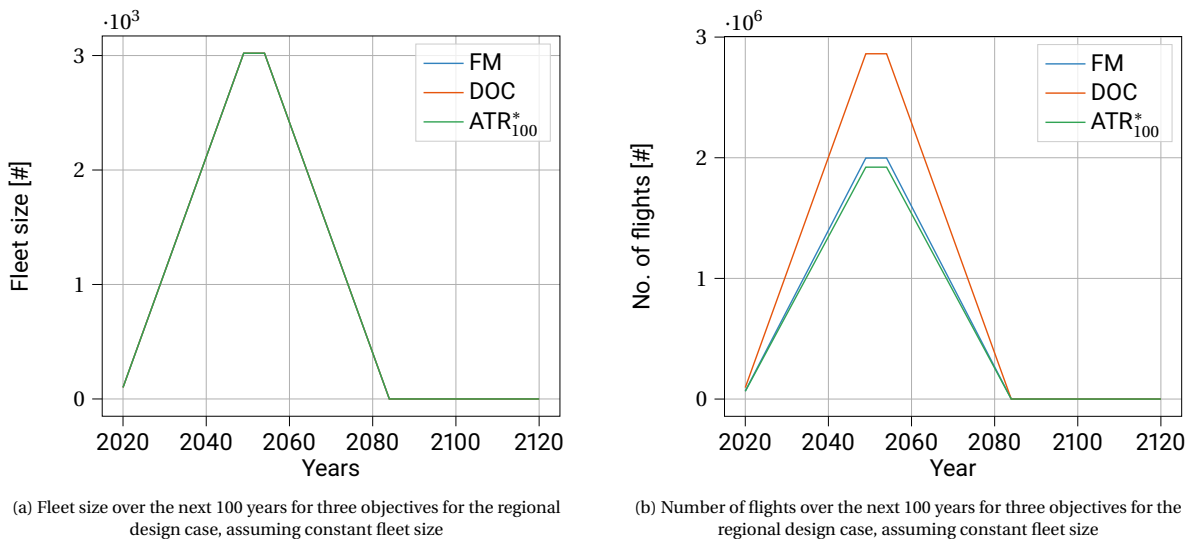


Figure 8.13: Fleet size and number of flights performed for the regional design case, assuming constant fleet size

8.2.2. Constant Productivity Scenario

The results for the constant productivity scenario, with a constant value of $1.31 \cdot 10^{11}$ rpk are shown in Table 8.12 the ATR*₁₀₀ and the FM objective are again similar with only negligible difference in both the fuel mass and ATR₁₀₀ between the objectives. The shift from the DOC to ATR*₁₀₀ objective in this scenario results in 22% reduction in costs and a 24% increase in ATR₁₀₀. The shift to the FM objective results in similar changes in costs and ATR₁₀₀. Additionally, the FM and ATR*₁₀₀ are again similar objectives as seen in the objective values. The relative differences seen in this scenario are comparable to that of the medium-range design case.

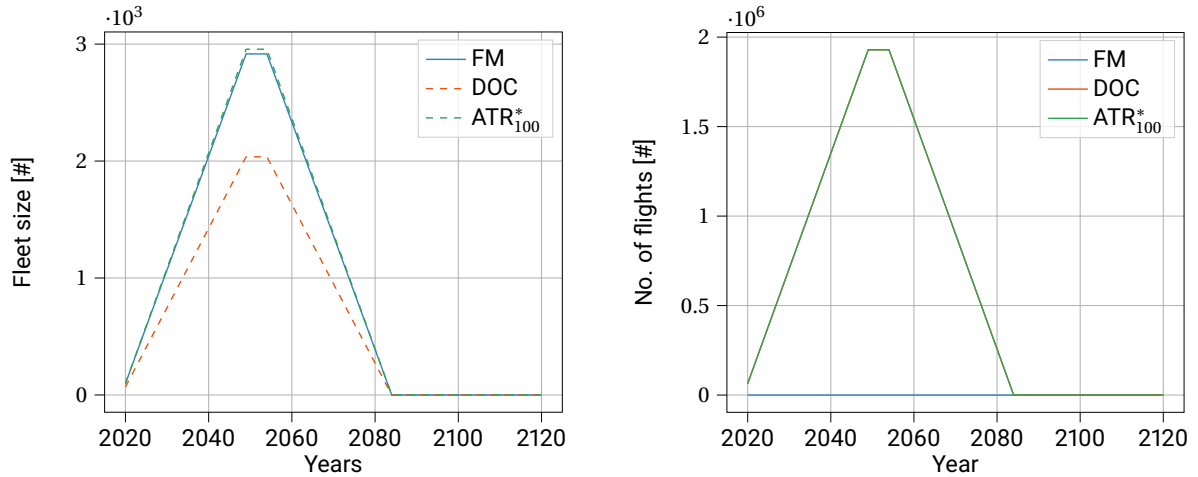
The costs, when compared to the medium-range design case, tend to be higher. The lower range and capacity makes the costs per seat-nm higher than the medium range costs. The total costs however are lower.

Table 8.12: Objective function values for the regional design case, assuming constant productivity

Objective	Numerical Value			Relative difference		
	m_{fuel} [kg]	DOC [\$/seat-nm]	ATR ₁₀₀ [mK]	Fuel Mass	DOC	ATR ₁₀₀
FM	$1.6 \cdot 10^2$	0.31	0.24	N.A	+29%	+0.1%
DOC	$2.1 \cdot 10^2$	0.25	0.30	+31%	N.A	+24%
ATR* ₁₀₀	$1.6 \cdot 10^2$	0.32	0.24	+0.1%	+30%	N.A

Figure 8.14 shows the fleet size and productivity over the time horizon in Figure 8.14a and Figure 8.14b respectively. A solid line is used for the FM objective to easier distinguish the lines. Similar to the medium-range design case, the lower block time of the DOC objective results in the lowest required fleet size. An increase of 43% in fleet size is required when shifting from the DOC to the FM objective. From the discussion in the medium-range previous design case this is expected. Interestingly, the relative difference in the small fleet size is similar to that of the medium-range design case, where the fleet size is significantly larger. If shown from a different perspective the DOC objective, needs a little of two-thirds (70%) of the fleet size that is needed for the FM and ATR*₁₀₀ objective. In other words to reduce the climate impact a larger fleet size is needed to maintain the same amount of productivity.

The design variables shown in Table 8.13, generally show the same trends as the medium-range design trend. The TIT and compressor pressure ratio follow the exact same trend for all objectives, while the cruise altitude for the FM and ATR*₁₀₀ objective is similar to that of the medium-range design case. The cruise Mach number for these objectives is also relatively low, as the time versus fuel consumption is less prominent in this design case. Ideally, the cruise Mach number would be even lower, but this is prevented by the buffet onset lift coefficient constraint. The cruise Mach number of the DOC aircraft is close to that of the DHC Dash



(a) Fleet size over the next 100 years for three objectives for the regional design case, assuming constant productivity

(b) Number of flights over the next 100 years for three objectives for the regional design case, assuming constant productivity

Figure 8.14: Fleet size and number of flights performed for the regional design case, assuming constant productivity

8-400², which is 0.53 compared to the 0.52 shown in Table 8.13.

The wing-loading for both the FM and ATR₁₀₀ objective is unconstrained, which is not true for the DOC objective. The lower wing-loading results in a larger wing and lighter engine. Thus the lighter engine is more beneficial than a smaller wing. The aspect ratio of 17 for the FM objective is unrealistic and structural support is necessary to maintain that. The ATR₁₀₀ objective has an even lower-wing loading and results in a lower aspect ratio, that is till constrained by the imposed maximum of 36 m. The DOC objective has a similar trend to the medium-range design case and has the smallest wing. The power-loading diagrams for the aircraft are shown in Appendix C.

Table 8.13: Optimal design variables values for the regional design case, assuming constant productivity

Design Variable	FM	DOC	ATR ₁₀₀ *
W/S [kN/m ²]	3.1	3.9	2.9
A [-]	17	11.0	15.8
TIT [K]	1376	1644	1415
Π _{compressor} [-]	25	25	25
h _{cruise} [km]	4.8	6.0	5.4
M _{cruise} [-]	0.30	0.52	0.29

Table 8.14: Aircraft parameters and characteristics for the regional design case, assuming constant productivity

AC Parameter	FM	DOC	ATR ₁₀₀ *
MTOM [metric tonnes]	24.0	24.1	24.0
OEM [metric tonnes]	14.5	14.2	14.5
S [m ²]	76	61	82
W/P [N/W]	0.070	0.055	0.076
t _{block} [hrs]	4.1	2.8	4.1
N _{ac,max} [10 ³ #]	2.9	2.0	3.0
EI _{NO_x,cruise} [kg/kg]	0.011	0.091	0.010

The effect of the lower-wing loading is clearly seen in the larger wing area shown in Table 8.14. The effect on the MTOM and OEM however is small between the objectives. The FM and ATR₁₀₀ objective have similar masses, with little differences, because of the similar design variables. The DOC objective has a lower wing mass, but this is offset by the higher fuselage mass, due to the pressurization of the fuselage. The difference in fuel mass then results in a similar MTOM. The block hours shown for the FM and ATR₁₀₀ are high in comparison to the DOC objective, which results in the large difference in fleet size seen earlier.

The aircraft design variables design the optimal aircraft geometries as seen in Figure 8.15. The FM and ATR₁₀₀ have similar geometries, while the aircraft of the DOC objective has a smaller stabilizer area and a smaller wing, which result from the lower aspect ratio and higher wing-loading. It has to be noted that a regional aircraft with a span of 36 in the current market unrealistic, however the airport category and current optimization allows this. The span for the DOC objective is more reasonable at 26 m.

²DHC dash-8 400 data obtained on 27-12-2021 from <https://customer.janes.com/Janes/Display/JAWA0096-JAWA>

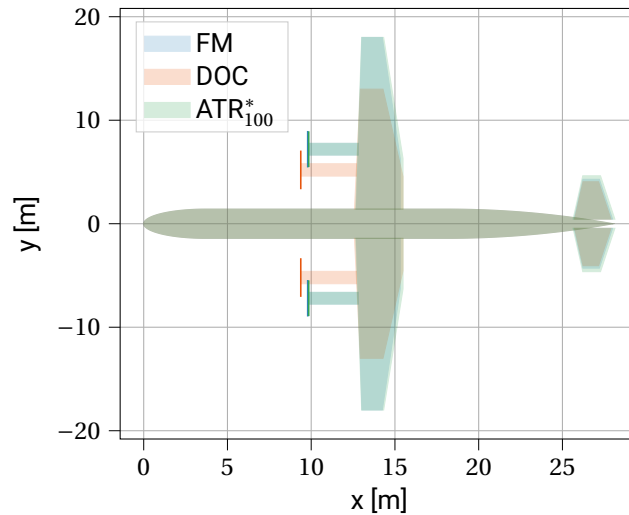


Figure 8.15: Optimal aircraft geometry comparison for the regional design case, assuming constant productivity

For this scenario within the regional design case, the sea-level temperature change over the time horizon is shown in Figure 8.16. Markers are added to highlight the overlap between the FM and ATR₁₀₀* objective. Logically, the main contribution is CO₂ with small contribution by the short-lived emissions and NO_x. During the operational lifetime the increase for these emissions is slightly noticeable, as the effects die out when the aircraft does not fly. The overall impact of NO_x and the short-lived emissions on the ATR₁₀₀, however, is negligible. The formation of persistent contrails is avoided for all objectives, as the atmospheric conditions are even more unfavorable than for the medium-range design case.

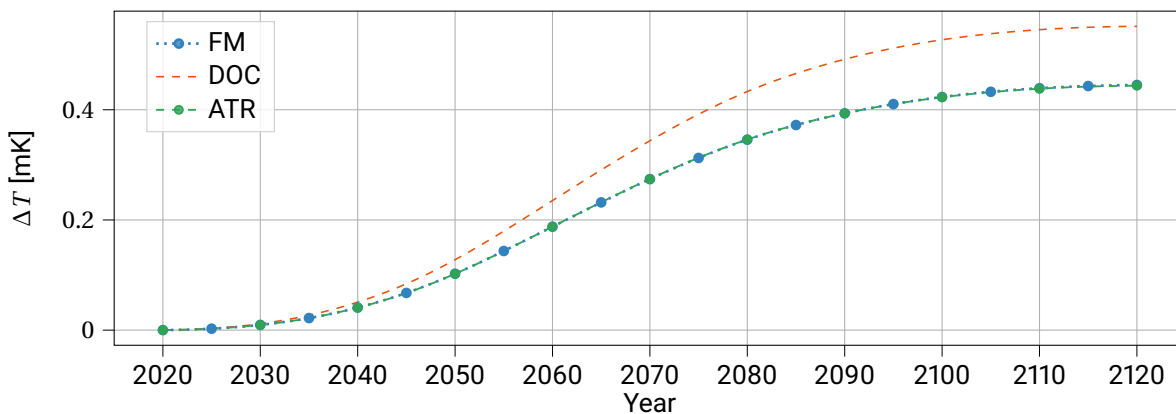


Figure 8.16: Sea-level temperature change for the regional design case, assuming constant productivity

8.3. Regional and medium-range Design Case Trends

The discussion of the results of both the regional and medium-range design gives insight in the climate impact, design variables, and the scenario itself. Some trends apply to both design cases, while others are exclusive. The aspects summarized are the scenario, the objective values and the design variables.

8.3.1. Constant Fleet Size versus Constant productivity scenario

The comparison and discussion between the constant fleet size scenario and constant productivity scenario can be held short. The DOC objective for both design cases outperforms the FM and ATR₁₀₀* objective. In the constant fleet size this leads to an unfair climate impact comparison, because more flights are performed. This is beneficial for the airliner, but not for the environment. This makes the constant productivity scenario a better comparison, as the same number of missions are performed. This is likely applicable to any design

case that are subjected to these future fleet scenarios.

8.3.2. Objective Values

The numerical objective values between the design cases are incomparable, because of the difference in productivity. The trends regarding the values itself however is comparable. For both constant productivity scenarios it is observed that the FM and ATR_{100}^* are overlapping objectives. For the medium-range design case this is more apparent, as less changes in the design variables are seen. For the regional design case the overlap is potentially coincidental, due to the optimization and uncertainties seen. Meaning that the overlap in objective values is caused by the relatively small ATR_{100} . Still it is clear that in the scenario for the regional design case have a great overlap. The overlap in the medium-range with the current climate model is logical, but is likely not the case if a more robust climate model is applied. The total overlap is not completely true if the block time constraint is applied, but all three objectives are in that case similar.

For both design cases the shift to the DOC objective results in a similar relative increase in costs and reduction in ATR_{100} . If the block time constraint is applied for the medium-range design case. Overall it can be said that the trends are generally applicable to both design cases.

8.3.3. Design Variables

Generally speaking the trends seen in the design variables are applicable to both design cases. In the current design cases, the FM and ATR_{100}^* objective minimize the fuel consumption by employing a relatively low cruise Mach number and cruise altitude. As the range increases, the cruise Mach number increases as well due to the influence of range on the fuel consumption. For example, in the medium-range design a trade-off is seen between the block time and TSFC. A lower TSFC can be achieved, but this increases the mission duration, which increases the fuel consumption. This problem increases with range and is thus less of an issue for the regional design case. The optimal DOC cruise Mach number and cruise altitude is generally higher to reduce the mission duration.

The engine design variables follow the same trend for both design cases. The TIT is constrained by the TIT at takeoff, while the compressor pressure ratio is bounded. The main differences is seen in the wing-loading for the FM and ATR_{100}^* objective between both design cases. The lighter engine is better for the regional design case, as the mass increase for the wing is lower. Additionally, a high aspect ratio in the regional design case can be achieved, which would not be possible if a lower-wing loading would be chosen in the medium-range design case. The high aspect in the regional design case is often not seen and likely unfeasible in actual aircraft design. The effect of the lower wing-loading however is seen in the regional design case.

8.3.4. Summary

Overall the trends regarding the objective values, scenarios and design variables are applicable to both design cases with the exception of the wing-loading. This is hard to predict or make general rules for it. The lower wing-loading might be the best option in the current design space, as said the aspect ratio of 17 is highly infeasible and will likely not be used in actual aircraft design. For that reason the trend of a high aspect ratio for reducing the fuel consumption is most important. The impact of the range on the mission design variables is such that the aircraft starts to fly faster the longer the mission is. It is thus expected that for a even longer mission range, the aircraft will fly even faster.

9

Sensitivity Analysis

The propeller efficiency has a direct influence on the aircraft design, climate impact and costs. The 88% used for the propeller efficiency in Chapter 8 is optimistic and creates a great benefit for the propeller aircraft. To put the results in perspective, a sensitivity analysis is performed to see the effects to see the effect of the propeller efficiency on the results. The optimizations performed in this chapter is for the ATR_{100}^* objective for the medium-range design case, assuming constant productivity scenario. Additionally, the possible causes for the propeller aircraft climate impact benefit, when compared to the turbofan, is discussed. First, Section 9.1 discusses the various causes for the climate impact benefit. Second, Section 9.2 discusses the propeller efficiency sensitivity analysis for the normal optimization. Lastly, Section 9.3 discusses the sensitivity analysis with the block time constraint applied.

9.1. Aircraft Performance Overestimation

The performance of the aircraft in Subsection 8.1.3 showed an optimistic benefit from utilizing propeller aircraft on the medium route. For the optimistic benefit two main reasons have been identified. The first is the assumed propeller efficiency, while the second reason is the optimum total enthalpy ratio used to size the engine. Both have a direct consequence on the aircraft designed for each objective.

The propeller efficiency assumed for the optimizations discussed is 88%. Normally a value between 80-85% is logical for the conceptual design phase, but it was assumed that technological advancement were made in the future and thus the 88% is used during the main results [64]. The change of the propeller efficiency directly influences the fuel consumption, climate impact and aircraft design.

The optimum total enthalpy ratio used during the sizing of the engine causes the engine performance to work optimally with the combination of the TIT and the compressor pressure ratio. This has an impact on the engine performance, but is expected to be small.

Between the turboprops the relative differences will likely remain the same, as all objectives have both mentioned reasons. As the effect of the chosen total enthalpy ratio is expected to be small, the focus of this Chapter is on the sensitivity of the propeller efficiency.

9.2. Propeller Efficiency Sensitivity Analysis

The propeller efficiency sensitivity analysis is solely performed for the ATR_{100}^* objective, assuming constant productivity, as mentioned earlier. The ATR_{100}^* objectives with different propeller efficiencies are then compared to the turbofan data to put the results in perspective. The efficiencies assumed, range from 65% to 90% with increments of 5%.

Changing the maximum propeller efficiency from 65% to 90%, results in distinct objective values for the ATR_{100}^* objective, as shown in Table 9.1. The propeller efficiency of 88% used during the normal optimization is added for comparison. The trend for increasing propeller efficiency is that fuel mass, costs and ATR_{100} all decrease, which is expected. The fuel mass is reduced from $13 \cdot 10^3$ kg to $4.7 \cdot 10^3$ kg, between the highest and lowest efficiency. For the costs this is from 0.32 \$/seat-nm to 0.22 \$/seat-nm, while the ATR_{100} is reduced from 15 mK to 7.0 mK. A significant decrease for changing the propeller efficiency. Comparing these values with the turbofan data, shown in Table 9.2, helps put them all in perspective. The aircraft using a propeller

efficiency of 75% has a similar fuel mass and ATR_{100} compared to the ATR_{100}^* turbofan objective. This indicates that for the turboprop to be beneficial for the climate, a propeller efficiency of at least 75% is necessary. If a higher value is achieved the climate benefit will become more significant. Thus for a propeller efficiency of 80% a reduction of 15% is realized in ATR_{100} , which is increased to 27% for a propeller efficiency of 85%.

The effect of the propeller efficiency on the costs is not only a reduction in fuel costs, but also the depreciation and maintenance costs, because the aircraft mass reduces with increasing propeller efficiency. Comparing the costs, the 75% propeller efficiency objective shows that for a similar ATR_{100} the turbofan is the better option due to the lower costs. The objectives for 80% and 85% are still more expensive than the ATR_{100}^* turbofan objective and signify that for a reduction in ATR_{100} the costs are higher. The costs comparison from the main results are then showed from a different angle. The costs still seem to be underestimated, as this is the sensitivity for the ATR_{100}^* turboprop objective. The costs for the DOC turboprop objective will be lower than the values seen in Table 9.1.

Table 9.1: Objective function value comparison for the ATR_{100}^* for various propeller efficiencies

Value	$\eta_{prop} = 0.65$	$\eta_{prop} = 0.70$	$\eta_{prop} = 0.75$	$\eta_{prop} = 0.80$	$\eta_{prop} = 0.85$	$\eta_{prop} = 0.88$	$\eta_{prop} = 0.90$
m_{fuel} [10^3 kg]	13	9.6	7.5	6.4	5.4	4.9	4.7
DOC [\$/seat-nm]	0.32	0.28	0.26	0.25	0.24	0.23	0.22
ATR_{100} [mK]	15	12	11	9.4	8.0	7.4	7.0

Table 9.2: Objective function values for the turbofan objectives

Value	FM	DOC	ATR_{100}^*
m_{fuel} [10^3 kg]	7.2	7.7	7.7
DOC [\$/seat-nm]	0.22	0.20	0.23
ATR_{100}	26	26	11

The cruise Mach number and cruise altitude, shown in Table 9.3, see little to no change between the objectives. The optimal cruise conditions do not change with a change in propeller efficiency. The change in block time is thus non-existent for the different propeller efficiencies assumed. While the different propeller efficiencies give a similar fleet size that is shown in Figure 8.5a, the DOC per flight do differ. This increases the amount of costs per flight with a decreasing propeller efficiency even though the fleet size stays constant.

Similar to the cruise altitude and the cruise Mach number, the wing-loading and compressor pressure ratio also see no change between the different propeller efficiencies assumed. The only two design variables that do see a significant change are the aspect ratio and the TIT. The TIT increases with increasing propeller efficiency, because the propeller converts the supplied power easier to thrust. This causes a lower throttle setting with the takeoff segment and thus an increase in TIT. The trend seen for the aspect ratio required knowledge about the aircraft as well, which is shown in Table 9.4. The MTOM decreases with decreasing propeller efficiency, which with the constant wing-loading results in a higher wing area. The increase in wing area then allows for a smaller aspect ratio, as the span constraint is active. The trend seen regarding the MTOM

Table 9.3: Optimal design variables comparison for the ATR_{100}^* for various propeller efficiencies

Value	$\eta_{prop} = 0.65$	$\eta_{prop} = 0.70$	$\eta_{prop} = 0.75$	$\eta_{prop} = 0.80$	$\eta_{prop} = 0.85$	$\eta_{prop} = 0.88$	$\eta_{prop} = 0.90$
W/S [kN]	5.8	5.8	5.8	5.8	5.8	5.8	5.8
A [-]	9.8	11.2	12.1	12.9	13.6	13.9	14.1
TIT [K]	1395	1402	1407	1412	1414	1415	1416
$\Pi_{compressor}$ [-]	25	25	25	25	25	25	25
h_{cruise} [km]	5.0	5.0	5.0	5.0	5.0	5.0	5.0
M_{cruise} [-]	0.40	0.40	0.40	0.40	0.40	0.40	0.40

and wing area in Table 9.4, is also true for the OEM, because the lower wing area lowers the wing mass and

thus the OEM. The small changes are caused by the increase in aspect ratio, which changes the performance of the aircraft for the loading requirements slightly. This changes the loading requirements slightly. Logically, the TSFC during the cruise segment improves with increasing propeller efficiency, since less fuel is needed for the same amount of thrust. Lastly, the EI_{NO_x} is indifferent cause the cruise altitude and the compressor pressure ratio see no change between the different propeller efficiencies. The TIT does change, but this has no effect on the determination of the EI of NO_x (Equation 5.2).

Table 9.4: Aircraft parameter and characteristics comparison for the ATR_{100}^* , with the block time constraint applied, for various propeller efficiencies

Value	$\eta_{prop} = 0.65$	$\eta_{prop} = 0.70$	$\eta_{prop} = 0.75$	$\eta_{prop} = 0.80$	$\eta_{prop} = 0.85$	$\eta_{prop} = 0.88$	$\eta_{prop} = 0.90$
MTOM [metric tonnes]	78.7	68.9	63.2	59.5	56.7	55.3	54.6
OEM [metric tonnes]	36.9	33.4	31.4	30.0	29.1	28.5	28.4
S [m ²]	132	115	106	100	95	93	92
W/P [N/W]	0.046	0.048	0.050	0.052	0.053	0.053	0.053
TSFC _{cruise} [g/kN·s]	10.5	9.7	9.1	8.4	8.0	7.6	7.6
$EI_{NO_x,cruise}$ [kg/kg]	0.011	0.011	0.011	0.011	0.011	0.011	0.011

When compared to the ATR_{100}^* turbofan objective aircraft parameters, shown in Table 9.5, the most similar aircraft regarding the MTOM, OEM and wing area compared to the climate aircraft is the one with a propeller efficiency assumed of 75%. This results in a similar aircraft, which is slightly lighter but with a similar wing area. The FM turbofan objective is similar, in mass and wing area, to the objective with a propeller efficiency of 75%.

Table 9.5: Optimal turbofan aircraft parameters and characteristics

Parameter	FM	DOC	ATR_{100}^*
MTOM [metric tonnes]	67.2	65.8	66.3
OEM [metric tonnes]	37.2	36.0	35.5
S [m ²]	115	110	107
F/W [N/N]	0.31	0.30	0.32
TSFC _{cruise} [g/kN·s]	14.9	16.1	14.6
$EI_{NO_x,cruise}$ [kg/kg]	0.025	0.011	0.017

While a small difference was observed between the ATR_{100}^* turboprop objective with and without the block time constraint, the change in propeller efficiency has a clear change effect on the aircraft geometry. In Figure 9.2 the geometry comparison for three different propeller efficiencies can be seen. The wing area and horizontal tail area is clearly seen in Figure 9.2. Both are a direct result of the higher MTOM of the aircraft, which subsequently also leads to a higher stabilizer area. The length of the nacelle for the lower propeller efficiencies are relatively long and unrealistic, but the effect of the propeller efficiency on the nacelle size is clear.

The sea-level temperature change over the time horizon all show the same trend, as shown in Figure 9.1. The ATR_{100}^* turbofan has been added for comparison with the green dashed line. As the propeller efficiency increases the total sea-level temperature change decreases. The amount of emitted CO_2 , H_2O , soot and sulfate becomes smaller and smaller with the increase of the propeller efficiency, which reduced the climate effects due to these emissions. As EI_{NO_x} is constant for the change in propeller efficiency, the amount NO_x emitted is also reduced. The reduced the warming effect of NO_x , but also the cooling effects. This causes the overall negative contribution of NO_x on the ATR_{100} to become smaller with increasing propeller efficiency.

The comparison with the ATR_{100}^* turbofan objective shows the great impact of the short-term ozone production due to NO_x . During the operational lifetime the sea-level temperature change is even higher than the objective with a propeller efficiency of 70%. At the end however, it is more close to that of 75%.

Throughout the discussion of the sensitivity analysis it is observed that for the gain of increasing the propeller efficiency is higher for lower values, e.g. between 65% and 70% than for 85% to 90%. When the propeller

efficiency is lower, the 5% increase is, relative to its original value, higher and results in more benefit in absolute terms. This trend is seen in Table 9.1 and Table 9.4. Additionally, it is also seen in Figure 9.1.

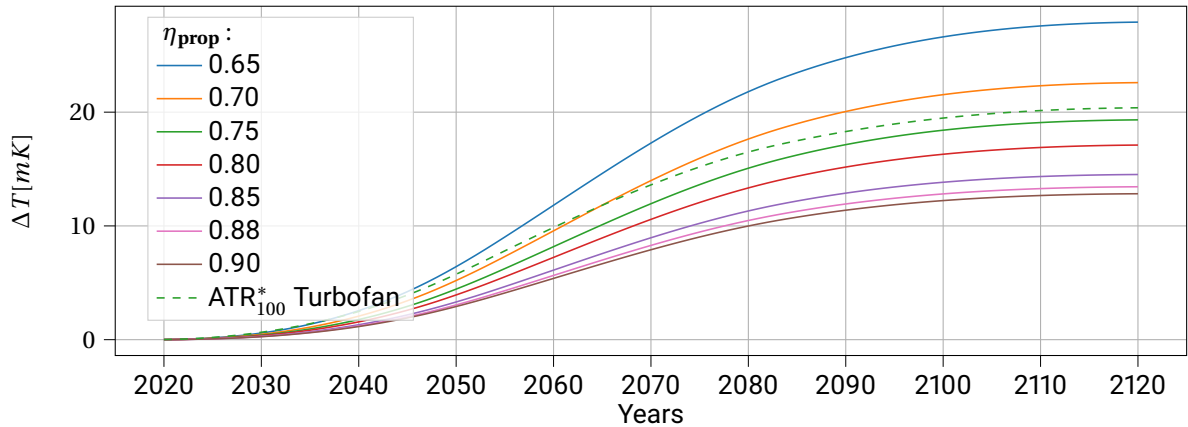


Figure 9.1: Sea-level temperature change for ATR*₁₀₀ objective for various propeller efficiencies, including ATR*₁₀₀ turbofan objective

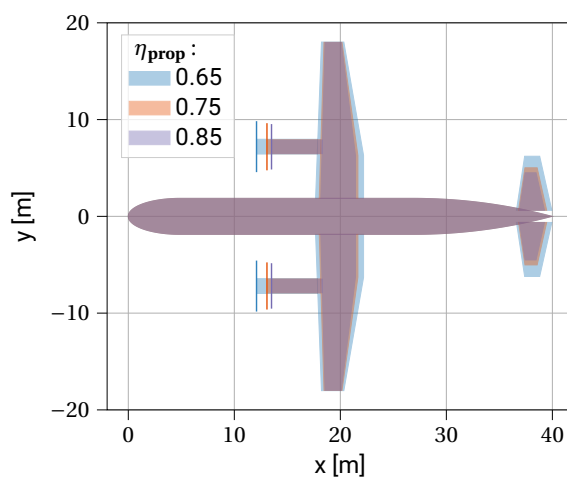


Figure 9.2: Optimal geometry comparison for the ATR*₁₀₀ objective with a propeller efficiency of 65%, 75%, and 85%

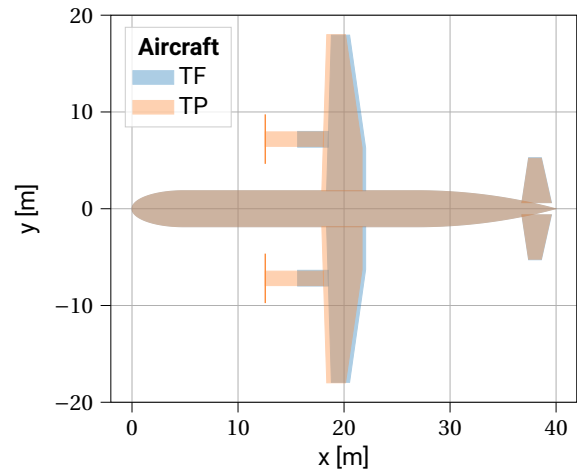


Figure 9.3: Optimal geometry comparison for the ATR*₁₀₀ turbofan objective and the ATR*₁₀₀ turboprop objective with a propeller efficiency of 75%

9.3. Block Time Sensitivity Analysis

In order to get the full picture in the sensitivity analysis, the propeller efficiency is also varied for the ATR*₁₀₀ turboprop objective with the block time constraint applied. The values are again compared to the turbofan values.

The objective values for the climate optimized aircraft with the block time constraint applied are shown in Table 9.6. The impact of changing the propeller efficiency follows the same trend as for the normal sensitivity analysis. Compared to normal sensitivity analysis the fuel mass and ATR₁₀₀ are higher, while the costs are lower. The latter is due to same reasons mentioned in Subsection 8.1.4. When compared to the ATR*₁₀₀ turbofan objective, the minimum propeller efficiency needed for a similar climate impact is increased to around 80%. This is a shift of approximately 5% from 75%, which is caused by the lower block times.

Due to the decrease in block time, the costs shown in Table 9.6 are reduced when compared with Table 9.1. The trend for decreasing costs with increasing propeller efficiency still holds, but as mentioned in Chapter 8 the costs are optimistic and must be viewed critically. A propeller efficiency of 80% is normal for propeller aircraft to achieve, and a direct operating cost of 0.21 \$/seat-nm, in comparison with the turbofan, is low.

Table 9.6: Objective function value comparison for the ATR_{100}^* , with the block time constraint applied, for various propeller efficiency

Value	$\eta_{prop} = 0.65$	$\eta_{prop} = 0.70$	$\eta_{prop} = 0.75$	$\eta_{prop} = 0.80$	$\eta_{prop} = 0.85$	$\eta_{prop} = 0.88$	$\eta_{prop} = 0.90$
m_{fuel} [10^3 kg]	14	11	8.7	7.3	6.2	5.7	5.3
DOC [\$/seat-nm]	0.28	0.25	0.23	0.21	0.20	0.20	0.19
ATR_{100} [mK]	16	14	12	11	9.3	8.5	8.1

Table 9.7 shows the design variables for the various assumed propeller efficiencies. Similar to the trend seen in Table 9.3, only the TIT and aspect ratio vary with the change in propeller efficiency. Note that the TIT for the lowest propeller efficiency (65%) in Table 9.7, is higher than the highest TIT for the highest propeller efficiency (90%), shown in Table 9.3. The effect of the cruise Mach number on the TIT is thus larger than the effect of the propeller efficiency.

Table 9.7: Optimal design variables value comparison for the ATR_{100}^* , with the block time constraint applied, for various propeller efficiencies

Value	$\eta_{prop} = 0.65$	$\eta_{prop} = 0.70$	$\eta_{prop} = 0.75$	$\eta_{prop} = 0.80$	$\eta_{prop} = 0.85$	$\eta_{prop} = 0.88$	$\eta_{prop} = 0.90$
W/S [kN]	5.8	5.8	5.8	5.8	5.8	5.8	5.8
A [-]	9.65	10.8	11.7	12.4	12.9	13.2	13.5
TIT [K]	1487	1510	1528	1540	1550	1555	1560
$\Pi_{compressor}$ [-]	25	25	25	25	25	25	25
h_{cruise} [km]	7.4	7.4	7.4	7.4	7.4	7.4	7.4
M_{cruise} [-]	0.59	0.59	0.59	0.59	0.59	0.59	0.59

The variance in the TIT, aspect ratio and propeller efficiency in combination with the other design variables, results in the aircraft parameters shown in Table 9.8. Comparing the TSFC for the cruise phase in the current sensitivity analysis for a propeller efficiency of 85% is comparable to the TSFC for a propeller efficiency of 65% shown in Table 9.4. This shows that applying the block time constraint, results in non-optimal cruise conditions and that even a 85% propeller efficiency is needed to compensate that. The EI of NO_x does not change for the same reasons mentioned earlier.

Table 9.8: Aircraft parameter and characteristics comparison for the ATR_{100}^* , with the block time constraint applied, for various propeller efficiencies

Value	$\eta_{prop} = 0.65$	$\eta_{prop} = 0.70$	$\eta_{prop} = 0.75$	$\eta_{prop} = 0.80$	$\eta_{prop} = 0.85$	$\eta_{prop} = 0.88$	$\eta_{prop} = 0.90$
MTOM [metric tonnes]	79.7	71.2	65.7	62.0	59.2	57.9	57.1
OEM [metric tonnes]	38.5	35.4	33.4	32.0	31.0	30.6	30.3
S [m^2]	134	120	111	104	100	98	96
W/P [N/W]	0.040	0.042	0.043	0.044	0.045	0.046	0.046
TSFC _{cruise} [g/kN·s]	13.9	12.9	12.1	11.3	10.7	10.3	10.1
EI _{NO_x,cruise} [kg/kg]	0.0097	0.0097	0.0097	0.0097	0.0097	0.0097	0.0097

The geometry follows the same trend that is observed in Figure 9.2. For that reason the comparison with the turbofan (TF) is of more interest and is shown in Figure 9.3. The turboprop (TP) used in the comparison has an assumed propeller efficiency of 75%. Similar stabilizer and wing size are observed between the two.

To conclude, the sea-level temperature change for the different propeller efficiencies is illustrated in Figure 9.4. The turbofan has been added again for the comparison. As NO_x has a total warming effect for the conditions with the block time, an increase in propeller efficiency decreases the contribution of NO_x to the ATR_{100} . This increase in propeller efficiency also decreases the effect of the short-lived emissions and CO_2 .

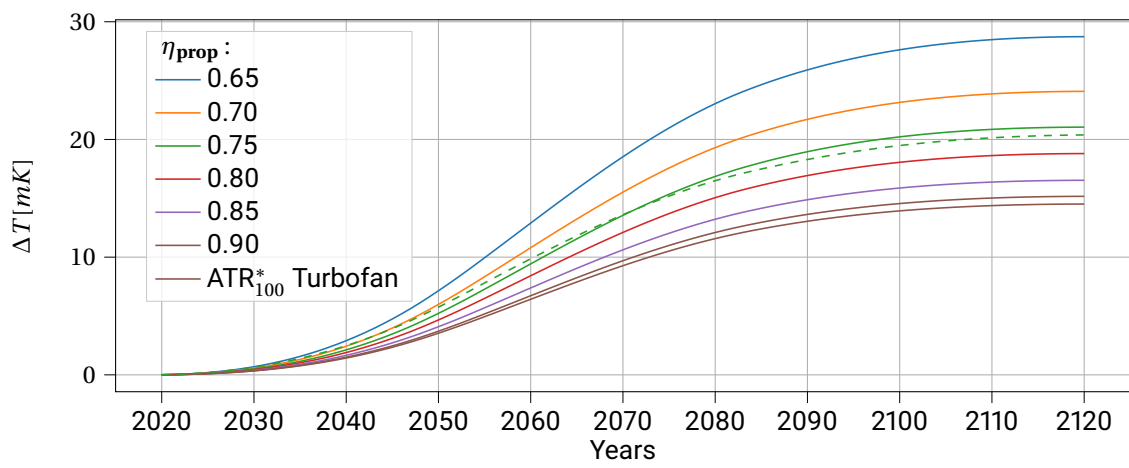


Figure 9.4: Sea-level temperature change for ATR*₁₀₀ objective, with block time constraint applied, for various propeller efficiencies, including ATR*₁₀₀ turbofan objective

10

Conclusion

This study aims to investigate the climate impact by utilizing propeller aircraft for sustainable aviation industry. The main objective is to conceptually design an optimal propeller aircraft for three different objectives and how the change between the objectives affects the aircraft design variables, climate impact and costs. The three objectives chosen are the fuel mass (FM) objective, the direct operating costs (DOC) objective, and the average temperature response objective (ATR). The latter is set over a time horizon of 100 years (ATR_{100}) and the objective is denoted by ATR_{100}^* . For each of the objectives the aircraft is conceptually designed for by optimizing the airframe, engine, and mission design variables. The optimization are executed for both a medium-range design case and a regional design case, since the turbofan aircraft is currently dominant for the former, while propeller aircraft is more present on the regional routes. Additionally, both design cases are subjected to two scenarios, where either the fleet size or the productivity is held constant over the time horizon of 100 years.

To design the propeller aircraft using the airframe, engine, and mission design variables, changes are made to the optimization structure. The main changes are the new propulsion module and the new loading diagram, which sizes the takeoff power of the propeller aircraft. Additionally, alterations are made to the weight estimation, cost estimation and mission analysis to design the aircraft with a high-wing configuration, T-Tail and wing mounted turboprop engines. These changes are also incorporated in the extended design structure matrix (XDSM) to correctly show the flow of the design variables, which are the wing-loading, the aspect ratio, the turbine inlet temperature (TIT), the compressor pressure ratio, the cruise Mach number, and the cruise altitude. The new propulsion module and the complete aircraft design loop are verified and validated respectively. Both are within the 5% margin.

Using the validated aircraft design loop, the change in design variables between the objectives for the medium-range design case is clear. The wing-loading and compressor pressure ratio are maximized by the approach constraint and the upper bound respectively. The TIT follows the same trend for all objectives, because for all objectives this is constrained by the TIT at takeoff. A higher TIT is obtained by the DOC objective, due to the larger cruise Mach number. The objective cruises at Mach 0.61, which has a relative to 0.39 for the FM objective, a lower throttle setting to the takeoff segment and thus a higher TIT can be set (1564 K vs 1412 K). The shift from the DOC objective to the ATR_{100}^* objective results in a lower cruise Mach number and cruise altitude, which are approximately 0.4 and 5.0 km respectively. The aspect ratio increases with this shift, but is limited by the span constraint of 36 m.

Regarding the objective values the change from the DOC objective to the ATR_{100}^* objective reduced the ATR_{100} is reduced by 40% for the constant fleet size scenario, which is caused by the 50% more flight performed by DOC objective. This makes the ATR_{100} comparison for the constant fleet size scenario biased. For that reason the constant productivity scenario is preferred for the change in ATR_{100}^* between the objectives, since the amount of flights are constant.

In the constant productivity the shift from the DOC objective to the ATR_{100}^* objective reduces the ATR_{100} by 15%, increases the costs 21%, and increases the required fleet size by 35%. The higher ATR_{100} for the DOC objective is caused by the increase in fuel consumption and thus the effects of CO_2 , H_2O , sulfate and soot are increased the DOC objective. The effects of NO_x for the DOC objective are in total positive, due to the higher forcing factor of the short-term ozone formation. The NO_x contribution is almost negligible compared to the

effect of CO₂ is for both the FM and ATR₁₀₀^{*} objective. The formation of persistent contrails are prevented by the unfavorable atmospheric conditions for all objectives. The ATR₁₀₀ for both the FM and ATR₁₀₀^{*} objective is thus directly dependent on the amount of fuel consumed. From this observation it is concluded that optimizing for the FM objective also results in minimum ATR₁₀₀. The formation of persistent contrails is avoided by all objectives, strengthening the conclusion. Additionally, the compliance in objectives is also seen in the design variables and the aircraft parameters.

Comparing the objective values of the turbofan with that of the turboprop for the medium-range design case, a benefit or reduction of 32% in ATR₁₀₀ is achieved by utilizing the ATR₁₀₀^{*} turboprop objective instead of the ATR₁₀₀^{*} turbofan objective. This reduction is caused by the lower fuel consumption of the ATR₁₀₀^{*} turboprop objective and the reduced climate impact of NO_x for the turboprop. The change from turbofan to turboprop does come at a 32% increase in fleet size, because of the increase in block time. The DOC turboprop objective attains a reduction of 7.4% compared to the DOC turbofan objective. This contradicts literature and the costs in the study must be looked at critically. Because of the large fleet size difference a maximum block time of 4 hours.

The lower block lessens the ATR₁₀₀ benefit between both ATR₁₀₀^{*} objectives from 32% to 22%, which also reduced the required fleet size and costs. The reduction is achieved by increasing by increasing the cruise Mach number, cruise altitude, and the TIT. The aspect ratio is reduced, because the wing area increases. The overlap between the FM and ATR₁₀₀^{*} is, with the lower block time, apparent. The clear conflicts between the objectives is with the block time constraint slight, but noticeable.

The ATR₁₀₀ benefits indicated are achieved with an optimistic propeller efficiency of 88%, which is used to account for technological advancements. When a realistic propeller efficiency of 80% is employed the 32% ATR₁₀₀ benefit, without the maximum block time is reduced to 15%. This becomes 5% if similar block times are wanted. To put this into perspective a propeller efficiency of approximately 75% must be realized during cruise to have the ATR₁₀₀ benefit between both ATR₁₀₀^{*} objectives. This requirements shift to approximately 80% if similar block times are wanted.

The general trends regarding the objective values, design variables, and the scenarios itself are also applicable for the regional design case. The uneven ATR₁₀₀ comparison problem in the constant fleet size problem is still present. For the constant productivity scenario, optimizing for minimum fuel again results in minimal ATR₁₀₀ for the same reasons as for the medium-range design case. Compared to the medium range design case, the cruise Mach number is significantly lower (0.29 vs 0.4), as the range of the mission shorter, resulting also in a lower cruise altitude. The wing-loading is not constrained for the FM and ATR₁₀₀^{*} objective as a smallest wing is less crucial, due to the lower aircraft mass.

This study has shown that optimizing propeller aircraft for minimum fuel results in the minimum climate impact and designing for minimum fuel mass results also in the minimum climate impact. Employing the climate impact optimal propeller aircraft on the medium-range route, results in a lower climate impact, due to the lower fuel consumption and avoidance of persistent contrails. This reduction in climate impact does come at the cost of an increase in fleet size. In short, employment of propeller aircraft are a sustainable and feasible manner to reduce the climate impact for a sustainable future of the aviation industry.

11

Future Recommendations

Having concluded the results of this study, a number of recommendations are proposed for improvements on this study and for future research. These are discussed and proposed in this Chapter.

The first improvement identified for this study is a different approach for the thermodynamic cycle analysis in the propulsion module. have been identified. The current on-design point thermodynamic analysis allows every combination of TIT and the compressor pressure ratio. This is the cause for the high TIT and compressor pressure ratio throughout the different optimizations, as the optimum total turbine enthalpy ratio is chosen. Potentially, this slightly overestimates the engine performance and might give a wrong trend regarding the engine design variables.

Adding to the improvement, is the recommendation for a more extensive propeller model. In this study, the propeller efficiency varies with the Mach number, without taking into account the rotations per minute (RPM), advance ratio, or the propeller diameter. It is a valid approach for the conceptual methods employed, but ideally all parameters are accounted for. The actuator disc theory (ADT), blade element momentum theory (BEM), or even a propeller map are options that could be explored. This increases the accuracy of the propeller model and thus the aircraft performance, but also increases the computational effort.

The second improvement is a more thorough cost estimation. The cost module is critically looked at during this study and potentially favors the turboprop. The current cost estimation is fine for if the downsides are known, but a more detailed cost estimation is needed if the current conceptual oriented design start to become more detailed.

Next to the cost module, a more in depth climate impact is proposed that models the influence of NO_x and persistent contrails more accurately and include the effects of both the unburned hydrocarbons (UHC's) and other types of aerosols.

For the optimization itself it is of interest to include noise in the study. This can either be the cabin noise or ground noise, but including the objective or constraint helps determine if the aircraft meet the noise requirements currently set. For propeller aircraft the noise generated is a big problem and with more stringent noise requirements the aircraft design is potentially limited by the noise itself.

Another recommendation regarding the optimization is to perform a multi-objective optimization. The multi-objective optimization for costs, fuel mass, climate impact, and potentially noise objective will give insights in the relation between the cost and the other objectives. This can be visualized with a Pareto front for an easy overview.

The last recommendation is to use the designed aircraft or optimization in more realistic routes with varying ranges and payload, resulting in a more realistic climate impact. The current future fleet scenario is a great first estimation of how the fleet size and productivity changes for the objectives chosen. The utilization in a more realistic route network will give insights in how the utilization of the turboprop or turbofan changes if both are utilized in the same fleet. This is also possible with a fuel pricing sensitivity for the costs comparison.

Applicable for all improvements and recommendations is the recommendation for different engine and aircraft configurations. For example, the contra rotating open rotor (CROR) is not chosen in this study for applicability reasons, but does show climate impact potential. Employing this type of propeller propulsion

allows for differ aircraft configuration as well. Implementing it in a future study will show its feasibility.

The new aircraft configuration could be paired with new design cases that change the range, the maximum structural payload or even the amount of engines. These can be easily thought of and are easily implemented with the current optimization architecture implemented.

A

Input Data Engine Verification

This Appendix shows the input parameters used for the engine verification for both the performance and parametric analysis. An overview of the paper verification for missions is also shown.

A.1. Parametric Paper Verification Inputs & Results

For the parametric analysis verification with the use of the paper by Dinç [77] The input parameters for all ten mentioned missions in the study are given in Table A.1. Additionally, the constant input parameters for all missions is shown in Table A.2.

Table A.1: Input parameters for the different engine parameters

Input Parameter	Mission #1	Mission #2	Mission #3	Mission #4	Mission #5	Mission #6	Mission #7	Mission #8	Mission #9	Mission #10
$\Pi_{\text{compressor}}$ [-]	10.37	10.37	10.37	10.37	10.37	10.37	10.37	10.37	10.37	10.37
TIT [10^3 K]	1368.7	1368.7	1368.7	1368.7	1368.7	1368.7	1368.7	1368.7	1368.7	1368.7
M_0 [-]	0.151	0.182	0.268	0.326	0.339	0.329	0.270	0.339	0.326	0.145
Altitude [km]	0.0	0.0	6.096	6.096	9.144	9.144	9.144	9.144	6.096	0.0
Ambient pressure [kPa]	101.325	101.325	46.56	46.56	30.08	30.08	30.08	30.08	46.56	101325
Ambient temperature [K]	288.15	288.2	248.5	248.5	228.7	228.7	228.7	228.7	248.5	288.15

Table A.2: Constant input parameters for the parametric analysis verification with the paper by Dinç [77]

Parameter	Value	Parameter	Value
$\eta_{\text{compressor}}$ [-]	0.795	$\eta_{\text{mech,hpt}}$ [-]	0.995
η_{HPT} [-]	0.86	η_{prop} [-]	0.8
η_{LPT} [-]	0.86	Π_{inlet} [-]	0.997
$\eta_{\text{combustor}}$ [-]	0.999	Cooling 2 [%]	0.07
$\eta_{\text{mech,LPT}}$ [-]	0.995	$P_{\text{off-take}}$ [W]	0.0

These ten different missions indicate ten different design points for the parametric analysis. Three of the main results are shown in the main document in Chapter 6. A percentage difference overview for some of the main parameters is shown in Figure A.1.

The mission numbers are found on the x-axis in the figure, while the y-axis shows the absolute percentage difference. The four main parameter chosen are the turbine inlet pressure ($p_{t,4}$), the turbine outlet temperature ($T_{t,5}$), the total thrust, and the TSFC. Overall the parametric analysis shows great compliance. The percentage difference lies between +4.8% and -1.7%. This is within the 5% bound for the conceptual design phase. The main outliers are the TSFC and the total thrust. The temperature and pressure are accurately estimated. Especially the former, as this is low for all missions.

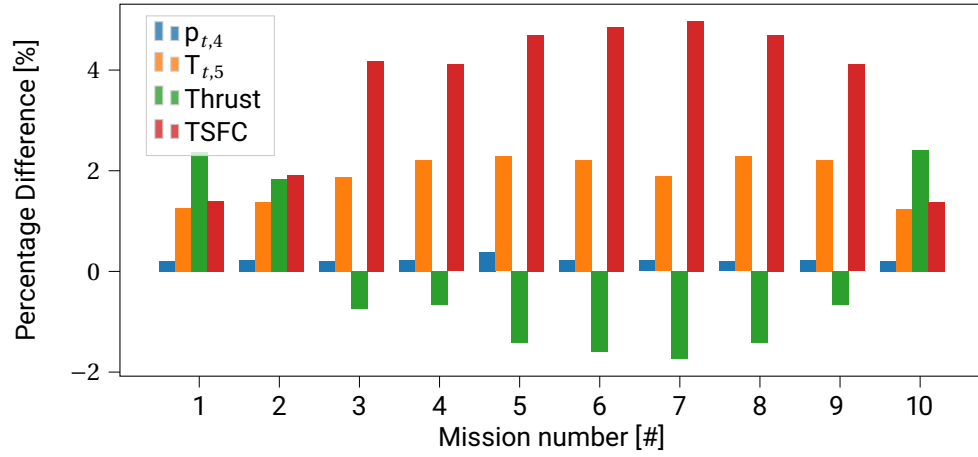


Figure A.1: Parametric analysis verification for specific engine parameters for the paper by Dinç [77]

A.2. GasTurb Verification Input Parameters

For the parametric and Performance analysis, the constant values assumed are same and shown in Table A.3. These are constant throughout all parametric and performance analyses using the GasTurb program.

Table A.3: Parametric and Performance analysis GasTurb input parameters

Parameter	Value	Parameter	Value
Π_{inlet} [-]	0.99	η_{HPT} [-]	0.85
$\Pi_{\text{combustor}}$ [-]	0.97	$\eta_{\text{mech,HPT}}$ [-]	0.95
Π_{outlet} [-]	0.98	$\eta_{\text{mech,LPT}}$ [-]	0.975
$\eta_{\text{combustor}}$ [-]	0.97	η_{prop} [-]	0.9
η_{LPT} [-]	0.9	LHV [MJ/kg]	43.124
$P_{\text{off-take}}$ [kW]	0.0	Cooling [%]	0.0

B

Regional Design Case Values

This appendix shows the regional design case results for the constant fleet scenario. The discussion is held short in Chapter 8, due to the skewed comparison. The full results are shown here.

Table B.1 shows the design variables for the regional design case, assuming constant fleet size.

Table B.1: Optimal design variables values for the regional design case, assuming constant fleet size

Design Variable	FM	DOC	ATR₁₀₀*
W/S [kN/m ²]	3.1	3.9	2.9
A [-]	17	11.0	15.9
TIT [K]	1376	1564	1386
$\Pi_{\text{compressor}}$ [-]	25	25	25
h_{cruise} [km]	4.8	6.0	4.8
M_{cruise} [-]	0.30	0.515	0.26

For the design variables a similar trend is seen in comparison to the medium-range design case, assuming constant fleet size. The ATR₁₀₀* objective tries to minimize the number of flights performed resulting in low cruise Mach number with a low cruise altitude. The lower wing-loading results in a lower aspect ratio compared to the FM objective, as the span constraint is active. Lastly, for ATR₁₀₀* objective the TIT at takeoff constraint limits the TIT during cruise, similar to the other objectives.

Table B.2 shows the aircraft parameters and characteristics for the regional design case assuming a constant fleet size. Again, the overall aircraft weight is similar between the different objectives, while the power-loading is higher due to the lower wing-loading for the FM and ATR₁₀₀*. That is also the reason for the larger wing area for the ATR₁₀₀* objective. The number of flights is a direct consequence of the difference in block time between the objectives.

Table B.2: Aircraft parameters and characteristics for the medium-range design case, assuming constant productivity

AC Parameter	FM	DOC	ATR₁₀₀*
MTOM [metric tonnes]	24.0	24.1	23.9
OEM [metric tonnes]	14.5	14.2	14.4
S [m ²]	76	61	81
W/P [N/W]	0.070	0.055	0.075
t_{block} [hrs]	4.1	2.8	4.2
N_{flights} [10 ³ #]	$1.9 \cdot 10^6$	$2.9 \cdot 10^6$	$1.9 \cdot 10^6$
EI _{NO_x} , cruise [kg/kg]	0.011	0.0091	0.011

The aircraft geometry comparison is a similar one to the constant productivity scenario. The geometry is seen in Figure B.1. This geometry match close when compared to the constant productivity scenario and the differences are negligible between both scenarios.

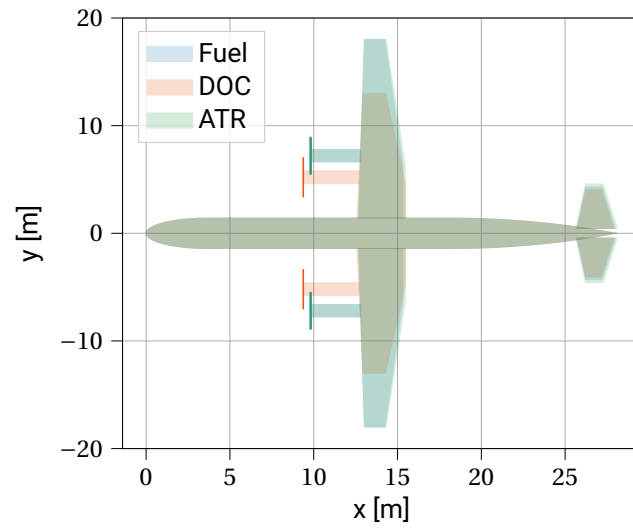


Figure B.1: Optimal aircraft geometry comparison for the regional design case, assuming constant fleet size

C

Power-Loading Diagrams

In this Appendix the power-loading diagrams for the different objectives can be seen. The power-loading diagrams shown are limited to the constant productivity scenario.

C.1. Medium-Range Design Case

For the medium-range design case the Figure C.1, C.2, and C.3 show the power-loading diagram for the ATR_{100}^* , DOC and FM objective, assuming constant productivity, respectively.

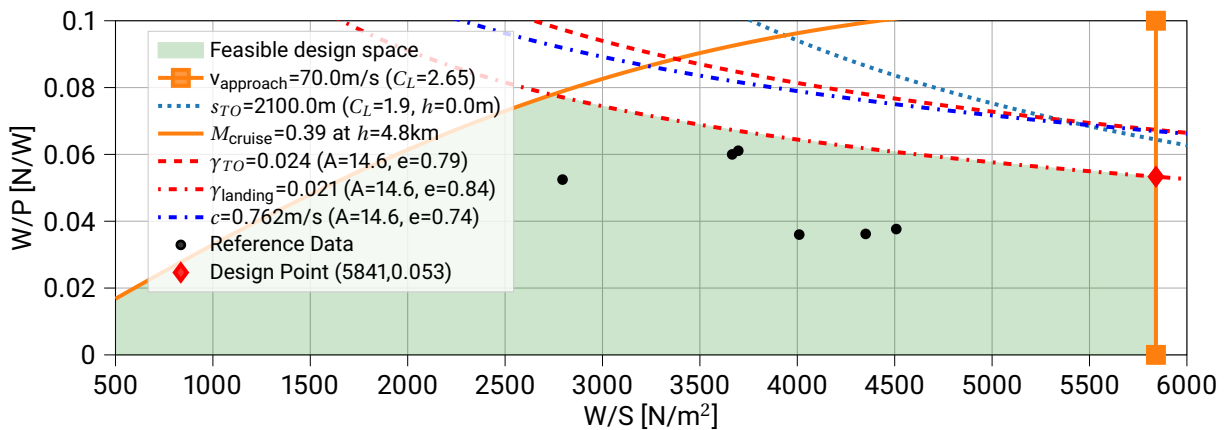


Figure C.1: Power-Loading diagram of the FM objective for the medium-range design case, assuming constant productivity

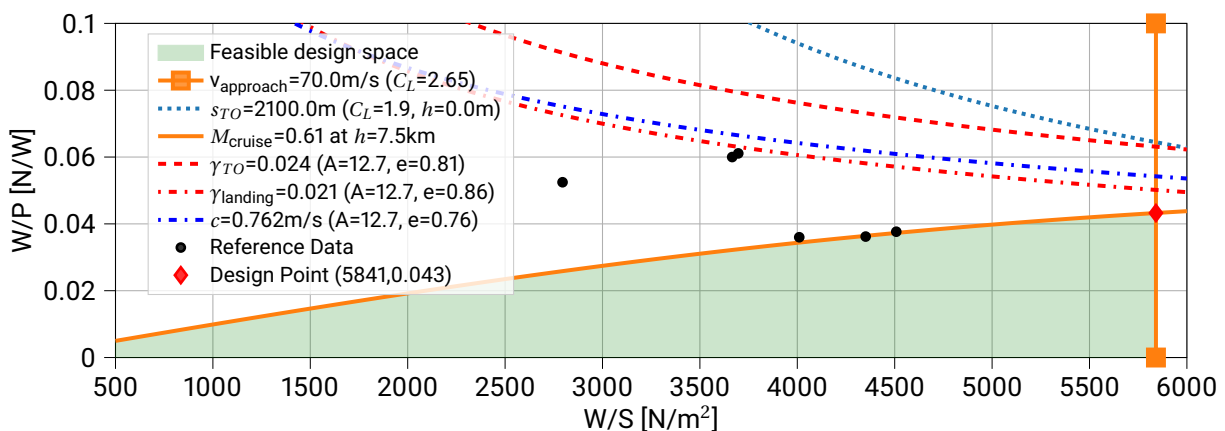


Figure C.2: Power-Loading diagram of the DOC objective for the medium-range design case, assuming constant productivity

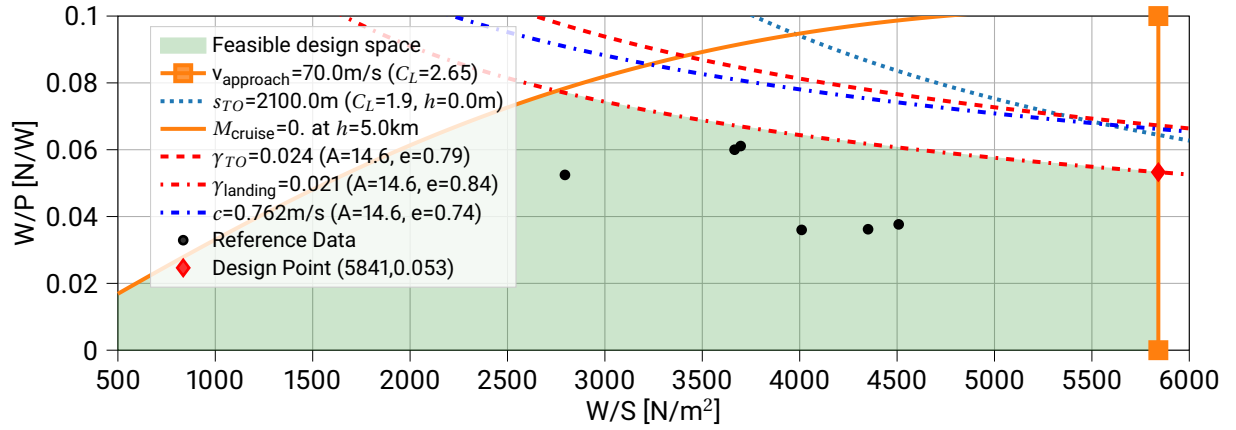


Figure C.3: Power-Loading diagram of the ATR_{100}^* optimised objective for the medium-range design case, assuming productivity

C.2. Medium-Range Design Case with Block Time Constraint

Figure C.4 and Figure C.5 show the power-loading diagram for the FM and ATR_{100}^* objective, assuming constant productivity, respectively. Note that for these two power-loading diagrams the and with the block time constraint applied respectively.

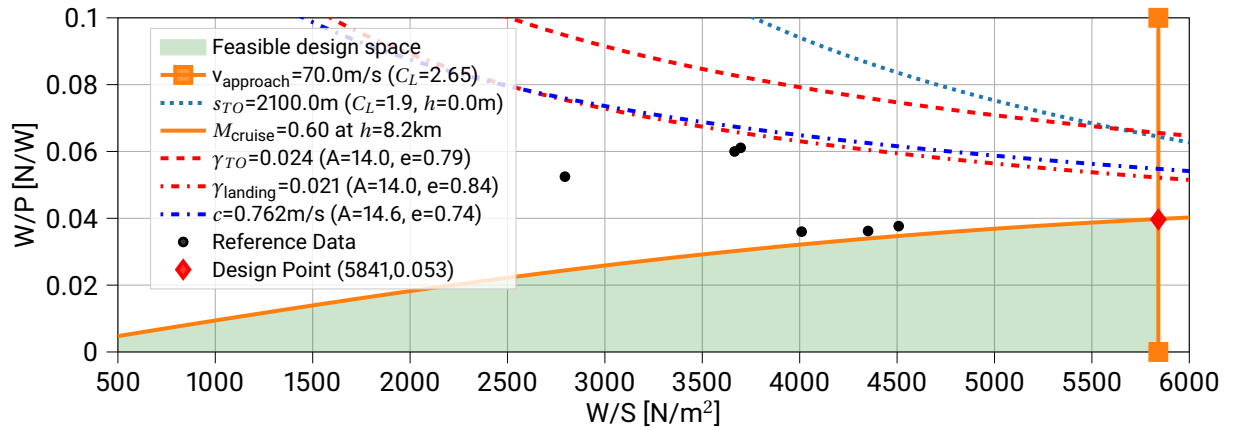


Figure C.4: Power-Loading diagram of the FM objective for the medium-range design case with block time constraint applied, assuming constant productivity

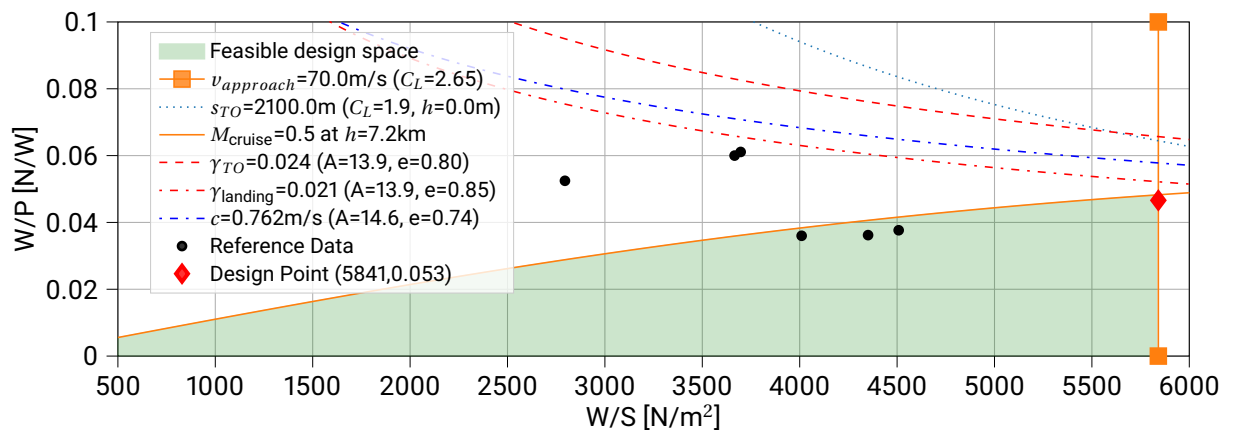


Figure C.5: Power-Loading diagram of the ATR_{100}^* objective for the medium-range design case with block time constraint applied, assuming constant productivity

C.3. Regional Design Case

For the Regional design case the Figure C.6, C.7, and C.8 show the power-loading diagram for the FM, DOC, ATR_{100}^* objective, assuming constant productivity, respectively.

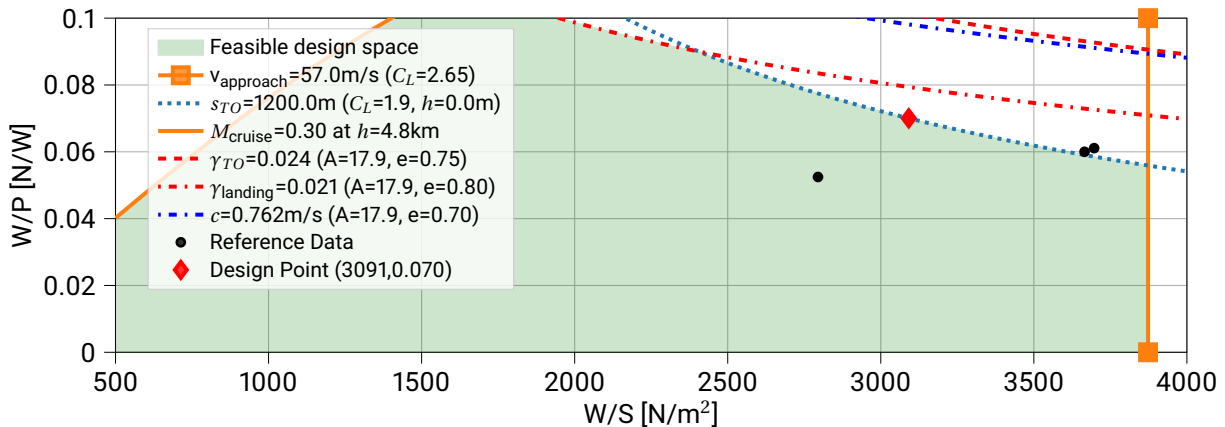


Figure C.6: Power-Loading diagram of the FM objective for the regional design case, assuming constant productivity

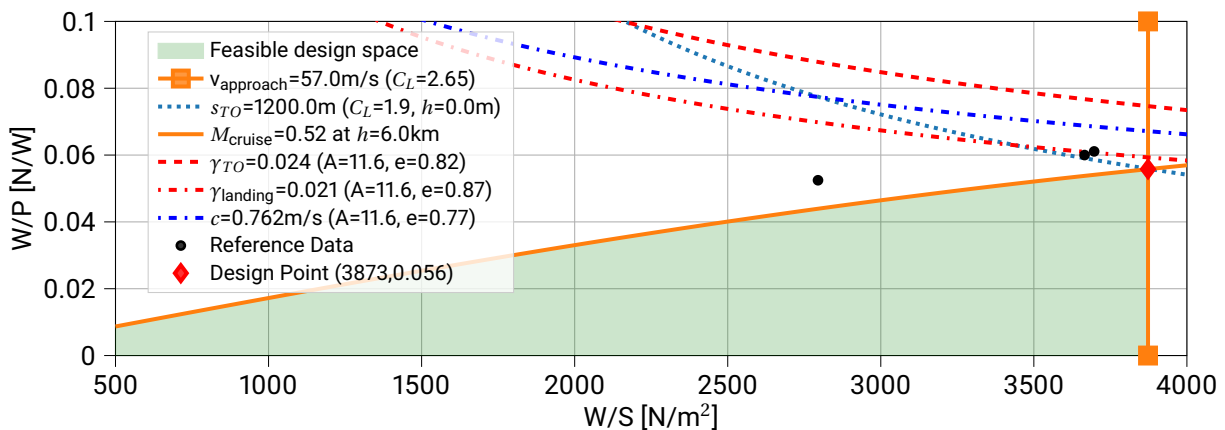


Figure C.7: Power-Loading diagram of the DOC objective for the regional design case, assuming constant productivity

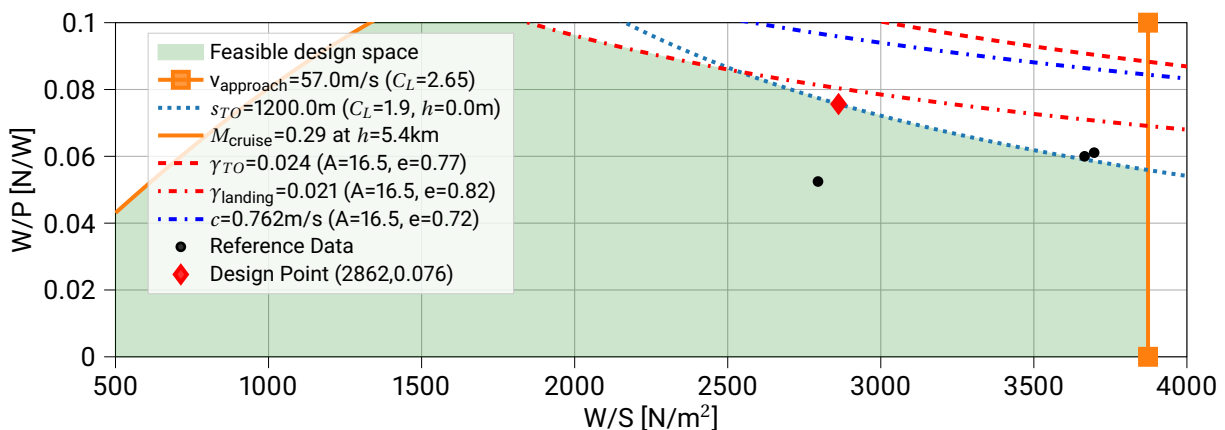


Figure C.8: Power-Loading diagram of the ATR_{100}^* objective for the regional design case, assuming constant productivity

D

Performance Discussion

The main discussion in Chapter 8 focused on the climate impact, design variables and aircraft parameters between the different aircraft for each objective. The performance of each of the designed aircraft was purposely avoided to keep the focus. The performance, measured with the help of the payload-range diagram, is shortly discussed in this Chapter. Note that the focus is on the constant productivity scenario for both design cases.

Section D.1 discusses the normal optimization performed for both design cases, while Section D.2 discusses the sensitivity analysis performed.

D.1. Aircraft Design Cases

For the generation of the payload-range diagram there are three main ranges. The first is the harmonic range with maximum payload. The second is with maximum fuel with payload that can be brought with at that weight. The last range is with zero payload and maximum fuel. With these three points payload-range diagram can be constructed.

The maximum fuel mass ($m_{\text{fuel, max}}$) that the aircraft can carry is important in the overall performance. This value determines the overall payload-range diagram. The maximum fuel mass estimation is based on the volume of the fuel tanks multiplied with the density of the fuel (ρ_{fuel}). The estimation is shown in Equation D.1 [48]. Note that multiplication with 0.91 is due to a subtraction of 5% for fuel expansions and 4% for the structural tanks.

$$m_{\text{fuel, max}} = 0.91 \cdot \rho_{\text{fuel}} \cdot \left(0.54 \cdot \frac{S^2}{b} \cdot (t/c)_{\text{root}} \cdot \frac{1 + \lambda\sqrt{\tau} + \lambda^2 \cdot \tau}{(1 + \lambda)^2} \right) \quad (\text{D.1})$$

Within Equation D.1, λ is the taper ratio, t/c is the thickness to chord ratio, S is the wing area, b is the span and τ is ratio between the t/c of the tip with that of the root.

Using Equation D.1 to calculate the maximum fuel mass for both design cases, gives a outlook on the different maximum fuel mass for all objectives. The overview is shown in Table D.1 for the propeller objectives, while Table D.2 shows the performance for the turbofan objectives. The range parameter (P_r) is obtained by multiplying the total engine efficiency with the lift-over-drag ratio (Equation 4.15). For the regional objectives a maximum fuel mass of 5000 kg has been imposed, as the equation greatly overestimates the fuel mass for the regional design case. The 5000 kg keeps the comparison more realistic. This is not done for the medium-range (MR) design case and the medium-range with the block time constraint applied.

Table D.1: Maximum fuel mass and range parameter for the objective within each design case

Parameter	Regional			medium-range (MR)			MR Block		
	FM	DOC	ATR* ₁₀₀	FM	DOC	ATR* ₁₀₀	FM	DOC	ATR* ₁₀₀
$m_{\text{fuel, max}}$ [10^3 kg]	5.0	5.0	5.0	15.0	17.4	15.0	16.6	17.4	16.6
Range Parameter	7.4	5.5	7.4	6.6	6.4	6.7	6.7	6.4	6.6

Table D.2: Maximum fuel mass and range parameter for the turbofan objectives

Parameter	FM	DOC	ATR* ₁₀₀
$m_{\text{fuel, max}}$ [10^3 kg]	16.7	18.2	18.4
Range Parameter	6.2	5.9	5.5

The maximum fuel mass for the medium-range turboprop and turbofan do seem to have a clear difference. The DOC turboprop and DOC turbofan objective have a similar maximum fuel mass, with a difference of 1000 kg. The difference between both ATR*₁₀₀ objectives is significant. More fuel can be brought for the turbofan aircraft, due to the larger wing size. The same is true for the FM turbofan objective. The FM turboprop objective is again similar to the ATR*₁₀₀ objective for the same aircraft. The range parameter of the turboprop is significantly higher. Logically, the maximum fuel mass increases for the turboprop with the block time constraint applied. The range parameter increases slightly. The range parameters of the FM and ATR*₁₀₀ objective are relatively on the high side, due to the high lift-over-drag ratio.

The payload-range diagram for the regional design case is shown in Figure D.1. The harmonic range requirement set for maximum payload can clearly be seen by the straight line. From that point the deviation between the objectives becomes clear. For this design case the regional aircraft is less fuel efficient and can reach a lower range with the same amount of fuel. The high engine efficiency of the FM and ATR*₁₀₀ objective results in higher maximum range. This range obtained is optimistic and is due to the high range parameter. The range parameter of the ATR 72 in the 90's was approximately 4.6 [56]. The 7.4 is significantly higher and causes the higher range. The maximum range achieved by the DOC objective is reasonable, with a range parameter of 5.5, as technological advancements have been made.

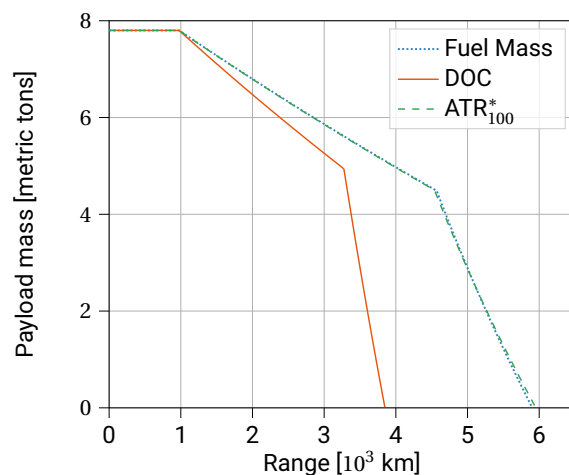


Figure D.1: Payload-range diagram for the regional design case, assuming constant productivity

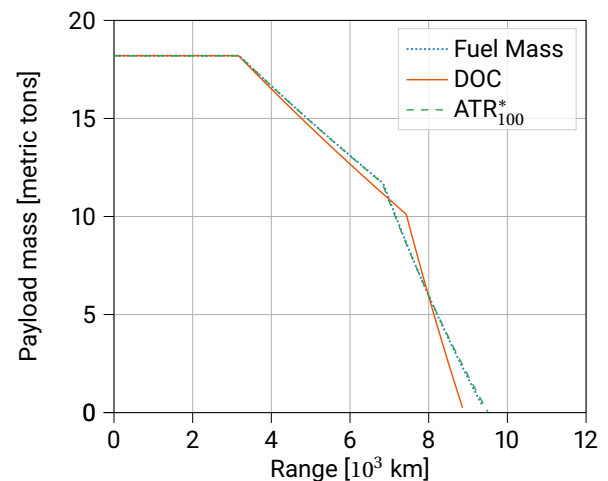


Figure D.2: Payload-range diagram for the medium-range design case, assuming constant productivity

The payload-range diagram of the medium-range design case is shown in Figure D.2. The DOC outperforms both the FM and ATR*₁₀₀ objective at the second point. The aircraft can carry more fuel resulting in the higher range. This advantage is outdone by the more fuel efficient FM and ATR*₁₀₀ objective. Even though less fuel is brought with, when the payload is decreased, the achievable range is higher. The range achieved for all objectives is on the high side. A maximum range of almost 10000 km is optimistic for the current aircraft designed. Comparing it to Figure D.4, the range increase is extensive as an extra 1500 km can be flown for the same requirements. The extension is because of the optimistic propeller efficiency assumed. The difference is expected to be less with a lower propeller efficiency.

The range achieved is logically lessened for the FM and ATR*₁₀₀ objective with the block time constraint applied due to the change in cruise Mach number. The range for these objective is similar to the DOC objective, as the design variables and aircraft design are also found similar. Compared to the turbofan aircraft an increase in maximum range of 1000 km is still seen. The intertwining of the performance for the three ob-

jectives is however similar between the turbofan (Figure D.4) and MR with the block time constraint applied (Figure D.3).

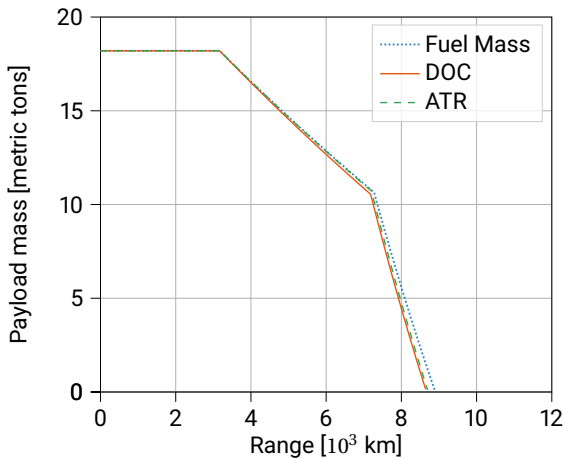


Figure D.3: Payload-range diagram for medium-range design case, with the block time constraint applied, assuming constant productivity

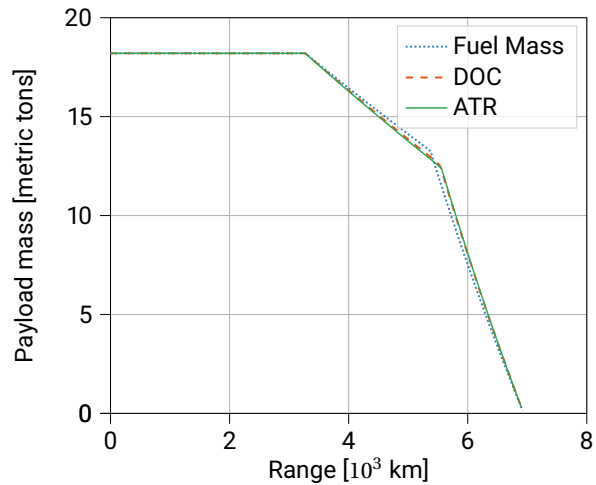


Figure D.4: Payload-range diagram for the turbofan objectives, assuming constant productivity

D.2. Sensitivity Analysis

The optimistically estimated performance, due to the high set propeller efficiency, is put into perspective with the performed sensitivity analysis. Figure D.5 shows the performance for the various propeller efficiencies assumed during the sensitivity analysis. Due to the higher overall engine efficiency with higher propeller efficiency, the range parameter increases. The opposite is true for the maximum fuel mass. As the propeller increases, the wing area decreases as a consequence and thus the maximum fuel mass decreases as well. The same trend is observed for the sensitivity analysis with the block time constraint applied. The results for that sensitivity analysis are shown in Table D.4.

The extra fuel does not result in a higher maximum range, as shown in Figure D.5. The benefit of the higher range parameter or overall engine efficiency clearly outweighs the larger fuel tanks. The aircraft with the higher propulsive efficiency can fly farther and outperforms the other clearly. Compared to the turbofan aircraft the propeller efficiency of 75% results in a similar maximum distance. For the sensitivity with the block time constraint applied, this similarity is achieved with for a propeller efficiency of 80%. The latter is shown in Figure D.6. The trend in the figure is again similar to that of Figure D.6. Lastly, it is noteworthy that the gradient of the last segment of the payload-range diagram is almost similar with changing propeller efficiency. As the higher maximum fuel mass and lower range parameters counteract each other. This is not true for the other gradient as it is still flown at MTOM. The ratio between the MTOM, fuel mass and payload differs more.

Table D.3: Maximum fuel mass and the range parameter for $ATR_{thesensitivity}^*$ for various propeller efficiencies

Parameter	$\eta_{prop} = 0.65$	$\eta_{prop} = 0.70$	$\eta_{prop} = 0.75$	$\eta_{prop} = 0.80$	$\eta_{prop} = 0.85$	$\eta_{prop} = 0.90$
$m_{fuel, max} [10^3 \text{ kg}]$	30.4	23.4	19.7	17.4	15.8	14.7
Range Parameter	3.2	3.9	4.6	5.3	6.1	7.0

Table D.4: Maximum fuel mass and the range parameter for $ATR_{thesensitivity}^*$, with the block time constraint applied, for various propeller efficiencies

Parameter	$\eta_{prop} = 0.65$	$\eta_{prop} = 0.70$	$\eta_{prop} = 0.75$	$\eta_{prop} = 0.80$	$\eta_{prop} = 0.85$	$\eta_{prop} = 0.90$
$m_{fuel, max} [10^3 \text{ kg}]$	31.3	25.0	21.4	19.0	17.3	16.1
Range Parameter	3.4	4.1	4.8	5.5	6.2	7.0

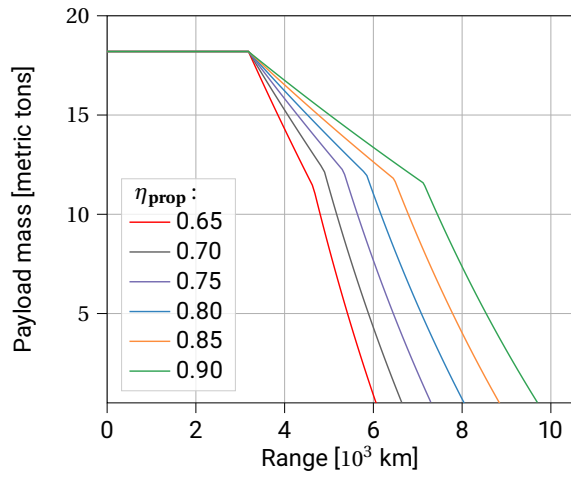


Figure D.5: Payload-range diagram for the ATR_{100}^* objective for various assumed propeller efficiencies

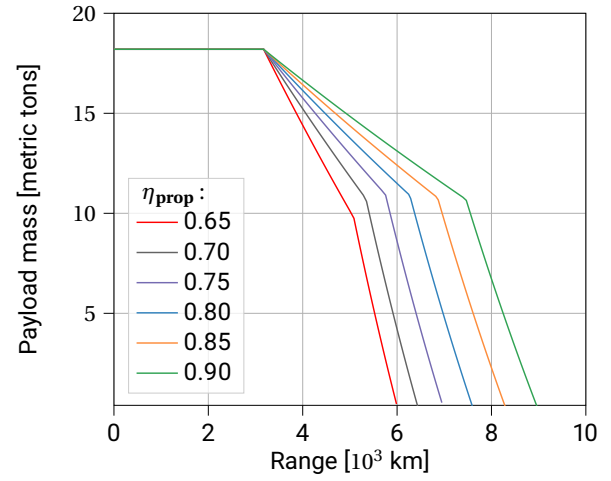


Figure D.6: Payload-range diagram for the ATR_{100}^* objective with the block time constraint applied for various assumed propeller efficiencies

E

Contrail Formation

In this Appendix the contrail formation for the medium-range case will be shortly discussed. The medium-range design case does not form any contrails for all objectives and the formation is discussed with the help of the Schmidt-Appleman criterion. The regional design case and medium-range design, case with block time constraint applied, are not shown. The atmospheric conditions for the former are worse than the ones discusses, while the latter are similar to the medium-range DOC objective. The objectives mentioned are all for the constant productivity scenario.

Figure E.1, E.3, and E.5 show the critical contrail formation plot for the FM, DOC and ATR_{100}^* objective respectively. Additionally, Figure E.2, E.4, and E.6 show the same plots in the same order, but for the turbofan aircraft. In the figures the lines shown, include the ice saturation pressure line, the water saturation pressure line, the mixing line and the critical mixing line. The green area is the area when persistent contrail can form. Looking at DOC turboprop objective in Figure E.1, it can be seen that the end point of the mixing line is below the critical mixing line and between the ice and water saturation pressure line. This indicates that no water droplets form as the mixing line does not cross the water saturation pressure line. Comparing this to the DOC turbofan objective in Figure E.2, the mixing line is clearly "above" the critical mixing line and contrail can form. The line crosses the water saturation pressure line and droplets can form, making the contrail visible. The particles then freeze and the contrail persists. As the mixing line ends in the green zone the contrails stays persistent and does not dissolve easily behind the engine, resulting in a climate impact due to the persistent contrail. In similar reasoning Figure E.4 can be explained.

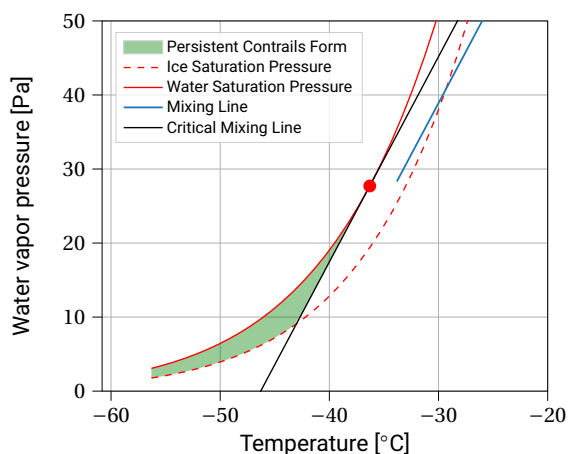


Figure E.1: Critical contrail formation plot during cruise for the DOC turboprop objective for the medium-range design case

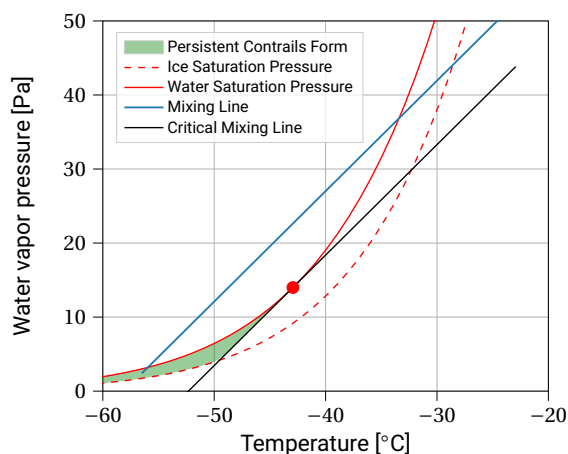


Figure E.2: Critical contrail formation plot during cruise for the DOC turbofan objective

Regarding the ATR_{100}^* turbofan objective, seen in Figure E.6, a similar reasoning can be applied to that of the DOC turboprop objective. As the aircraft fly at similar cruise altitudes the plot is similar, with small differences. The slop of the mixing line is different due to the difference in total engine efficiency. The other is the

atmospheric conditions, but these are very minor. This results in similar critical contrail formation plots, as observed. Again since the end point of the mixing line does not cross or ends the green indicated area, no persistent contrails are formed and thus no climate impact due to formation of contrails.

The last plots to discuss are the FM and ATR_{100}^* turboprop objective, seen in Figure E.3 and Figure E.5 respectively. These aircraft fly at a low altitude that the atmospheric conditions are not close to forming contrails due to the exhaust of water vapor at the engine. The mixing line end point is way off from the green area making the formation near impossible at this altitude. Both plots are also more zoomed out, as otherwise the mixing line was not visible.

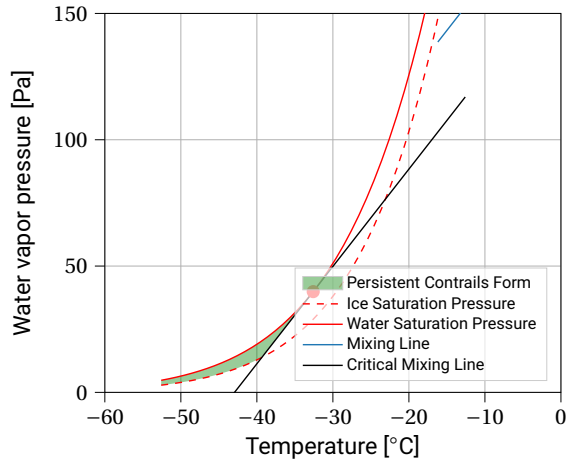


Figure E.3: Critical contrail formation plot during cruise for the FM turboprop objective for the medium-range design case

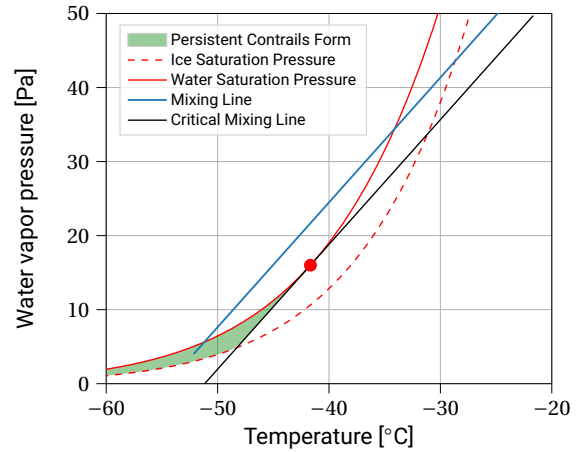


Figure E.4: Critical contrail formation plot during cruise for the DOC turbofan objective

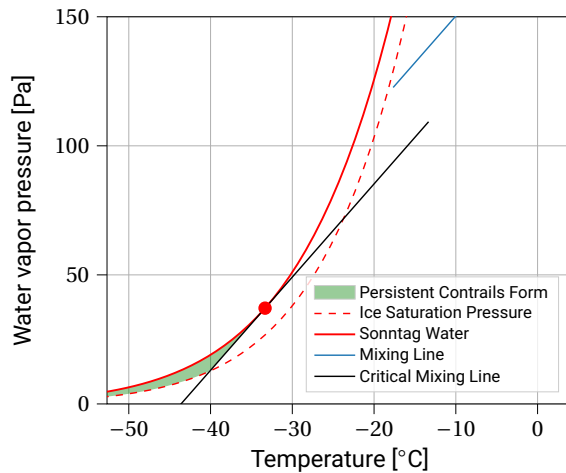


Figure E.5: Critical contrail formation plot during cruise for the ATR_{100}^* turboprop objective for the medium-range design case

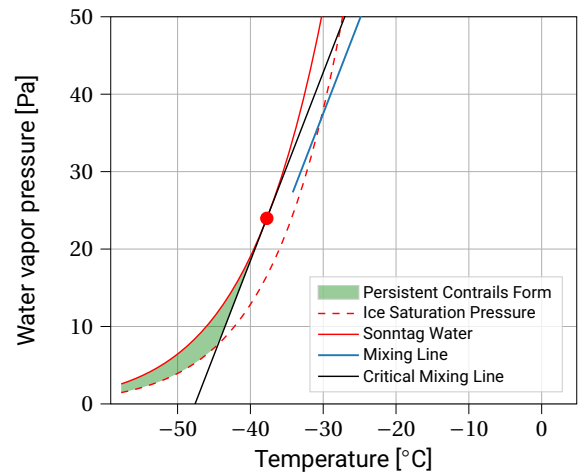


Figure E.6: Critical contrail formation plot during cruise for the ATR_{100}^* turbofan objective

Bibliography

- [1] D. S. Lee, D. W. Fahey, P. M. Forster, P. J. Newton, R. C. Wit, L. L. Lim, B. Owen, and R. Sausen. Aviation and global climate change in the 21st century. *Atmospheric Environment*, 43(22-23):3520–3537, 2009. ISSN 13522310, doi:10.1016/j.atmosenv.2009.04.024.
- [2] J. Wallace and P. Hobbs. *Atmospheric Science: An Introductory Survey*. International geophysics series. Elsevier Academic Press, 2006. ISBN 9780127329512, doi:10.1016/C2009-0-00034-8.
- [3] D. S. Lee, D. W. Fahey, A. Skowron, M. Allen, U. Burkhardt, Q. Chen, S. Doherty, S. Freeman, P. Forster, J. Fuglestvedt, A. Gettelman, R. De León, L. Lim, M. Lund, R. Millar, B. Owen, J. Penner, G. Pitari, M. Prather, R. Sausen, and L. Wilcox. The contribution of global aviation to anthropogenic climate forcing for 2000 to 2018. *Atmospheric Environment*, 244(September 2020):117834, 2021. ISSN 13522310, doi:10.1016/j.atmosenv.2020.117834.
- [4] Airbus. Cities, airports and aircraft 2019-2038, 2019.
- [5] Boeing. Commercial market outlook 2020–2039, 2020.
- [6] D. Xue, K. K. H. Ng, and L.-T. Hsu. Multi-Objective Flight Altitude Decision Considering Contrails, Fuel Consumption and Flight Time. *Sustainability*, 12(15):6253, aug 2020. ISSN 2071-1050, doi:10.3390/su12156253.
- [7] D. S. Lee, G. Pitari, V. Grewe, K. Gierens, J. E. Penner, A. Petzold, M. J. Prather, U. Schumann, A. Bais, T. Berntsen, D. Iachetti, L. L. Lim, and R. Sausen. Transport impacts on atmosphere and climate: Aviation. *Atmospheric Environment*, 44(37):4678–4734, 2010. ISSN 13522310, doi:10.1016/j.atmosenv.2009.06.005.
- [8] G. Brasseur, R. Cox, D. Hauglustaine, I. Isaksen, J. Lelieveld, D. Lister, R. Sausen, U. Schumann, A. Wahner, and P. Wiesen. European scientific assessment of the atmospheric effects of aircraft emissions. *Atmospheric Environment*, 32(13):2329–2418, jul 1998. ISSN 13522310, doi:10.1016/S1352-2310(97)00486-X.
- [9] E. Schwartz. Aircraft Design for Reduced Climate Impact. PhD thesis, Stanford University, 2011.
- [10] C. Fichter, S. Marquart, R. Sausen, and D. S. Lee. The impact of cruise altitude on contrails and related radiative forcing. In *Meteorologische Zeitschrift*, volume 14, pages 563–572. 2005, doi:10.1127/0941-2948/2005/0048.
- [11] T. Hendriks. Contrail mitigation. *MSc Thesis, Delft University of Technology*, 2015.
- [12] J. Lee and J. Mo. Analysis of Technological Innovation and Environmental Performance Improvement in Aviation Sector. *International Journal of Environmental Research and Public Health*, 8(9):3777–3795, sep 2011. ISSN 1660-4601, doi:10.3390/ijerph8093777.
- [13] N. E. Antoine and I. M. Kroo. Aircraft Optimization for Minimal Environmental Impact. *Journal of Aircraft*, 41(4):790–797, jul 2004. ISSN 0021-8669, doi:10.2514/1.71.
- [14] R. P. Henderson, J. R. R. A. Martins, and R. E. Perez. Aircraft conceptual design for optimal environmental performance. *The Aeronautical Journal*, 116:1–22, jan 2012. ISSN 0001-9240, doi:10.1017/S000192400000659X.
- [15] P. Proesmans and R. Vos. Airplane Design Optimization for Minimal Global Warming Impact. In *AIAA Scitech 2021 Forum*, Reston, Virginia, jan 2021. American Institute of Aeronautics and Astronautics. ISBN 978-1-62410-609-5, doi:10.2514/6.2021-1297.

- [16] V. Grewe and K. Dahlmann. How ambiguous are climate metrics? And are we prepared to assess and compare the climate impact of new air traffic technologies? *Atmospheric Environment*, 106:373–374, 2015. ISSN 18732844, doi:10.1016/j.atmosenv.2015.02.039.
- [17] L. Stingo, P. Della Vecchia, G. Cerino, F. Nicolosi, and A. De Marco. MDO applications to conventional and novel turboprop aircraft within agile European project. *31st Congress of the International Council of the Aeronautical Sciences, ICAS 2018*, pages 1–10, 2018.
- [18] P. Della Vecchia, L. Stingo, F. Nicolosi, A. De Marco, G. Cerino, P. D. Ciampa, P. S. Prakasha, M. Fioriti, M. Zhang, A. Mirzoyan, B. Aigner, and D. Charbonnier. Advanced turboprop multidisciplinary design and optimization within AGILE project. In *2018 Aviation Technology, Integration, and Operations Conference*, pages 1–17, Reston, Virginia, jun 2018. American Institute of Aeronautics and Astronautics. ISBN 978-1-62410-556-2, doi:10.2514/6.2018-3205.
- [19] J. S. Fuglestedt, T. K. Berntsen, O. Godal, R. Sausen, K. P. Shine, and T. Skodvin. Metrics of climate change: Assessing radiative forcing and emission indices. *Climatic Change*, 58(3):267–331, 2003. ISSN 01650009, doi:10.1023/A:1023905326842.
- [20] R. Hager and D. Vrabel. *Advanced Turboprop Project*. NASA SP-495. Scientific and Technical Information Division, NASA, 1988.
- [21] M. Guynn, J. Berton, W. Haller, E. Hendricks, and M. Tong. Performance and environmental assessment of an advanced aircraft with open rotor propulsion. 2012, doi:10.13140/RG.2.1.4847.3687.
- [22] E. Torenbeek. *Advanced Aircraft Design: Conceptual Design, Analysis and Optimization of Subsonic Civil Airplanes*. Aerospace Series. Wiley, 2013. ISBN 9781118568095, doi:10.1002/9781118568101.
- [23] D. Raymer. *Aircraft Design: A Conceptual Approach, Sixth Edition*. AIAA education series. American Institute of Aeronautics and Astronautics, Incorporated, 2018. ISBN 9781624104909.
- [24] P. Alves, M. Silvestre, and P. Gamboa. Aircraft Propellers—Is There a Future? *Energies*, 13(16):4157, aug 2020. ISSN 1996-1073, doi:10.3390/en13164157.
- [25] M. H. Sadraey. *Aircraft Performance: An Engineering Approach*. CRC Press, January 2017, doi:10.1201/9781315366913.
- [26] F. Nicolosi, S. Corcione, V. Trifari, P. Della Vecchia, and A. De Marco. Design Guidelines for High Capacity Innovative Regional Turboprop Aircraft. In *AIAA Scitech 2019 Forum*, number January, pages 1–16, Reston, Virginia, jan 2019. American Institute of Aeronautics and Astronautics. ISBN 978-1-62410-578-4, doi:10.2514/6.2019-0256.
- [27] N. van Arnhem, R. de Vries, R. Vos, and L. L. Veldhuis. Aerodynamic performance of an aircraft equipped with horizontal tail-mounted propellers. *AIAA Aviation 2019 Forum*, (June):1–19, 2019, doi:10.2514/6.2019-3036.
- [28] A. Mirzoyan, A. Isianov, G. Cerino, P. D. Vecchia, L. Stingo, M. Fioriti, L. Boggero, F. Tomasella, and P. S. Prakasha. Comparative Study of Advanced Turboprop Aircraft with Wing and Rear Mounted Propulsion System in the Agile EU project. In *2018 Joint Propulsion Conference*, pages 1–13, Reston, Virginia, jul 2018. American Institute of Aeronautics and Astronautics. ISBN 978-1-62410-570-8, doi:10.2514/6.2018-4849.
- [29] T. Schouten, M. Hoogreef, and R. Vos. Effect of Propeller Installation on Performance Indicators of Regional Turboprop Aircraft. In *AIAA Scitech 2019 Forum*, number January, pages 1–14, Reston, Virginia, jan 2019. American Institute of Aeronautics and Astronautics. ISBN 978-1-62410-578-4, doi:10.2514/6.2019-1306.
- [30] I. M. Goldsmith. A study to define the research and technology requirements for advanced turbo/propfan transport aircraft. In *Report No. CR-166138.*, 1981.
- [31] E. S. Hendricks, J. J. Berton, W. J. Haller, M. J. Tong, and M. D. Guynn. Updated Assessment of an Open Rotor Airplane using an Advanced Blade Design. In *49th AIAA/ASME/SAE/ASEE Joint Propulsion Conference*, volume 1 PartF, Reston, Virginia, jul 2013. American Institute of Aeronautics and Astronautics. ISBN 978-1-62410-222-6, doi:10.2514/6.2013-3628.

- [32] M. S. Ryerson and M. Hansen. The potential of turboprops for reducing aviation fuel consumption. *Transportation Research Part D: Transport and Environment*, 15(6):305–314, aug 2010. ISSN 13619209, doi:10.1016/j.trd.2010.03.003.
- [33] T. Mahieu. Regional Aircraft Design Space Exploration. *MSc Thesis, Delft University of Technology*, 2016.
- [34] M. S. Ryerson and X. Ge. The role of turboprops in China’s growing aviation system. *Journal of Transport Geography*, 40:133–144, 2014. ISSN 09666923, doi:10.1016/j.jtrangeo.2014.03.009.
- [35] S. J. Reid, R. E. Perez, P. W. Jansen, and C. Bil. Influence of Carbon Pricing on Regional Aircraft and Route Network Design. In *AIAA Scitech 2021 Forum*, number January, pages 1–17, Reston, Virginia, jan 2021. American Institute of Aeronautics and Astronautics. ISBN 978-1-62410-609-5, doi:10.2514/6.2021-0463.
- [36] E. S. Dallara, I. M. Kroo, and I. A. Waitz. Metric for comparing lifetime average climate impact of aircraft. *AIAA Journal*, 49(8):1600–1613, 2011. ISSN 00011452, doi:10.2514/1.J050763.
- [37] U. Schumann. Formation, properties and climatic effects of contrails. *Comptes Rendus Physique*, 6(4-5): 549–565, may 2005. ISSN 16310705, doi:10.1016/j.crhy.2005.05.002.
- [38] J. S. Fuglestvedt, K. P. Shine, T. Berntsen, J. Cook, D. S. Lee, A. Stenke, R. B. Skeie, G. J. Velders, and I. A. Waitz. Transport impacts on atmosphere and climate: Metrics. *Atmospheric Environment*, 44(37):4648–4677, 2010. ISSN 13522310, doi:10.1016/j.atmosenv.2009.04.044.
- [39] R. Sausen and U. Schumann. Estimates of the climate response to aircraft CO₂ and NO(x) emissions scenarios. *Climatic Change*, 44(1-2):27–58, 2000. ISSN 01650009, doi:10.1023/a:1005579306109.
- [40] R. Sausen, I. Isaksen, V. Grewe, D. Hauglustaine, D. S. Lee, G. Myhre, M. O. Köhler, G. Pitari, U. Schumann, F. Stordal, and C. Zerefos. Aviation radiative forcing in 2000: An update on IPCC (1999). *Meteorologische Zeitschrift*, 14(4):555–561, 2005. ISSN 09412948, doi:10.1127/0941-2948/2005/0049.
- [41] R. Egelhofer. Aircraft Design Driven by Climate Change. PhD thesis, Technische Universität München, 2008.
- [42] A. Koch. Climate impact mitigation potential given by flight profile and aircraft optimization. PhD thesis, Technischen Universität Hambrug-Harburg, 2013.
- [43] N. Antoine. Aircraft Optimization for Minimal Environmental Impact. PhD thesis, Stanford University, 2004.
- [44] E. Schwartz and I. Kroo. Aircraft Design for Reduced Climate Impact. In *49th AIAA Aerospace Sciences Meeting including the New Horizons Forum and Aerospace Exposition*, number January, Reston, Virginia, jan 2011. American Institute of Aeronautics and Astronautics. ISBN 978-1-60086-950-1, doi:10.2514/6.2011-265.
- [45] J. D. Mattingly, W. H. Heiser, and D. T. Pratt. *Aircraft Engine Design, Second Edition*. American Institute of Aeronautics and Astronautics, Reston, VA, jan 2002. ISBN 978-1-56347-538-2, doi:10.2514/4.861444.
- [46] European Union Aviation Safety Agency. Certification specifications and acceptable means of compliance for large aeroplanes cs-25: Amendment 26. dec 2020. <https://www.easa.europa.eu/document-library/certification-specifications/cs-25-amendment-26-0>.
- [47] R. Vos and S. Farokhi. *Introduction to Transonic Aerodynamics*, volume 110 of *Fluid Mechanics and Its Applications*. Springer Netherlands, Dordrecht, 2015. ISBN 978-94-017-9746-7, doi:10.1007/978-94-017-9747-4.
- [48] E. Torenbeek. *Synthesis of Subsonic Airplane Design: An introduction to the preliminary design of subsonic general aviation and transport aircraft, with emphasis on layout, aerodynamic design, propulsion and performance*. Springer Netherlands, 1982. ISBN 9789024727247.
- [49] M. Iwanizki, N. P. Randt, and S. Sartorius. Preliminary design of a heavy short-and medium-haul turboprop-powered transport aircraft. *52nd Aerospace Sciences Meeting*, pages 1–11, 2014, doi:10.2514/6.2014-0027.

- [50] J. R. R. A. Martins and A. B. Lambe. Multidisciplinary Design Optimization: A Survey of Architectures. *AIAA Journal*, 51(9):2049–2075, sep 2013. ISSN 0001-1452, doi:10.2514/1.J051895.
- [51] X. Vouvakos, Y. Kallinderis, and P. Menounou. Preliminary design correlations for twin civil turboprops and comparison with jet aircraft. *Aircraft Engineering and Aerospace Technology*, 82(2):126–133, 2010. ISSN 00022667, doi:10.1108/00022661011053427.
- [52] K. Ibrahim. Selecting Principal Parameters of Baseline Design Configuration for Twin Turboprop Transport Aircraft. In *22nd Applied Aerodynamics Conference and Exhibit*, volume 1, pages 567–577, Reston, Virginia, aug 2004. American Institute of Aeronautics and Astronautics. ISBN 978-1-62410-025-3, doi:10.2514/6.2004-5069.
- [53] B. G. Marinus and L. Quodbach. Data and Design Models for Civil Turbopropeller Aircraft. *Journal of Aircraft*, 57(6):1252–1267, nov 2020. ISSN 1533-3868, doi:10.2514/1.C035271.
- [54] E. Obert. Drag polars of nineteen jet transport aircraft at mach number $m = 0.40 - 0.60$, 2013.
- [55] J. Roskam. *Airplane Design V: Component weight estimation*. Airplane Design. Roskam Aviation and Engineering Corporation, 1989. ISBN 1884885500.
- [56] E. Torenbeek. The initial calculation of range and mission fuel during conceptual design. (Report LR-525), 1987.
- [57] G. Ruijgrok. *Elements of Airplane Performance*. VSSD, 2009. ISBN 9789065622327.
- [58] J. GODSTON and C. REYNOLDS. Propulsion system integration configurations for future prop-fan powered aircraft. 1983, doi:10.2514/6.1983-1157.
- [59] E. Hendricks and M. Tong. Performance and Weight Estimates for an Advanced Open Rotor Engine. In *48th AIAA/ASME/SAE/ASEE Joint Propulsion Conference Exhibit*, number August, pages 1–12, Reston, Virginia, jul 2012. American Institute of Aeronautics and Astronautics. ISBN 978-1-60086-935-8, doi:10.2514/6.2012-3911.
- [60] J. Mattingly. *Elements of Gas Turbine Propulsion*. AIAA education series. American Institute of Aeronautics and Astronautics, 2005. ISBN 9781563477782, doi:https://doi.org/10.2514/4.861789.
- [61] P. Walsh and P. Fletcher. *Gas Turbine Performance*. Wiley, 2004. ISBN 9780632064342, doi:10.1002/9780470774533.
- [62] M. Drela. TASOPT 2.00: Transport Aircraft System Optimization. Technical report, Massachusetts Institute of Technology, 2010.
- [63] P. Giannakakis, P. Laskaridis, T. Nikolaidis, and A. I. Kalfas. Toward a scalable propeller performance map. *Journal of Propulsion and Power*, 31(4):1073–1082, 2015. ISSN 15333876, doi:10.2514/1.B35498.
- [64] Y. Teeuwen. Propeller Design for Conceptual Turboprop Aircraft. *MSc Thesis, Delft University of Technology*, 2017. <http://repository.tudelft.nl/.%0Ahttps://repository.tudelft.nl/islandora/object/uuid:d746a647-25e1-463b-af3a-6c2c478e1b37/datastream/OBJ/download>.
- [65] R. Vos and J. Melkert. Propeller slipstream effects. Lecture Notes. Delft University of Technology, 2018.
- [66] L. Nicolai and G. Carichner. *Fundamentals of Aircraft and Airship Design*. Number v. 1 in AIAA education series. American Institute of Aeronautics and Astronautics, 2010. ISBN 9781600867514, doi:https://doi.org/10.2514/4.867538.
- [67] J. Roskam. *Airplane Design VIII: Airplane Cost Estimation: Design, Development, Manufacturing and Operating*. Number v. 1 in Airplane Design. DARcorporation, 1990. ISBN 9781884885556.
- [68] E. L. Thomas. *ATA Direct Operating Cost Formula for Transport Aircraft*. SAE International, February 1966, doi:10.4271/660280.
- [69] J. Roskam. *Airplane Design: Preliminary sizing of airplanes*. Airplane Design. DARcorporation, 1985. ISBN 9781884885426. <https://books.google.nl/books?id=usXVaf8Qu0cC>.

- [70] V. Grewe, S. Matthes, and K. Dahlmann. The contribution of aviation NO_x emissions to climate change: are we ignoring methodological flaws? *Environmental Research Letters*, 14(12):121003, dec 2019, doi:10.1088/1748-9326/ab5dd7.
- [71] V. Grewe and A. Stenke. AirClim: an efficient tool for climate evaluation of aircraft technology. *Atmospheric Chemistry and Physics*, 8(16):4621–4639, aug 2008. ISSN 1680-7324, doi:10.5194/acp-8-4621-2008.
- [72] L. Sherry and T. Thompson. Primer on Aircraft Induced Clouds and Their Global Warming Mitigation Options. *Transportation Research Record: Journal of the Transportation Research Board*, 2674(11):827–841, nov 2020. ISSN 0361-1981, doi:10.1177/0361198120951188.
- [73] K. Gierens and F. Dilger. A climatology of formation conditions for aerodynamic contrails. *Atmospheric Chemistry and Physics*, 13(21):10847–10857, 2013. ISSN 16807316, doi:10.5194/acp-13-10847-2013.
- [74] C. Zhou and J. E. Penner. Aircraft soot indirect effect on large-scale cirrus clouds: Is the indirect forcing by aircraft soot positive or negative? *Journal of Geophysical Research: Atmospheres*, 119(19):11,303–11,320, oct 2014. ISSN 2169897X, doi:10.1002/2014JD021914.
- [75] U. Schumann. Über Bedingungen zur Bildung von Kondensstreifen aus Flugzeugabgasen. *Meteorologische Zeitschrift*, 5(1):4–23, mar 1996. ISSN 0941-2948, doi:10.1127/metz/5/1996/4.
- [76] V. Grewe. Aircraft emissions and climate effects: Part 3. Lecture Notes. Delft University of Technology, 2016.
- [77] A. Dinç. Sizing of a turboprop unmanned air vehicle and its propulsion system. *Journal of Thermal Sciences and Technology*, 35:53–62, 01 2015.
- [78] Bombardier. Airport planning manual, 2014.
- [79] P. Nadot. Performance: Atr training & flight operations manual, 2009.
- [80] M. Husemann, K. Schäfer, and E. Stumpf. Flexibility within flight operations as an evaluation criterion for preliminary aircraft design. *Journal of Air Transport Management*, 71(April):201–214, 2018. ISSN 09696997, doi:10.1016/j.jairtraman.2018.04.007.
- [81] Avions de transport régional. Turboprop market forecast 2018-2037. Digital Document, 2018.
- [82] M. Scanavino, A. Vilardi, and G. Guglieri. An Experimental Analysis on Propeller Performance in a Climate-controlled Facility. *Journal of Intelligent and Robotic Systems: Theory and Applications*, 100(2):505–517, 2020. ISSN 15730409, doi:10.1007/s10846-019-01132-9.